SUPPLEMENT

to the No 3-4 of Vol 5. of the Publications of the Institute of Nuclear Research of the Hung. Acad. of Sciences /ATOMKI/ Debrecen

ПРИЛОЖЕНИЕ

к вып. 3-4 том. 5., Сообщения Института Ядерных Исследований Венгерской АН /ATOMKI/ Дебрецен.

Atomki Közlemények

V. kötet 1963. 3-4. szám

Subject matter reported by collaborators of the Institute at the Conference on Nuclear Physics of Tihany on 16-21. Sept. 1963. (Manuscript.)

Материалы, изложенные сотрудниками Института на Конференции по Ядерной Физике в Тихане с 16. 09. 1963. по 21. 09. 1963 г. (В качестве рукописи.)

M.T.A.
ATOMMAG KUTATÓ INTÉZETE
DEBRECEN
1963. december

CONTENTS

СОДЕРЖАНИЕ

INVESTIGATIONS ON THE $Mg^{25}(d,\alpha)Na^{23}$ NUCLEAR REACTION

O. Hansen - E. Koltay - B. Madsen*

Institute for Theoretical Physics,
University of Copenhagen. Denmark.

The correlation between the total cross-section for $Mg^{25}/d,\alpha/$ reactions to definite states in Na^{23} and the spin I of this states has been investigated experimentally. Bombarding energies from 3,35 to 3,70 MeV and from 7,1 to 7,7 MeV were employed. In the latter region the total cross-sections, when averaged over bombarding energy, were observed to be approximately proportional to /2I + 1/. This empirical relation is used to deduce the spin values for 7 excited states in Na^{23}. The interpretation based on the rotational model at the Na^{23} level scheme is briefly discussed. From the quantitative evaluation of the observed fluctuations of Ericson's type the averaged width of the excited compound nucleus were obtained.

I. Introduction

The experimental conditions chosen in the present investigations made it possible to get informations both for the life-time of the compound nucleus using the *Ericson* fluctuations and for the spin values of the different states in the residual nucleus by means of the (2I + 1)-rule.

Ericson has predicted, that in the case of sufficiently high resolution fluctuation should occur on the excitation functions by means of which the averaged width of the excited compound nucleus can be estimated. Namely the

$$F(\varepsilon) = \{[\sigma(E+\varepsilon) - \sigma_{AV}][\sigma(E) - \sigma_{AV}]\}_{AV} \qquad /1/$$

correlation function have to show an ε dependence of the from $\Gamma^2/(\Gamma^2+\varepsilon^2)$. The index *AV* denotes the averaging over bombarding energy [1, 2].

* Permanent adress: Institute of Nuclear Research of the Hungarian Academy of Sciences. Debrecen.

It has been shown theoretically by *Ericson* [1] and by *MacDonald* [3] and experimentally by *Hinds* and *Middleton* [4] and more recently by *Colli* et al. [5], that under certain bombarding conditions, the total cross-section $\sigma/I/$ for populating a definite final state with spin I in a nuclear reaction when averaged over bombarding energy may fullfied the (2I + 1)-rule, i.e.

$$\sigma_{AV}/I/ \propto /2I + 1/ \qquad /2/$$

The conditions relevant to such a situation are, according to the above authors:

1. The reaction mechanism should be compound nucleus formation.

2. The bombarding energy should be such that the compound states are situated in a region of many overlapping levels and the spin J of these states should satisfy the condition $J > I$.

3. The energy of the outgoing particles should be large enough to ensure that barrier penetration effects are negligible.

4. The cross sections $\sigma/I/$ should be averaged over "sufficiently" many compound states in order to destroy any special correlation, that may exist between the compound states and the final states.

The present experiment demonstrates that the reaction $Mg^{25}(d,\alpha)Na^{23}$ fullfills the /2I + 1/-rule for $I \leq 5/2$ for bombarding energies E_d between 3,35 and 3,70 MeV and for I at least up to $9/2$ when $7,1 \leq E_d \leq 7,7$ *MeV*.

From the 7 MeV measurements spin values for the states 3, 6, 7, 8, 9, 10 and 11 in Na^{23} are suggested by applying the /2I + 1/-rule. The level structure of Na^{23} is briefly discussed in the light of these new spin values.

II. Experimental Procedure

The 3,5 MeV measurements were done at the 4 MeV electrostatic generator whereas the 7 MeV experiment was carried out at the Tandem Accelerator Laboratory. In both cases the α-spectrum was recorded by a 2000 ohm-cm n-type silicon detector in connection with a 512 channel analyser. In the 3,5 MeV region an energy spread in the beam of ±4 keV was employed; the energy resolution as observed from the spectra was ≈40 keV. The corresponding numbers for the tandem data were ±15 keV and ≈60 keV.

In the 3 - 4 MeV runs the first seven α-groups from Mg^{25} appeared separated in the spectra, groups at lower energies than the sevenths were obscured by O/d,α/ groups and by pile up effects from the elastic deuterons. In the 7 MeV experiment the first 12 α-groups were clear of impurities and pile up effects, but the groups 4 - 5 and 8 - 9 could be resolved at back angles only.

The experimental procedure for the Mg^{25}/d,α/ reaction at 3,5 MeV was to measure angular distributions at 11 angles between 20° and 160° at bombarding energies with an interval of 50 keV. In the 7 - 8 MeV measurements the angular interval was 25° to 160° and the energy interval was 100 keV. The low energy data were averaged over 8 distributions the high energy data over 7 distributions. The statistical accuracy of the individual measurements was from 5 % to 15 %.

The Mg^{25} target was made by vacuum evaporation of Mg in metal form enriched to 95 % in Mg^{25} on to a 50 $\mu g/cm^2$ carbon film.

III. Results and discussion

The qualitative features of our data are in agreement with Ericson's predictions:

a./ The excitation functions for the different α-groups show well defined fluctuations.

b./ There are no correlations among the fluctuations on the different excitation curves corresponding to different final states (Fig. 1.).

c./ The angular distributions are not symmetrical with respect to 90° and change rapidly with the bombarding energy (Fig. 2.).

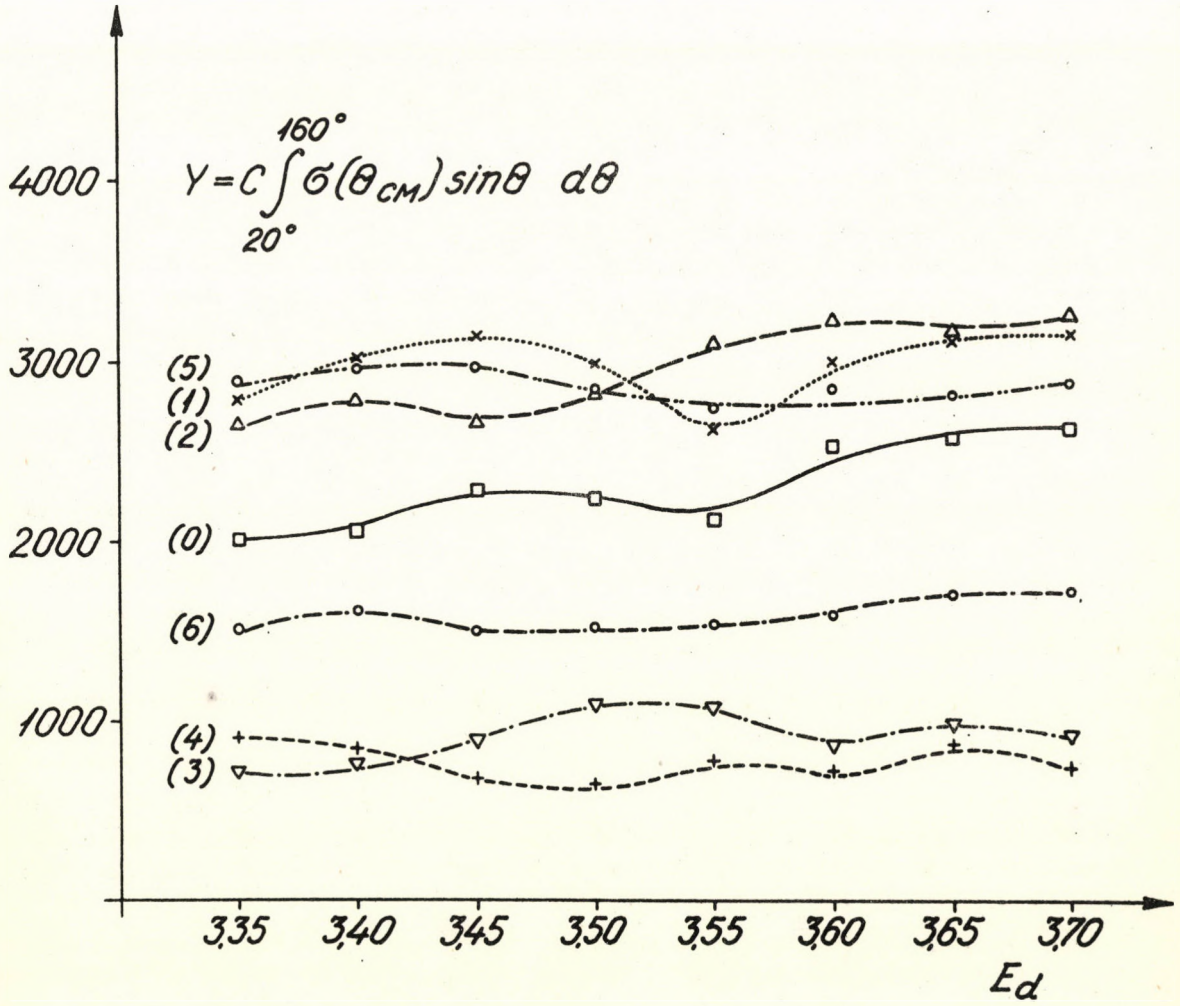

Fig. 1. The low energy excitation functions for the different α-groups emitted in the $Mg^{25}/d,\alpha/Na^{23}$ nuclear reaction. The group numbering refers to the level scheme as given in ref. [7].

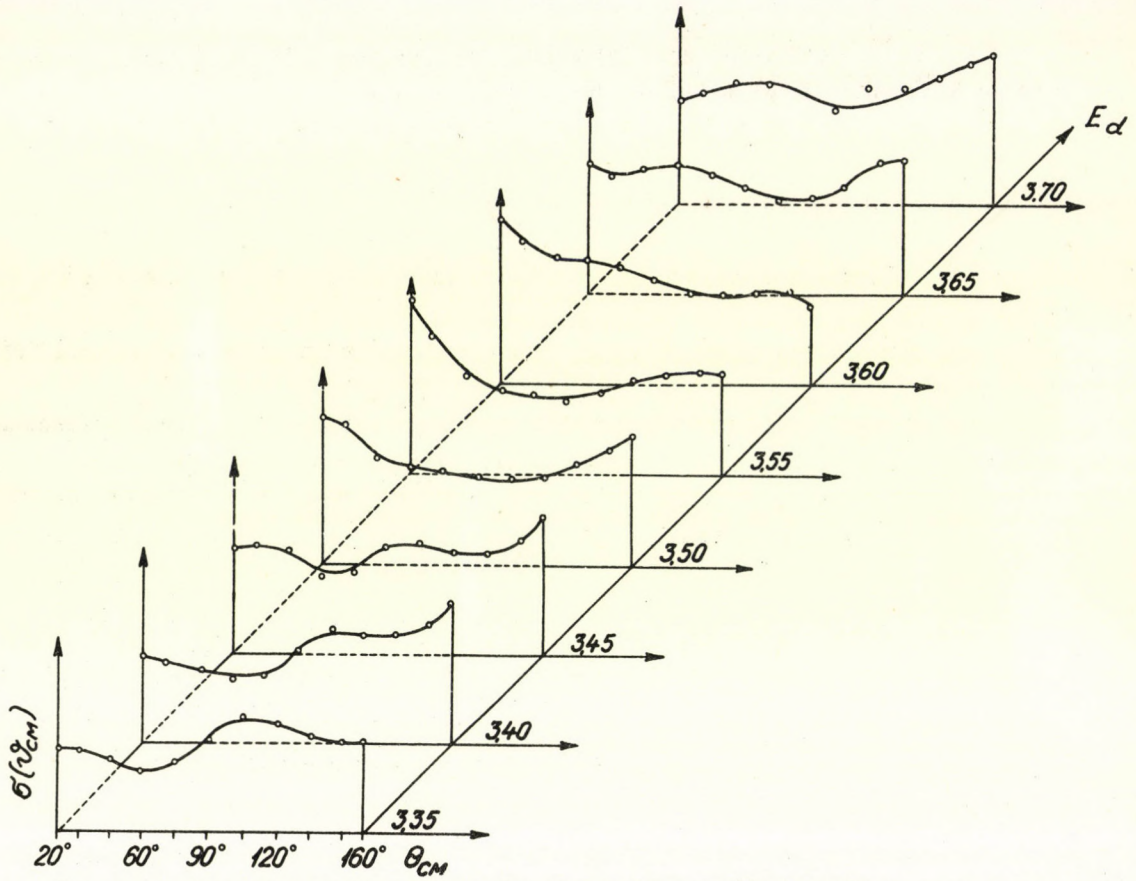

Fig. 2. Angular distribution curves for the reaction $Mg^{25}/d, \alpha/Na^{23}$ (ground state) as a function of the bombarding energy in C.M. system.

d./ When averaging over bombarding energy and/or final states the symmetry with respect to 90° comes back (Fig. 3.).

A more quantitative analysis for the low energy data was performed on the basis of the correlation function.

a./ Using the definition given by the formula /1/ and the theoretically predicted form of $F/\varepsilon/$ the Γ values corresponding to the best fitting of the both mentioned curves can be got for all the different α-groups. Two typical examples are given in the Fig. 4. and Fig. 5. The Γ values obtained are gathered in the Table 1. together with the averaged life time of the compound nucleus calculated from them.

b./ *Ericson* predicts, that the Γ dependence of the correlation function in the case of the differential cross-section has the same form as in the former case. For the sake of control we determined the Γ value for the third group over the 3,0 - - 4,2 MeV bombarding energy interval for $\theta_{lab} = 145°$ and got Γ = 74,5 keV. One possible reason for the deviation of this value from that got according to a./ is the invalidity of the assumption on the energy independence of σ_{AV} using such a large energy interval.

c./ It is customary to compare the quantities

$$\sqrt{(\sigma - \sigma_{AV})^2/2\sigma_{AV}^2} \quad ; \quad \text{and} \quad 1/\sqrt{n} \, ,$$

here n is the number of the final states ordinarily taken as 2I + 1 (see e.g. [6]

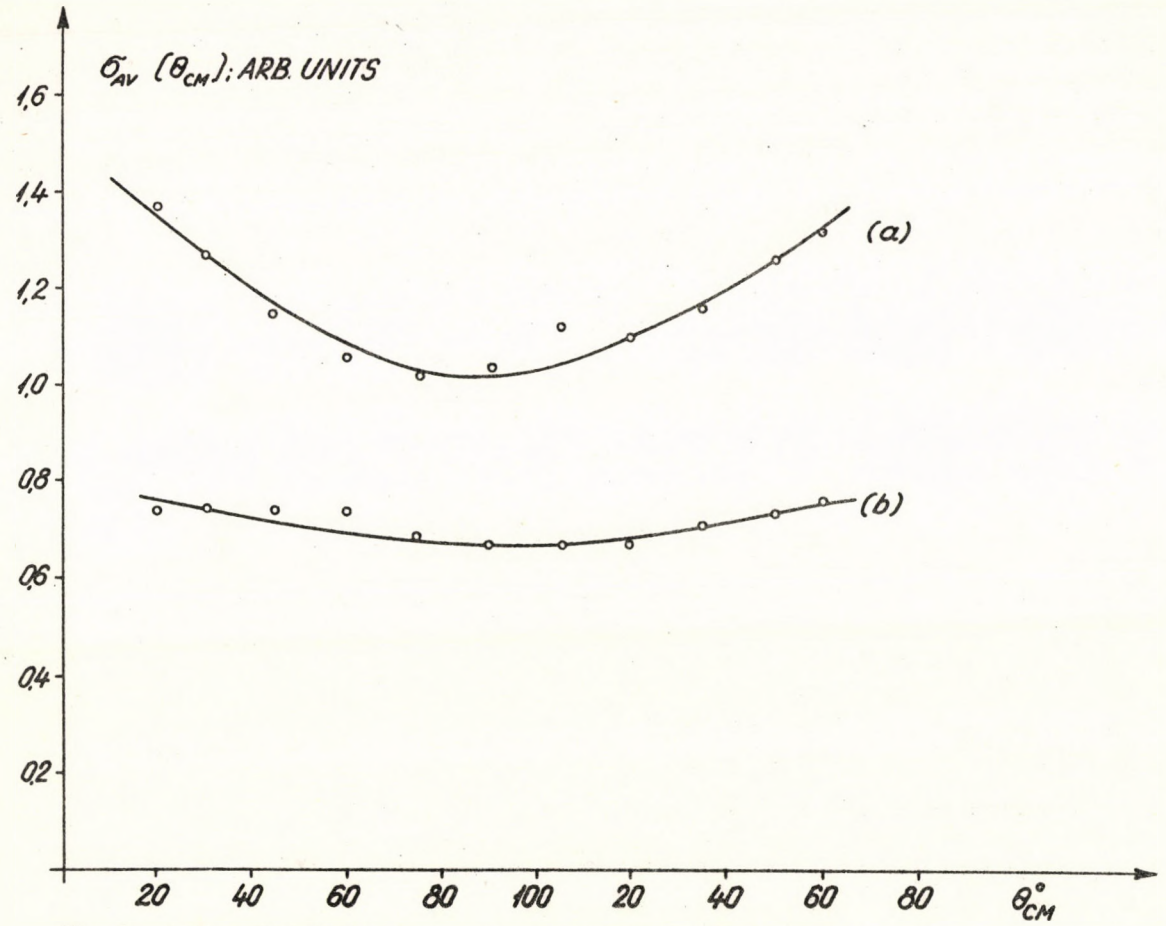

Fig. 3. Angular distribution curves for the reaction $Mg^{25}/d, \alpha/Na^{23}$
a./ averaged over bombarding energy interval $3,35 \leq E_d \leq 3,70$ MeV (ground state)
b./ averaged over bombarding energy interval $3,35 \leq E_d \leq 3,70$ MeV and final states from 0 to 6.

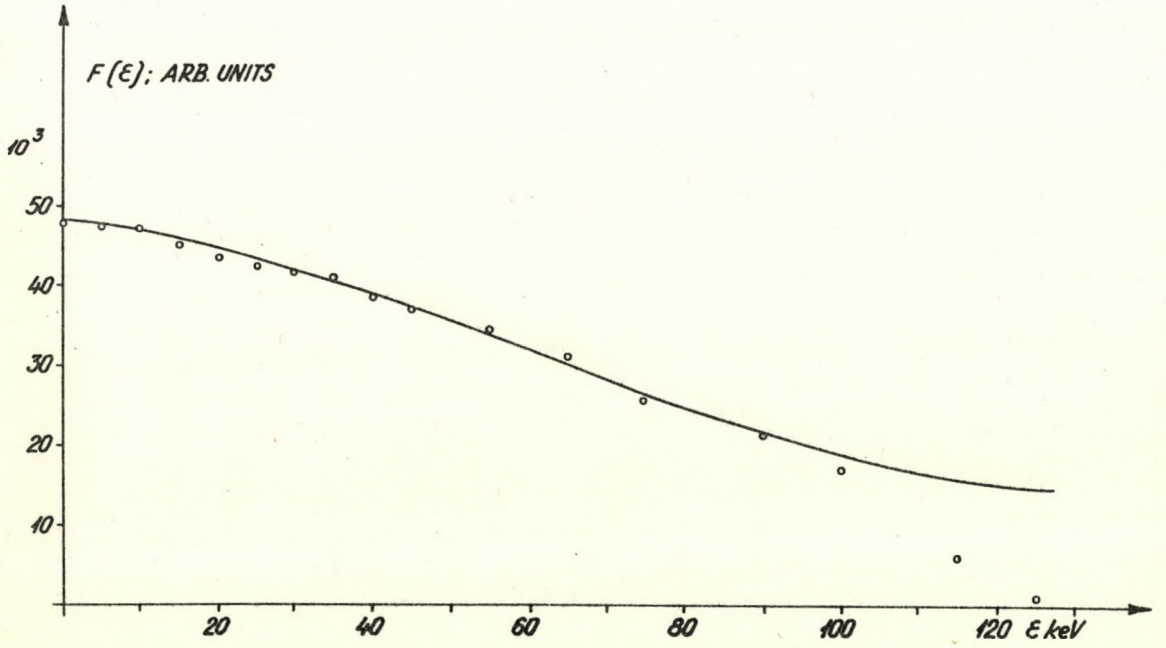

Fig. 4. Correlation function for the 2. α-group. (full line: $\Gamma^2/(\Gamma^2 + \varepsilon^2)$; $\Gamma = 82,4$ keV; normalised at $\varepsilon = 0$; points represent the experimental values).

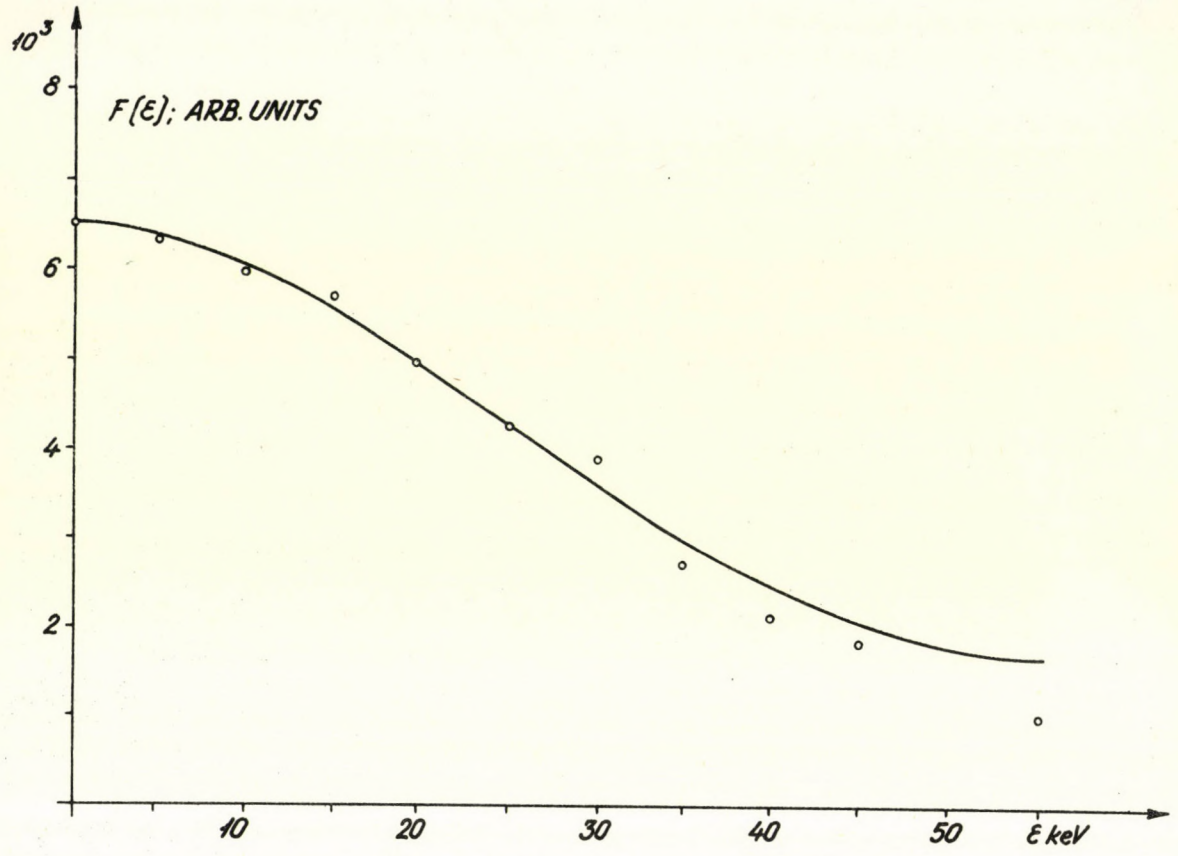

Fig. 5. Correlation function for the 4. α-group. Γ = 82,5 keV.

Table 2.). In the more recent paper [2] *Ericson* shows, that n should be the effective number of the entrance and exit channels where the angular momenta are to be taken into account. Because of the high spin values in our case the effective number of channels differs strongly from 2I + 1, as it can be seen on the Table 1.

Table 1.

Level No	Spin I	$\sqrt{\frac{(\sigma - \sigma_{AV})^2}{2\sigma_{AV}^2}}$	$\frac{1}{\sqrt{2I+1}}$	Γ_{exp}, keV in compound nucleus Al^{27}	τ sec (average)
0	3/2	0,055	0,5	83,1	
1	5/2	0,035	0,41	33,5	
2	7/2	0,052	0,35	82,5	$1,35.10^{-20}$
3	1/2	0,091	0,70	46,5	
4	1/2	0,074	0,70	32,5	
5	9/2	0,022	0,31	55,0	

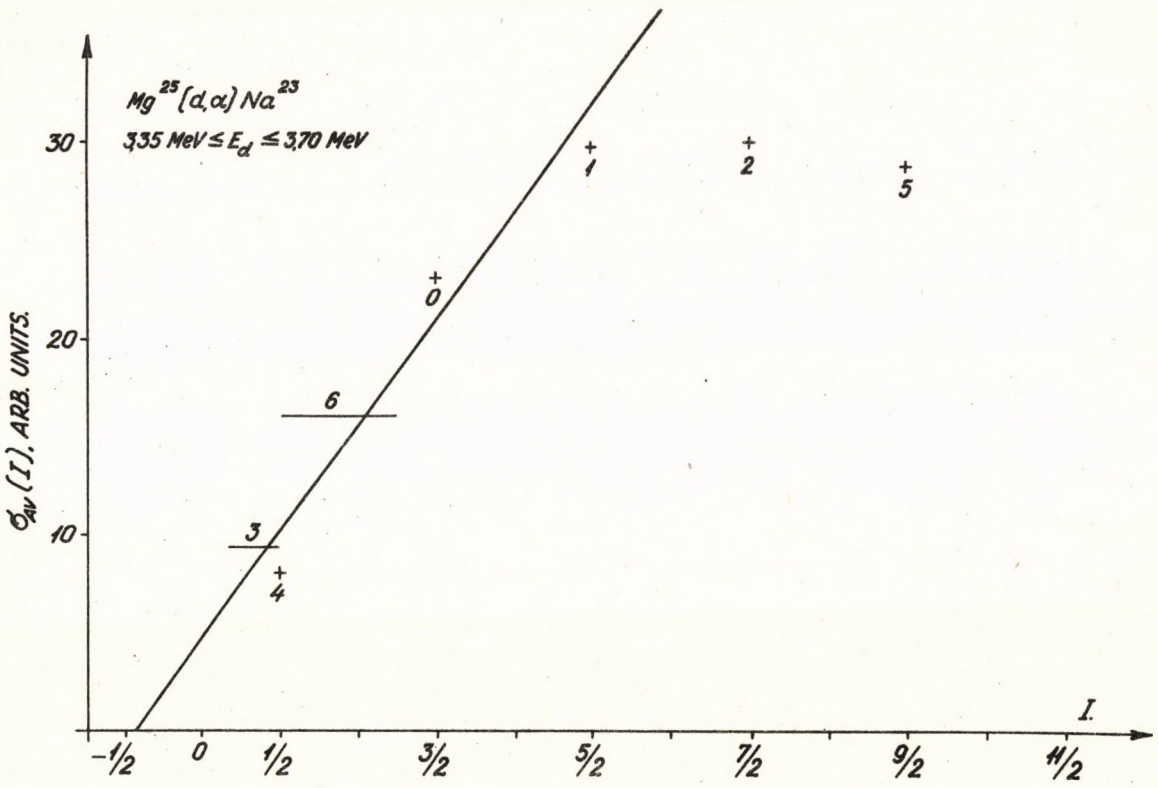

Fig. 6. $Mg^{25}/d,\alpha/Na^{23}$ yields integrated over scattering angles from θ = 20° to θ = 160° and averaged over 7 bombarding energies from E_d = 3,35 MeV to E_d = 3,70 MeV. The abscissa is the final state spin I. When I is known, (ref. [7]). $\sigma_{AV}/I/$ is marked with a cross. The straight line is drawn through the crosses only. σ_{AV} for final states of unknown I are marked by horizontal lines. The numbers appearing near the crosses or horizontal lines are the level numbers according to Fig. 8.

The measured $\sigma_{AV}/I/$ are shown in figs. 6. - 7. A cross marks the $\sigma_{AV}/I/$ for a final state whose I is given in [7], when I is not known a horizontal line indicates σ_{AV}. The curves shown are drawn through the points of known I.

Fig. 6. gives the 3 - 4 MeV $Mg^{25}/d,\alpha/$ data. An approximately linear correlation between σ_{AV} and I is observed for $I \leq 5/2$, for $I > 5/2$ σ_{AV} seems to become independent of I. A spin of 1/2 for group 3 is suggested.

The main trend of Fig. 6. especially the I independence for high values of I seems to be due mostly to two facts, a breakdown of the $J > I$ condition (i.e. E_d is too low) and barrier penetration effects on the α particles (i.e. E_α is too low).

The 7 - 8 MeV results on $Mg^{25}/d,\alpha/$ illustrated in Fig. 7. seem to follow the /2I + 1/-rule for all states observed, i.e. for I at least up to 9/2. The better validity of the /2I + 1/-rule at higher energies is qualitatively in accordance with the statistical model estimates, i.e. conditions 2./ and 3./ of section I. are fullfilled to a higher degree. That the condition 1./ (compound reaction mechanism) is relevant follows from Fig. 3.

We thus suggest that the I-values, that may read off from Fig. 7. (shown in the insert of this figure) for the states 3, 6, 7, 8, 9, 10 and 11 are identical to the spin of these states. It may be remarked that both high and low energy data yield $I = 1/2$ for level 3 (and $I = 3/2$ for state 6).

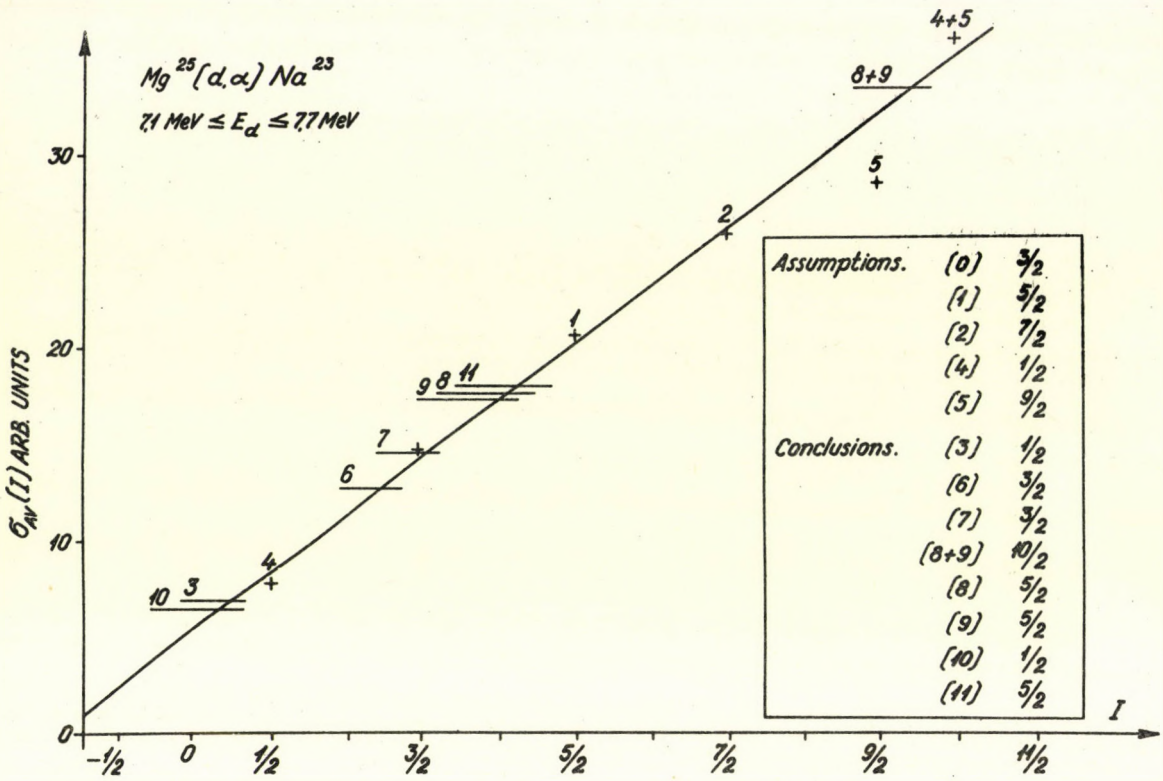

Fig. 7. $Mg^{25}/d,\alpha/Na^{23}$ yields integrated over scattering angles from $\theta = 25^\circ$ to $\theta = 160^\circ$ and averaged over bombarding energies from $E_d = 7{,}1$ MeV to $E_d = 7{,}7$ MeV. The α-groups corresponding to the levels 4 and 5 were resolved from each other for $\theta > 90^\circ$ only. Their yields were converted to total yields by multipying the $\sigma_{AV}[\theta > 90^\circ]$ by $[1 + \sigma_{AV}(\sigma < 90^\circ)/\sigma_{AV}(\theta > 90^\circ)]$ where the ratio is taken from the (4 + 5) data. A similar remark is valid for the groups 8 and 9. See otherwise caption Fig. 6.

IV. The Na^{23} level scheme

The level scheme of Na^{23} as given in ref. [7] is shown in fig. 8. The spin values of ref. [7] are stated to the left of the level diagram, those suggested by the present experiment are given to the right of the diagram. Our *I = 1/2* assignment for level 3 is in accordance with the measurements of *Clegg* et al. [8] and no assignment is in contradiction with other data (see e.g. refs. [7, 9] and [10].

In the right half of the figure we have indicated those states which must be considered as intrinsic states i.e. state 0, 3, 4 and 10. The ground state rotational band (see ref. [7]) is also shown. The remaining states cannot, we think, be interpreted uniquely as rotational sequencies or instrinsic states on the basis of present experimental data. The identification of the three spin 1/2 states, to some extent, changes the basis of most theoretical calculations (see e.g. ref. [9]). It may be remarks however, that at least three levels of *I = 1/2* are to be expected in the lower lying excitations of Na^{23} from the theoretical level diagrams of *Mottelson* and *Nilsson* [11]. An important clue to the understanding of the structure of Na^{23} would be the determination of the parities of the *I = 1/2* states, because it is not possible to identify these states in the *Nilsson-Mottelson* scheme without this knowledge and first after such an identification may the interband couplings be calculated on a safe basis.

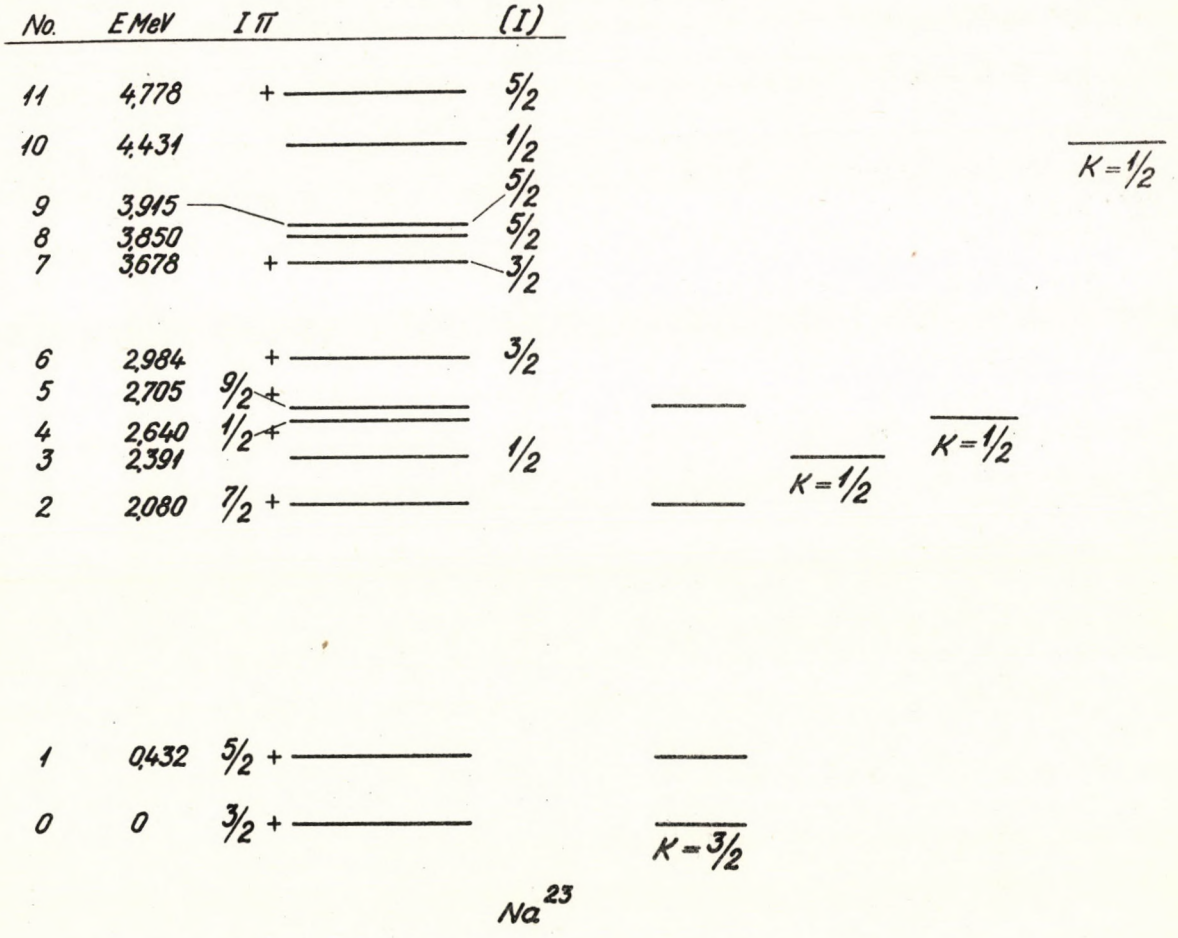

Fig. 8. Level scheme of Na^{23}. The level diagram and the spin values to the left are taken from ref. [7]. The spin values to the right are suggested by the present experiment. Also shown are the ground state rotational band and the three I = 1/2 levels which must be intrinsic states. Some of the remaining levels may of course also be intrinsic states.

Part of the evaluation work was carried out by *B. Gyarmati**.

We are indebted to *Dr. B. Elbek* for putting the tandem accelerator with the necessary electronic equipment at our disposal. One of us (E.K.) wishes to thank *Professors A. Bohr* and *T. Huus* for the kind hospitality extended to him at the Institute for Theoretical Physics in Copenhagen and the International Atomic Energy Agency for supporting his stay in Denmark.

* Institute of Nuclear Research of the Hungarian Academy of Sciences. Debrecen.

References

[1] *T. Ericson:* Advances in Physics, *9*/1960/415.

[2] *T. Ericson:* CERN 5419/TH 319, 10 December, 1962. (to be published in Annals of Physics).

[3] *N. MacDonald:* Nuclear Physics, *33*/1962/110.

[4] *S. Hinds - R. Middleton:* in Proc. Rutherford Int. Jubilee Conf., Manchester (Heywood Co., London, 1961) 305.

[5] *L. Colli - I. Iori - M.G. Marcazzan - M. Milazzo:* Nuclear Physics, *43*/1963/529.

[6] *L. Colli - U. Facchini - I. Iori - M.G. Marcazzan - M. Milazzo - E. Saetta Menichella - F. Tonolini:* Energia Nucleare, *9*/1962/439.

[7] *P.M. Endt - C. van der Leun:* Nuclear Physics, *34*/1962/1.

[8] *A.B. Clegg - K.J. Foley:* Phil. Mag., 7/1962/247.

[9] *D.W. Braben - L.L. Green - J.C. Willmott:* Nuclear Physics, *32*/1962/584.

[10] *J.H. Towle - W.B. Gilboy:* Nuclear Physics, *32*/1962/610.

[11] *B.R. Mottelson - S.G. Nilsson:* Mat. Fys. Skr. Dan. Vid. Selsk. *1*/1959/ no. 8.

ИССЛЕДОВАНИЕ УГЛОВЫХ РАСПРЕДЕЛЕНИЙ РЕАКЦИИ $He^3 + T$

Б. Кюн - В. Кленк

Измерены угловые распределения заряженных частиц для всех каналов реакции He^3+T при энергиях падающих тритонов: 460 Кэв; 665 Кэв; 900 Кэв и 1087 Кэв. Форма полученных распределений не изотропная и меняется с энергией. На основании угловых распределений и определения соотношений между каналами реакции получены полные сечения реакции и сечения для каждого отдельного канала.

1. Введение

Исследованию реакции

$$He^3 + T \longrightarrow He^4 + d + 14{,}31 \text{ Мэв} \qquad /1/$$
$$\longrightarrow He^4 + p + n + 12{,}08 \text{ Мэв} \qquad /2/$$
$$\longrightarrow He^5 + p + 11{,}18 \text{ Мэв} \qquad /3/$$
$$\longrightarrow He^4 + n + 0{,}9 \text{ Мэв}$$

посвящены три экспериментальные работы [1-3]. В работах *C.D. Moak* [2] и *Ли Га Ена* и др. [3] были найдены соотношения между ветвями реакции и определены полные сечения всех трех ветвей. Данные по полным сечениям получены на основании измерения дифференциальных сечений под углом 90° и последующего пересчета в предположении изотронности распределения выходов каждого из каналов реакции.

Поскольку предположения о сферической симметрии каждого канала реакции в интервале рассматриваемых энергий не имели экспериментального подтверждения, нами были проведены эти исследования.

2. Методика измерений

Измерения проводились с ионами трития, ускоренными электростатическим генератором ОИЯИ. Напряжение генератора стабилизировалось с точностью 0,1 - 0,2 % и калибровалось по резонансным пикам реакции $F(p,\gamma)$. Ионы трития, ускоренные электростатическим генератором, пройдя через магнитный анализатор и коллиматор ($\varnothing$ = 1,5 мм), попадали на входное окошко точечной газовой мишени, помещенной в центре вакуумной камеры [4].

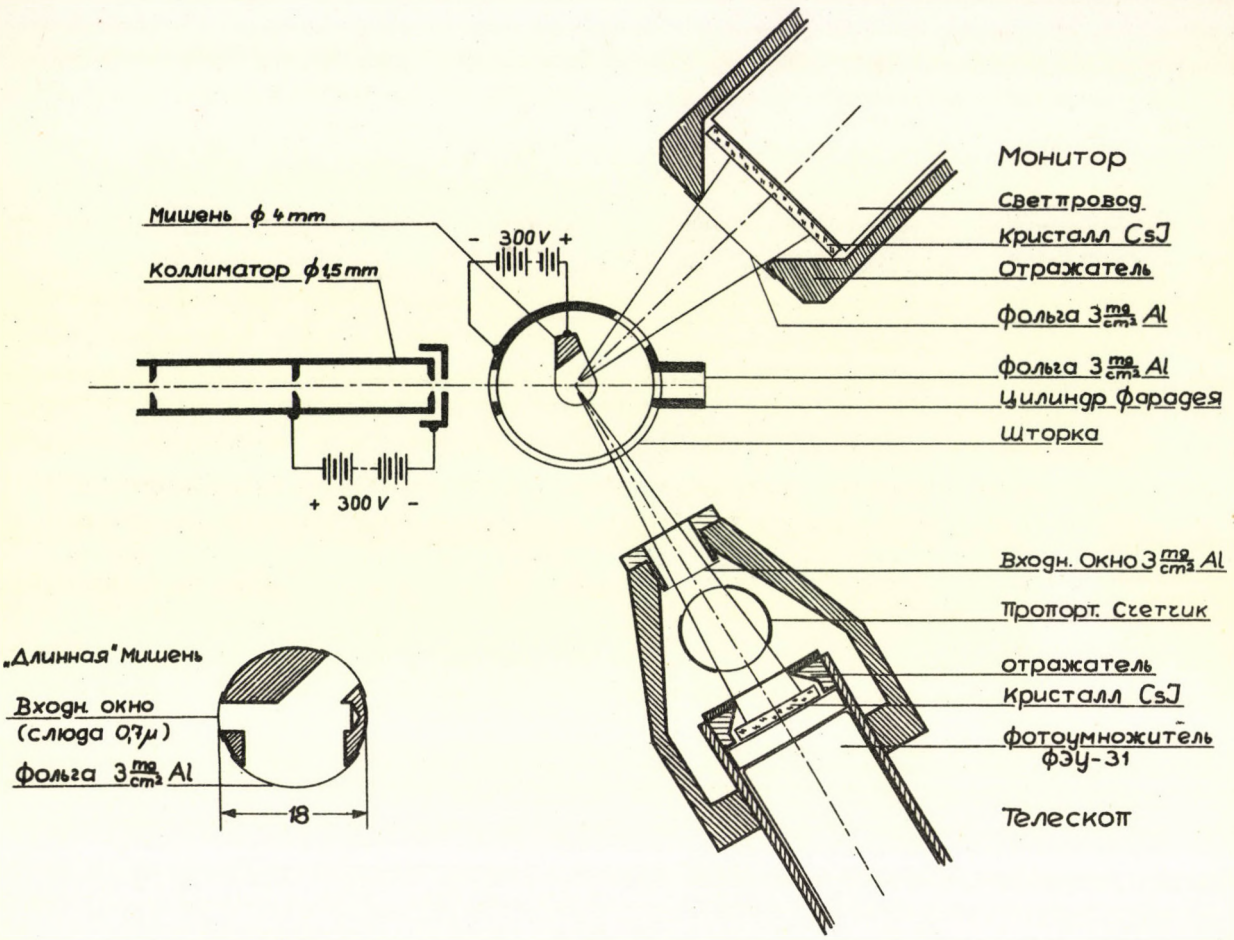

Рис. 1. Схема опыта.

Схема опыта представлена на рис. 1. Окошко газовой мишени закрывалось тонкой слюдяной пленкой (при E_T = 1 Мэв, $\Delta E \approx 35$ Кэв). Давление He^3 в мишени составляло 40 мм рт.ст. Ток падающих частиц измерялся цилиндром Фарадея, соединенным с интегратором тока. Расположение цилиндра Фарадея показано на рис. 1. Для проведения измерений под 0° дно цилиндра Фарадея заклеивалось тонкой фольгой из алюминия (3 мг/см^2), достаточной для поглощения пучка ускоренных ионов, но пропускающей продукты реакций.

Частицы, образующиеся в результате ядерной реакции, рефистрировались телескопом, состоящим из пропорционального счетчика и малогабаритного фотоумножителя ФЭУ-31 с кристаллом CsJ. Телесный угол телескопа составлял $1,34.10^{-2}$ стер., а угловое разрешение $7,5^\circ$. Пропорциональный счетчик и фотоумножитель были включены в схему совпадений что обеспечивало уменьшение фона от нейтронов и γ-квантов. Разрешение фотоумножителя для протонов с энергией 10 Мэв составляло 10 %. Импульсы от фотоумножителя после усиления подавались на многоканальный анализатор, работающий в режиме совпадения. Управляющими импульсами для многоканального анализатора являлись импульсы от пропорционального счетчика. Монитором служил фотоумножитель ФЭУ-С с кристаллом CsJ, расположенный под углом 45° к падающему пучку ионов трития.

Поскольку дейтроны из ветви /1/ и протоны из ветви /3/ имеют близкие энергии, они телескопом не разрешаются. Необходимое разрешение пиков протонов и дейтронов реакции /1/ и /3/ может быть получено путом использования различия тормозной способ-

ности для дейтронов и протонов в некотором веществе. В качестве такого вещества использовался алюминий. При проведении измерений под различными углами задача усложняется тем, что энергия дейтронов и протонов из реакций /1/ и /3/ меняется с углом. (При E_T = 900 Кэв, $E_d(0^\circ)$ = 12,4 Мэв, $E_d(153^\circ)$ = 7,8 Мэв, $E_p(0^\circ)$ = 11,5 Мэв и $E_p(153^\circ)$ = = 8,2 Мэв). Это требует использования при различных углах алюминиевых фольг различных толщин. Расчет показал, что при измерениях под углами от 0° до 60° хорошее разрешение можно получить с фольгой 90 мг/см^2, а при углах от 60° до 153° с фольгой 60 мг/см^2.

Поскольку эти толстые фольги срезают большую часть непрерывного спектра, соответствующего ветви /2/, необходимо дополнительное измерение без разделяющих фольг. Но та часть непрерывного спектра, на которую накладываются импульсы от α-частиц из какалов /1/, /2/ и /3/, остается ненаблюдаемой. В связи с этим измерение угловых распределений протонов из канала /2/ производилось с фольгой 7,4 мг/см^2, которая поглощала все указанные α-частицы. Эта фольга совместно с окошком и газом счетчика срезает непрерывный спектр от 0 до 2,6 Мэв. Полный спектр может быть получен разумной экстраполяцией экспериментально измеренной части спектра к нулю.

Таким образом, задача разделения каналов реакции включает:

а./ измерение угловых распределений в интервале углов 0° - 153° без разделяющей фольги;

б./ измерение угловых распределений в интервале углов 0° - 60° с фольгой 90 мг/см^2;

в./ измерение угловых распределений в интервале углов 60° - 153° с фольгой 60 мг/см^2.

При измерении угловых распределений на точечной газовой мишени форма непрерывного спектра искажается протонами из реакций $O^{18}(t,p)O^{18}$ и $C^{12}(t,p)C^{14}$, происходящих на окошке мишени. Для получения спектра в более чистом виде необходимо, чтобы продукты реакций, происходящих на окошке мишени, не попадали в телескоп. Этому требованию удовлетворяет "длинная" мишень, представленная на рис. 1. С помощью "длинной" мишени была изучена форма непрерывного спектра под углами 30° - 145° в интервале энергий 460 - 1087 Кэв. В пределах ошибок измерений форма спектра оказывалась всегда прямоугольной. Этот результат подтвердился при измерениях спектров с фольгами толщиной 90 и 60 мг/см^2, где часто было возможно наблюдать непрерывный спектр вблизи пика протонов реакции /3/.

3. Результаты измерений

На рис. 2. представлены (в системе центра масс) угловые распределения дейтронов канала /1/ реакции He^3 + T. Среднеквадратичная ошибка каждой точки распределений не превышает ±5 %. На оси ординат этого и последующих графиков нанесены дифференциальные сечения. Абсолютные величины этих сечений получены нормировкой относительного хода кривых по данным дифференциальных сечений под углом 90°, представленных в работе [3].

Из рисунка видно, что угловое распределение при 460 Кэв симметрично относительно 90° и имеет максимум при 90°. С увеличением энергии положение максимума не меняется, в то время как дифференциальное сечение в максимуме растет. При энергии 665 Кэв и выше наблюдается асимметрия в угловых распределениях, значение которой превышает ошибки измерений.

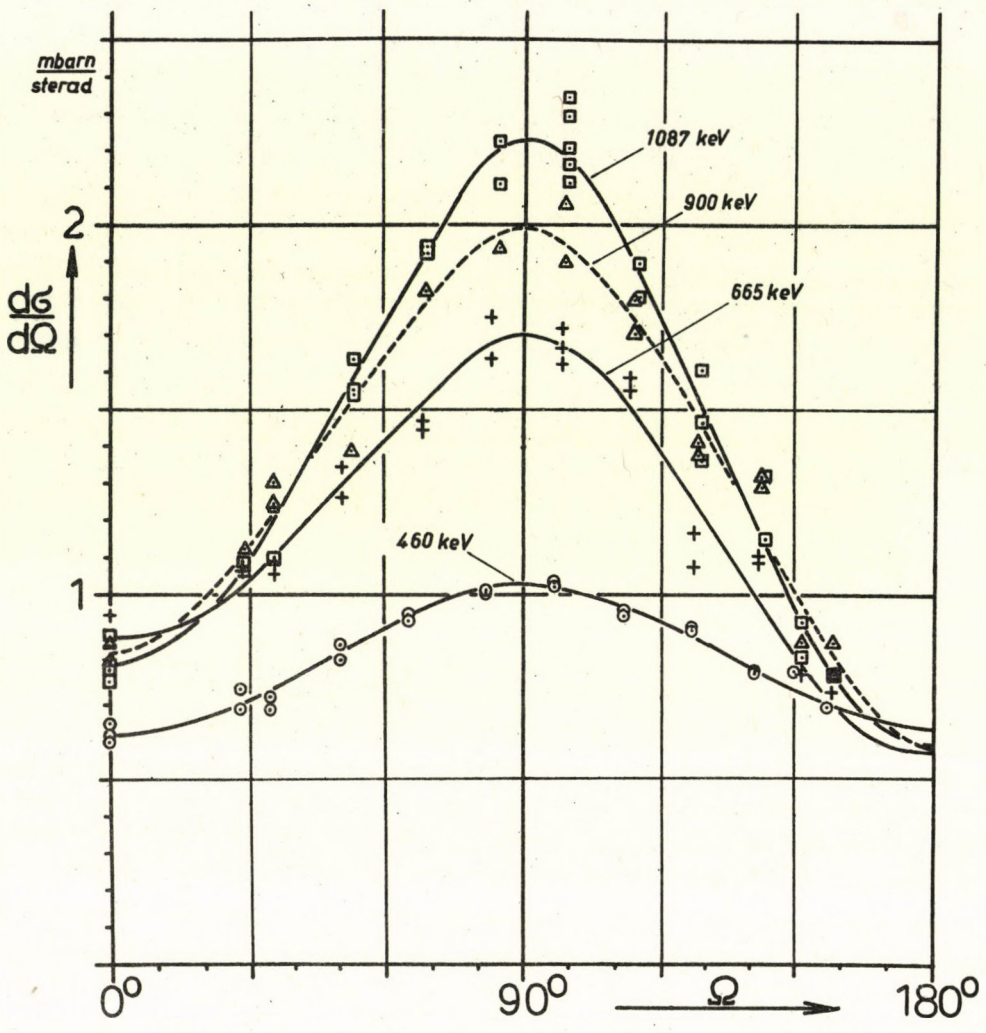

Рис. 2. Угловые распределения дейтронов канала /1/ реакции He^3 + T в системе центра масс.

На рис. 3. представлены угловые распределения протонов из канала /3/ реакции (в системе центра масс). Среднеквадратичная ошибка этих измерений составляет 20 - - 30 %. При энергии 665 Кэв в районе 40° появляется широкий максимум. С ростом энергий положение этого максимума смещается в сторону больших углов.

Угловые распределения непрерывной части спектра приведены на рис. 4. Эти распределения представлены в лабораторной системе координат. Среднеквадратичная ошибка каждой экспериментальной точки не превышает 12 %. Как видно из рисунка, полученные распределения асимметричны относительно угла 90°. Выход частиц в малые углы более вероятен. При возрастании энергии эта асимметрия увеличивается.

Полученные результаты показывают, что начиная уже с энергии 460 Кэв угловые распределения продуктов реакции каждого канала не изтропны.

На основании измерений спектров под углом 90° при энергиях 460, 665, 900 и 1087 Кэв определялись соотношения между выходами продуктов реакции каждого канала. Результаты измерений и их среднеквадратичные ошибки представлены в табл. 1. Как видно из таблицы, в пределах ошибок измерений эти соотношения не меняются.

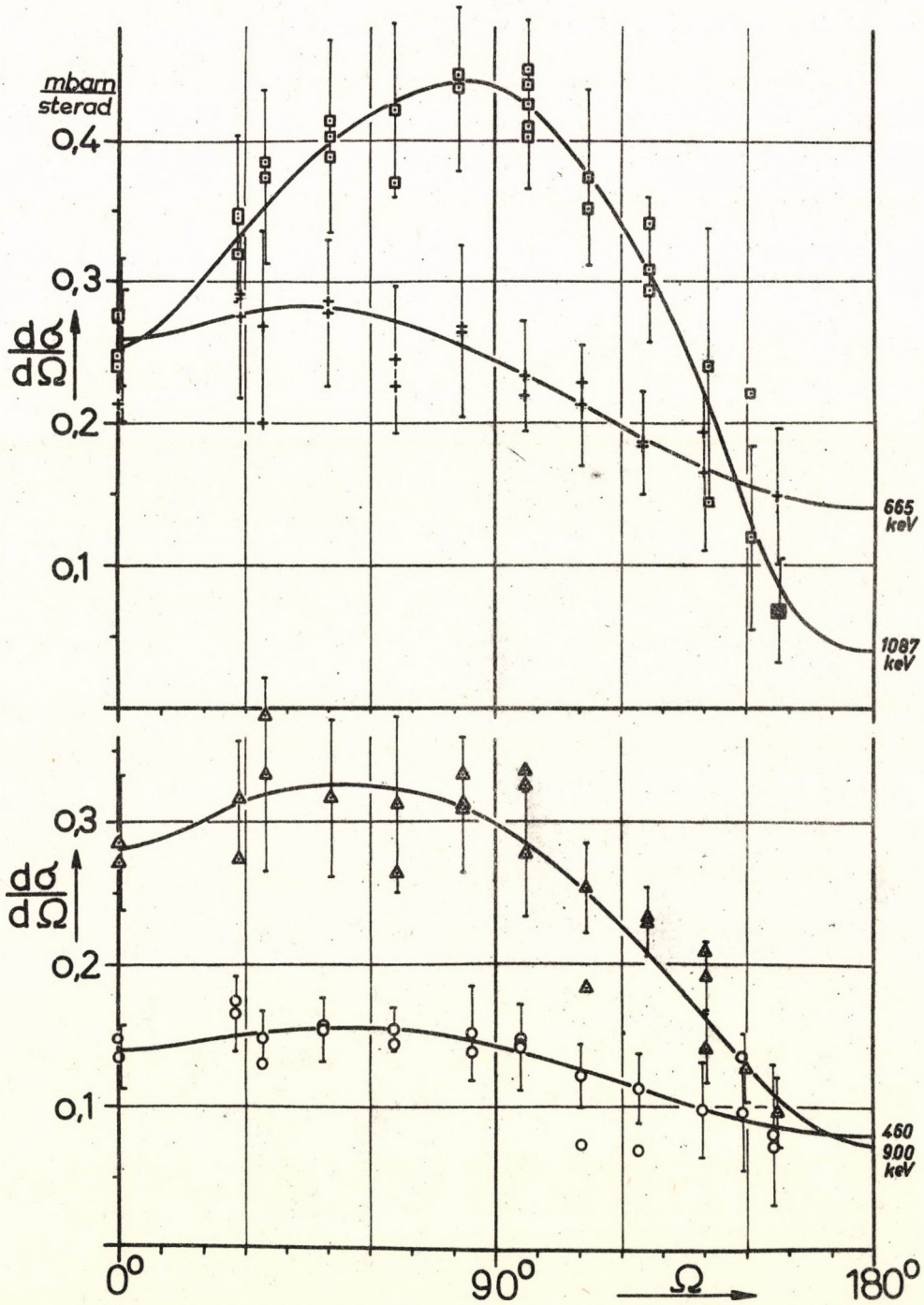

Рис. 3. Угловые распределения протонов канала /3/ реакции He^6 + T в системе центра масс.

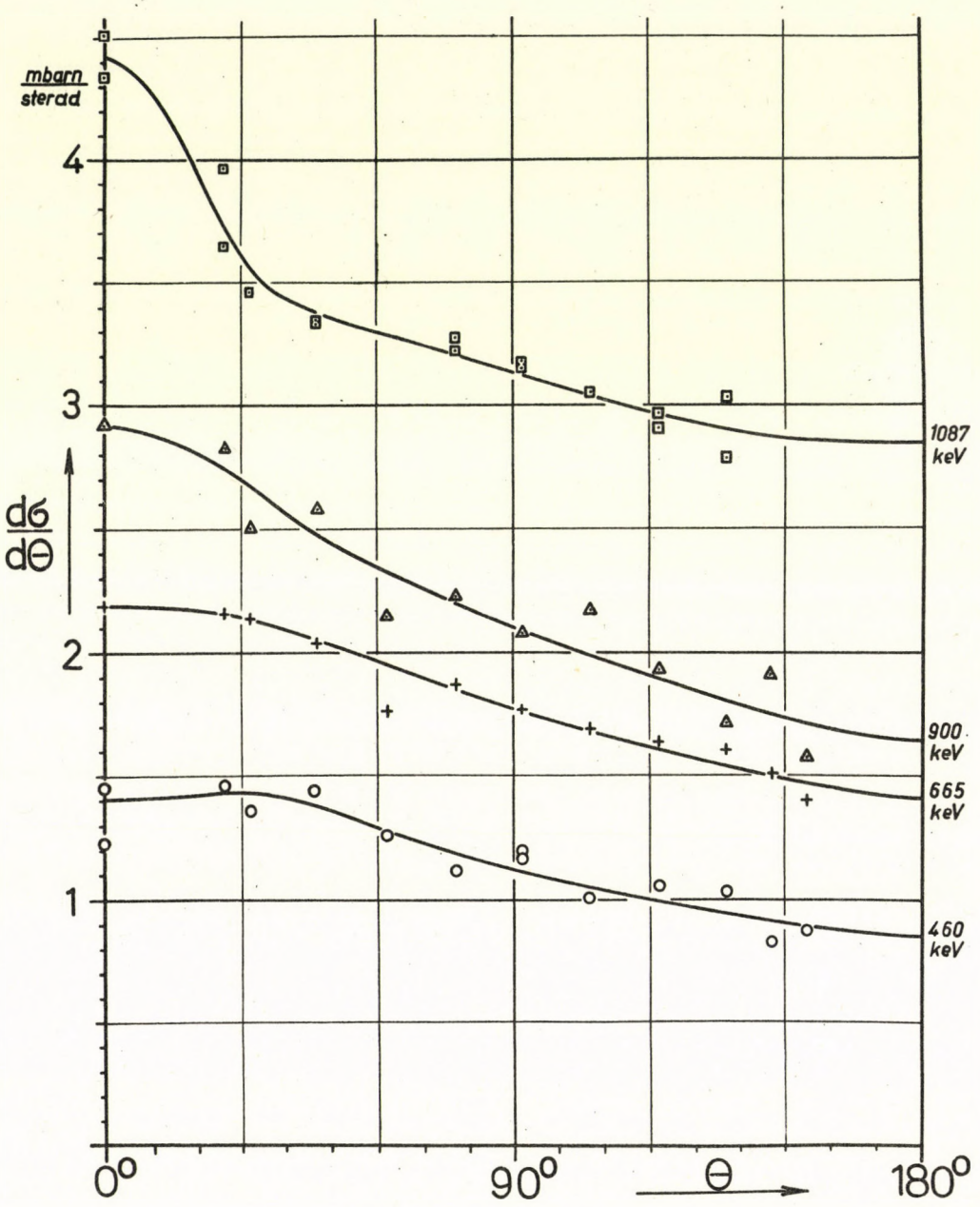

Рис. 4. Угловые распределения непрерывного спектра протонов канала /2/ реакции He^3 + T в лабораторной системе. (Шкала ординат кривой для 1087 Кэв смещена на 1 мб/стерад вверх.)

Таблица 1.

Соотношения между выходами разных каналов реакции He^3 + T

Энергия / Канал	460 Кэв	665 Кэв	900 Кэв	1087 Кэв
канал /1/	(43,5 ± 2) %	(45,5 ± 2) %	(45,5 ± 2) %	(46 ± 2) %
канал /2/	(50 ± 6) %	(48,5 ± 6) %	(46,5 ± 6) %	(45 ± 6) %
канал /3/	(6 ± 1,5) %	(6 ± 1,5) %	(7 ± 1,5) %	(9 ± 1,5) %

В таблице 2 и на рис. 5. представлены сечения каждого канала реакции и полное сечение реакции He^3 + T в интервале энергии 460 - 1087 Кэв. Сечения получены на основании угловых распределений, представленных на рис. 2., 3., 4. В этой таблице представлены среднеквадратичные ошибки в определении сечения. На рис. 5. также представлены кривая полного сечения реакции He^3 + T (кривая 5), измеренная *Ли Га Еном* и др. [3]. Из сравнения результатов видно, что начиная с энергий примерно 650 Кэв данные этих авторов существенно расходятся с данными настоящей работы. Это объясняется тем, что вычисление полных сечений реакции He^3 + T в работе [3] было проведено в предположении сферической симметрии угловых распределений продуктов реакции, высказанном впервые *C. D. Moak* [2]. Наши измерения не подтвердили это предположение.

Таблица 2.

Полные сечения реакции He^3 + T

Энергия / Канал	460 Кэв		665 Кэв		900 Кэв		1087 Кэв	
	σ (мбн)	A	σ (мбн)	A	σ (мбн)	A	σ (мбн)	A
канал /1/	11,2 ± 0,6	0,41	16,9 ± 0,8	0,40	19,6 ± 1,0	0,39	21,0 ± 1,0	0,40
канал /2/	14,4 ± 1,7	0,53	22,5 ± 2,7	0,53	27,1 ± 3,2	0,54	27,5 ± 3,3	0,52
канал /3/	1,7 ± 0,3	0,06	2,9 ± 0,6	0,07	3,3 ± 0,7	0,07	4,4 ± 0,9	0,08
полные	27,3 ± 1,8		42,3 ± 2,8		50,0 ± 3,4		52,9 ± 3,6	

(Данные в столбце A представляют долю выхода соответствующего канала по отношению к полному сечению реакции.)

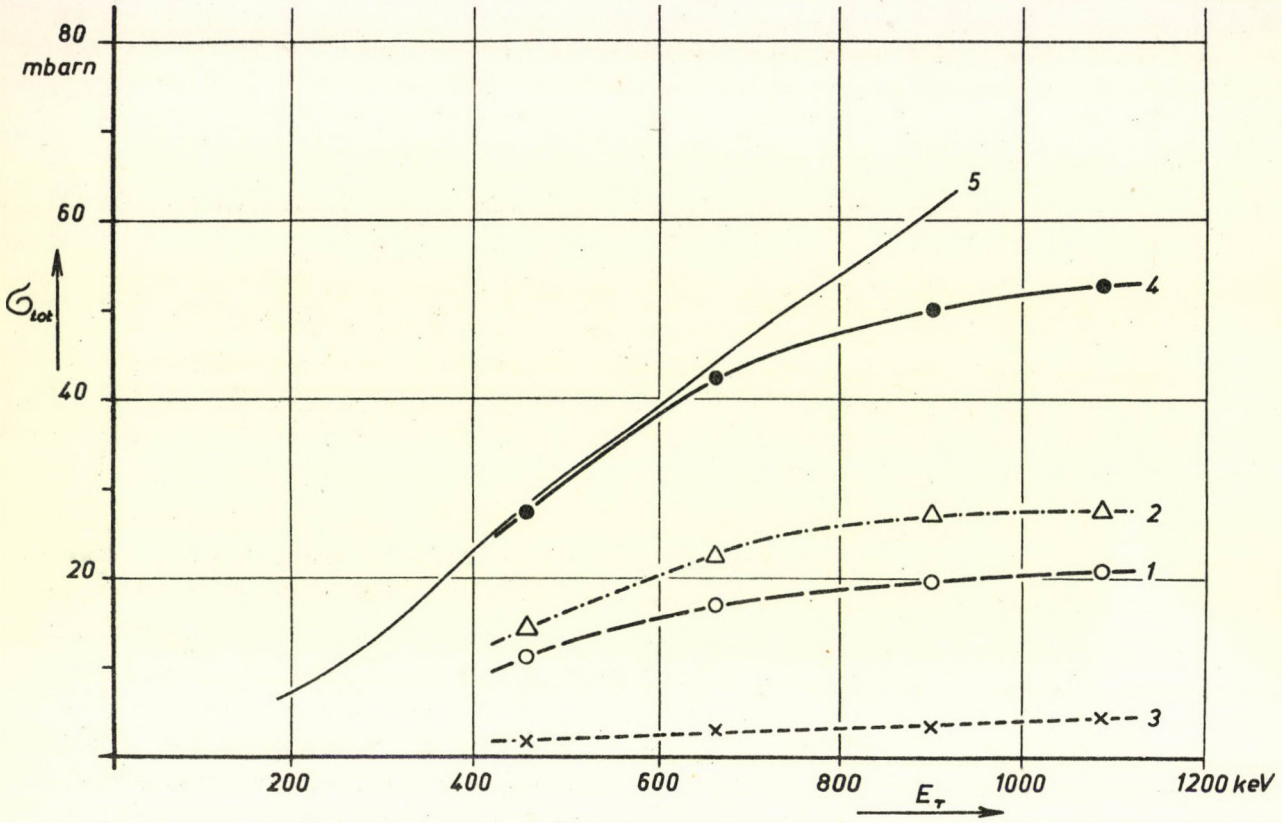

Рис. 5. Полные сечения реакции He^3 + T
Кривая 1 - канал /1/,
Кривая 2 - канал /2/,
Кривая 3 - канал /3/,
Кривая 4 - полное сечение реакции He^3 + T,
Кривая 5 - сечение реакции He^3 + T, взятое из работы *Ли Га Ена* и др. [3].

Авторы выражают глубокую благодарность *Г.М. Осетинскому* и *И.В. Сизову* за постоянный интерес и ценные обсуждения, *П.П. Костромину* за изготовления газовых мишеней, а также группе обслуживания электростатического генератора.

Литература

[1] *E. Almquist - K.W. Allen - J.T. Devan - T.P. Pepper:* Phys. Rev., *83*/1951/202.
[2] *C.D. Moak:* Phys. Rev., *92*/1953/383.
[3] *Ли Га Ен - Г.М. Осетинский - Н. Содном - А.М. Говоров - И.В. Сизов - В.И. Салацкий:* ЖЭТФ т. *39*, вып. 2. /8/ 1960 г. Препринт ОИЯИ, Р-426, 1956 г.
[4] *В;С. Сиксин - Л. Вайи - Б. Кюн:* Препринт ОИЯИ No. 621, 1960.

NUCLEAR RECOIL IN 14,8 MeV ENERGY NEUTRON REACTIONS

J. Csikai - Mrs. P. Bornemisza - I. Hunyadi
Institute of Nuclear Research of the Hungarian
Academy of Sciences, Debrecen, Hungary

1. Nuclear recoil and cross section measurement

The activation method is often applied for determining the fast neutron reaction cross sections. Generally thin foils are used for measuring (e.g. [1-4]). Nevertheless due to nuclear recoil during the activation a part of the active nuclei is breaking off from the foil, which must be taken into consideration if the cross section is determined from the measured activity. The ratio of the activities of the broken off nuclei (A_c) and that remaining in the foil (A_f) depends on the thickness of it. If the foil is thicker than the range (X_o) of the recoil nuclei having the maximum energy, then the activity of broken off nuclei is saturated, in which case there is a simple relation between the ratio A_c/A_f and the thickness X of the foil:

$$\frac{A_c}{A_f} = \frac{C}{X - C} \qquad /1/$$

For a given saturated thickness X the value of the constant C can be computed simply from the measurement of the ratio A_c/A_f. Knowing C the value of the ratio A_c/A_f can be given for any thickness $X > X_o$. The connection between the value $A = A_c + A_f$ which is necessary to determine the cross section and the activity A_f remaining in the foil is:

$$A = A_f \frac{X}{X - C} \qquad /2/$$

In many cases the relative method is used to determine the cross section values, mainly choosing the reactions $Al^{27}(n,\alpha)Na^{24}$ and $Cu^{63}(n,2n)Cu^{62}$ for the standardisation.

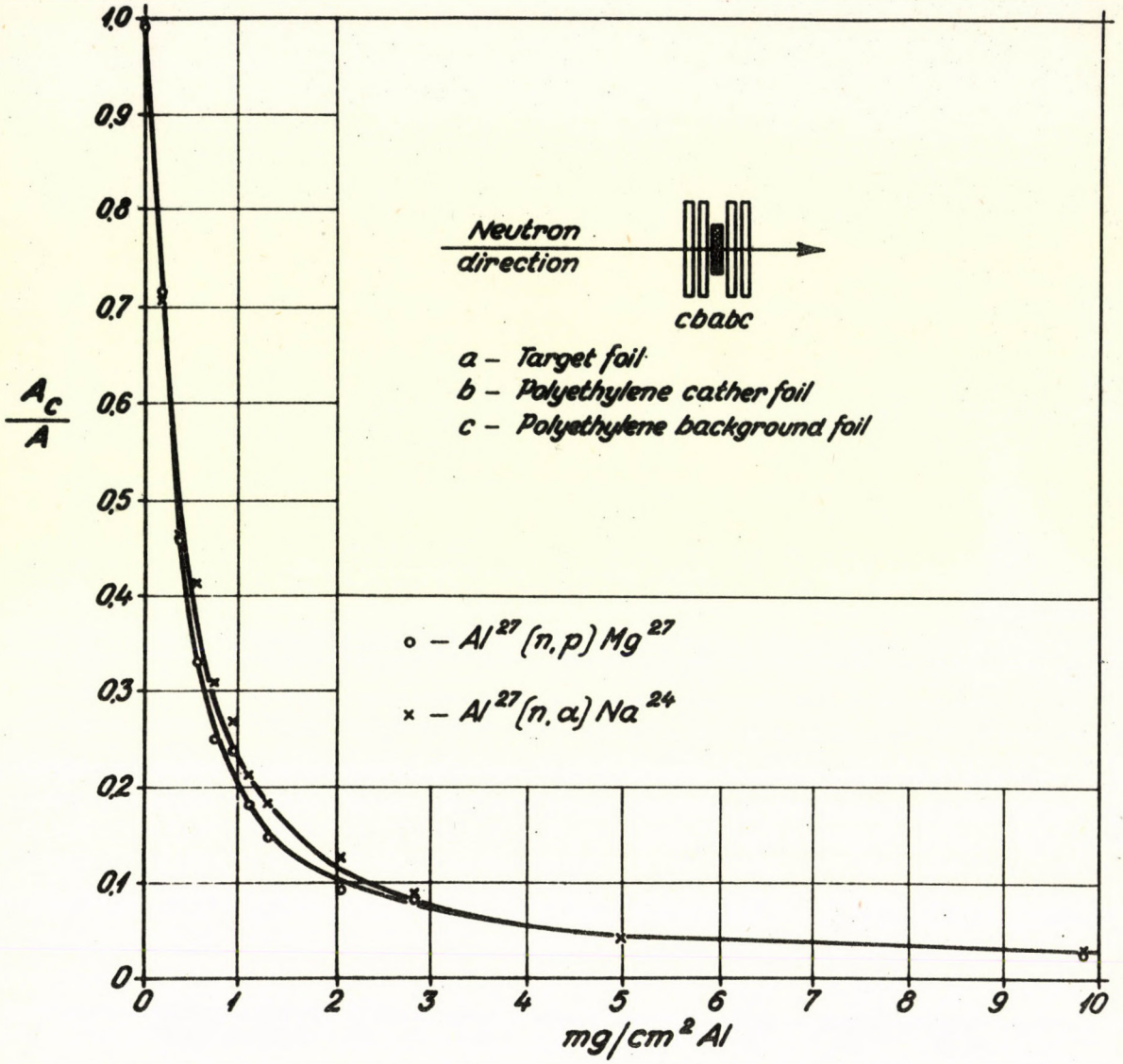

Fig. 1. Targeting arrangement for irradiation. Ratio of the broken off (A_c) and produced (A) active nuclei vs. target foil thickness.

We investigated the thickness dependence of the ratio of the broken off (A_c) and the total (A) activities in the case of $Al^{27}(n,p)Mg^{27}$ and $Al^{27}(n,\alpha)Na^{24}$ reactions. The irradiation were performed by 14,8 MeV energy neutrons, originating from $D + T$ reaction, the target arrangement can be seen in Fig. 1. The values of A_c and A_f belonging to the Mg^{27} and Na^{24} nuclei was determined from the measurements of the beta activities of the foils a, b, c. It can be seen from the ratios A_c/A plotted in the figure, that in the case of foil thickness used for the cross section measurements the broken off activity can reach 8 - 10 % of the total activity.

In table I.are given the C values occuring in relations /1/ and /2/ for some important reactions with 14,8 MeV bombarding neutron energy, in the case of substituting X mg/cm^2.

Table I.

Reaction	Maximum recoil energy (MeV)	C
$Al^{27}(n,\alpha)Na^{24}$	3,814	0,245
$Al^{27}(n,p)Mg^{27}$	1,951	0,197
$Co^{59}(n,\alpha)Mn^{56}$	2,17	0,104
$Cu^{63}(n,2n)Cu^{62}$	0,687	0,040
$Cu^{65}(n,2n)Cu^{64}$	0,728	0,040
$Cu^{65}(n,p)Ni^{65}$	0,853	0,050
$Ag^{107}(n,2n)Ag^{106}$	0,471	0,014
$Ag^{109}(n,2n)Ag^{108}$	0,476	0,012

2. The range of recoil nuclei

The range and the range straggling of slow moving atoms is not cleared up in the cases when the atomic number of the moving atom and the stopping medium is nearly equal [5]. The investigation of the range of the recoil nuclei originating from reactions (n,α); (n,p); (n,γ); $(n,2n)$ in target material can provide important data for the solution of the problem. Equations [1], [2] hold only in the cases of $X > X_0$, therefore the thickness $X = X_0$ beginning when the value of $A_C/A - C/X$ is not zero, is just the range of the maximum energy recoil nuclei. With this method we examined the range of recoil nuclei in aluminium, originating from reactions $Al^{27}(n,p)Mg^{27}$ and $Al^{27}(n,\alpha)Na^{24}$ in the case of 14,8 MeV neutron energy.

The range of the recoil nucleus can be measured by a simple method and with very great accuracy in case of certain neutron reactions, namely if the direction and size of the momentum of the recoil nucleus are nearly equal to those of the bombarding neutrons. This happens for example in the (n,γ) reactions and $(n,2n)$ reactions having high negative Q values. In these cases at the calculation of the recoil energy one does not need to take into account the negligible energy and momentum of the emitted particles, and so the experimentally measured range can be ordered to a rather well-defined energy. The energy of the recoil nucleus is given in a good approximation by the formula:

$$E_R = \frac{E_n}{A+1} \qquad /3/$$

where E_n is the energy of the bombarding neutron, and A the mass number of the target nucleus. If the incident neutron beam is perpendicular to the plane of the target

foil, the range of the recoil nuclei may be determined in the following way:

$$R = \frac{A_c}{A_c + A_f} X \qquad /4/$$

where X is the foil thickness and A_c and A_f are the activities that recoil into the catcher and retaind in the target foil, respectively. The value of X, A_c and A_f are taken from the experiments. The above relation is valid only in case $X > R$. With this method we determined the range of 140 keV Rh^{104} nuclei, originating from the reaction $Rh^{103}(n,\gamma)Rh^{104}$, in rhodium.

Nielson gives a theoretical expression for the range:

$$R = 0,6 \frac{(Z_1^{2/3} + Z_2^{2/3})^{1/2}}{Z_1 Z_2} \cdot \frac{A_1 + A_2}{A_1} \cdot A_2 E_1 \quad (\mu g/cm^2) \qquad /5/$$

where Z_1, A_1 and Z_2, A_2 are the atomic numbers and masses for the incoming particles and the tarteg atoms, respectively, and E_1 is the energy of the incoming particle in keV.

Table II. contains the range values determined experimentally and computed from the relation given by *Nielsen* [6].

Table II.

Recoil atom	Recoil energy (MeV)	Range (mg/cm^2)	
		Meas.	Calc.
Mg^{27}	1,95	0,800	1,329
Na^{24}	3,81	1,500	2,965
Rh^{104}	0,14	0,089	0,043

Comparing the values measured and calculated it turns out that the ranges determined by the *Nielsen* formula agree within a factor of two with our experimental results (however the direction of the deviation is not the same). An extensive experimental program is in progress with the above mentioned method, for the range measurement.

3. Observation of fast neutron reaction using recoil technique

The occurrence of a reaction is often proved by the appearence of a radioactivity due to a residual nucleus of known half-life. Nevertheless if any concurrent reaction of high cross section exists; it is practically impossible to show the presence of the low cross section activity, by analising the complex decay curve - especially if there is but a little difference between the half-lives. In the case of short half-lives even the chamical separation cannot be applied. In some cases the separation of the residual nuclei due to different reactions can be achieved through nuclear recoil. Investigating fast neutron reactions, recoil technique can be applied mainly in the observation of (n, α) processes. If the value of Q is negative the recoil nuclei from the (n,p) reaction cannot leave the foil backwards (i.e. ppposite the bombarding direction). Almost in every case of (n, 2n) reactions the recoil nucleus emerge only into the forward direction, because of the great negative value of Q, and so no disturbance arises when observing the (n, α) reaction of considerably lower cross section. In bombarding a Cu foil with 14,8 MeV neutrons we obrained an activity of half-lives 1,52 min. and 13,50 min. on the backward polyethylene which proves the presence of $Cu^{65}(n,\alpha)Co^{62,\,62m}$ reactions. We obtained as cross section ratio 1,4 however it belongs only to the transitions $E_\alpha \gtrsim 3,75$ *MeV* because nuclear recoil occurs in this case only backward.

Bombarding silver with neutrons, activities of half-lives 4,5 min. and 125 min. were observed in the backward direction, which proves the existence of reactions $Ag^{107}(n,\alpha)Rh^{104\,m}$ and $Ag^{109}(n,\alpha)Rh^{106\,m}$.

Some attempts will be made with the recoil technique to observe the (n,He^3) reactions, too, which were untill now unobservable, because of the great background effects.

References

[1] *I.L. Preiss - R.W. Fink:* Nucl. Phys., *15*/1960/326.

[2] *S.K. Mukherjee - A.K. Ganguly - N.K. Majumder:* Proc. Phys. Soc., 77/1961/508.

[3] *A. Poularikas - R.W. Fink:* Phys. Rev., *115*/1959/989.

[4] *E.T. Bramlitt - R.W. Fink - L.G. Gardner - A. Poularikas:* Phys. Rev., *125*/1962/297.

[5] *L. Winsberg - J.M. Alexander:* Phys. Rev., *121*/1961/518.

[6] *K.O. Nielsen:* Electromagnetically Enriched Isotopes and Mass Spectrometry (Academy Press, Inc., New York, and Butterworths Scientific Publications, Ltd., London, 1956)

ИССЛЕДОВАНИЕ ЭНЕРГЕТИЧЕСКОЙ ЗАВИСИМОСТИ ОТНОШЕНИЙ СЕЧЕНИЙ ИЗОМЕРОВ

Й. Бачо - Ю. Чикаи - М. Дароци

Институт Ядерных Исследований ВАН, Дебрецен

1. Введение

В ядерных реакциях кроме заряда, энергии, радиуса и четности участвующих ядер значительную роль играет также их момент количества движения. В случае высоких энергий возбуждения вместо момента количества движения отдельных уровней можно говорить только о распределении момента количества движения уровней в малом интервале энергии. *Бете* [1] и *Блох* [2] показали, что плотность уровней с моментом количества движения J при энергии возбуждения E дается уравнением:

$$\sigma(J) = \rho(o)\,(2J + 1)\; e^{-(J + 1/2)^2/2\sigma^2}$$

где $\sigma(o)$ плотность уровней с моментом количества движения O, σ параметр, дающий зависимость плотности уровней от спина.

В многочисленных ядерных реакциях конечное ядро имеет также долгоживущее метастабильное состояние, спин которого сильно, энергия немного отличается от спина и энергии основного состояния. Отношение вероятностей возникновения основного и метастабильного состояния (изомерной пары) называется отношением сечений изомеров или отношением выходов изомеров. Отношение сечений изомеров правильно отражает эффекты, причиненные моментом количества движения на ядерные реакции.

Определение параметра σ возможно путем сравнения отношений сечений изомеров, полученных экспериментально и по теории составного ядра [3-6]. Если составное ядро имеет большие моменты количества движения, тогда отношение сечений изомеров сильнее зависит от значения параметра σ, из-за этого исследование этого отношения в зависимости от энергии бомбардирующей частицы дает важные данные для определения зависимости плотности уровней от спина [5-8].

Цель нашей работы, кроме дополнения значений сечений реакций ядер Rh^{103}, In^{115} и Br^{81} с нейтронами, дать экспериментальные данные для зависимости параметра σ от энергии возбуждения.

2. Метод и аппаратура измерений

Измерения в случае родия и индия были проведены активационным методом термическими нейтронами и нейтронами с энергией 24 и 116 кэв, 2,5; 3,1 и 14,7 Мэв. При активации термическими нейтронами были применены Sb-Be фотонейтронный источник [9], помещенный внутри парафинового блока большого размера, и метод Cd-разности (рис. 1А). Нейтроны с энергией 24 кэв получились из Sb-Be фотонейтронного источника в нерассеивающей окружности (рис. 1Б). Нейтроны с энергией 116 кэв были полученны из реакции $C^{12}(d,n)N^{13}$, с энергией 2,5 и 3,1 Мэв из реакции $H^2(d,n)He^3$ на ускорителе АТОМКІ на 800 kV каскадного типа [10], а с энергией 14,7 Мэв из реакции $H^3(d,n)He^4$ на нейтронном генераторе на 100 kV [11]. Для обсолютного измерения потока нейтронов и для определения его временной флуктуации был использован "длинный счетчик" (рис. 1В). Для определения обсолютного значения потока нейтронов "длинный счетчик" колибровался источником Po-Be с известным потоком нейтронов [12]. Зависимость чувствительности от энергии учитывалась на основе работы *Вацета* и др. [13].

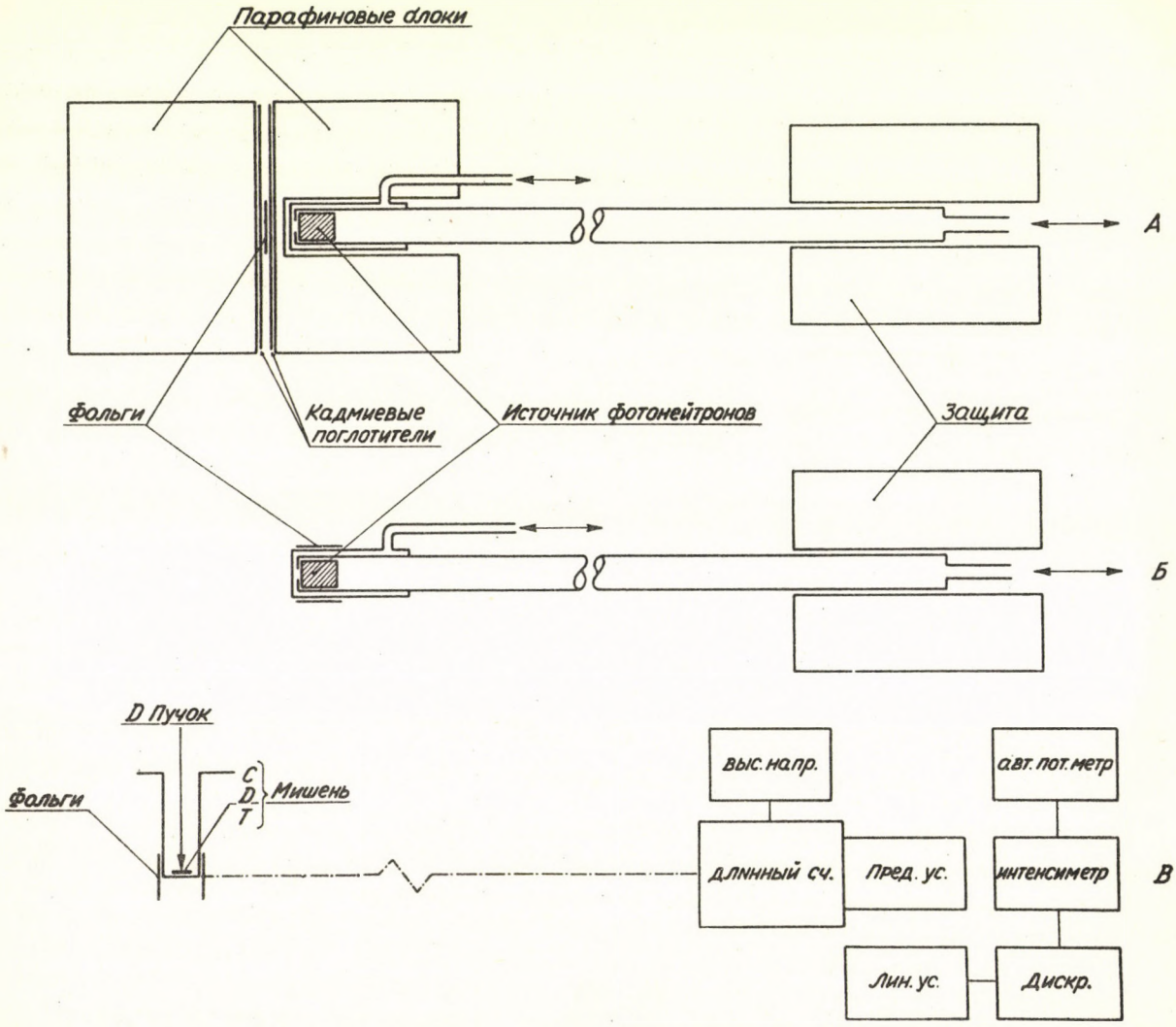

Рис. 1. Схемы активаций нейтронами различной энергии.

Толщины использованных в измерениях Rh и In фольг были 124 и 153 мг/см^2 соотвественно. β-активность фольг детектировалась торцевым счетчиком Гейгера, импульсы которого подавались на пересчетный прибор ПС-10000. Числа счета непрерывно работающего прибора в определенных моментах регистрировались киносъемочным аппаратом.

В случае In^{115} определялись отношения сечений, из-за этого необходимо было внести поправки только на различие в самопоглащении источника и в поглащении окна в следствие отличия максимальных энергий β-групп изомеров In^{116} и In^{116m}. Эти поправки были рассчитанны на основе разультатов *Бэкера* и *Каца* [14], и также *Броветто* и др. [15]. В случае Rh^{103} определялось и обсолютное значение сечения из обсолютной активности фольги. Для этого счетчик Гейгера калибровался стандартом UO_2SO_4, используя те же геометрические условия, как и в случае фольги, и учитывая отличия в толщинах и бета-спектрах источников.

3. Исследования энергетической зависимости отношений сечений возникновения изомеров $Rh^{104,104m}$ и $In^{116,116m}$ в реакции (n,γ)

По схеме распада Rh^{104} [16] ядро из метастабильного состояния с высоким спином ($I_m = 5$) переходит практически полностью в основное состояние с низким значением спина ($I_g = 1$). Чувствительностью нашего детектора к возникающим при этом переходе γ-лучам низкой энергии можно пренебречь; по колибровке источником Ce^{141} это меньше 0,4 %. Таким образом определение чисел ядер как в основном, так и в метастабильном состоянии производилось путем измерения β-эмиссии основного состояния. В этом случае и при постоянном потоке и активности насыщения отношение сечений изомеров (σ_g/σ_m) дается в зависимости от отношения активностей (A_g/A_m) выражением:

$$\frac{\sigma_g}{\sigma_m} = \frac{A_g}{A_m} \cdot \frac{\lambda_g}{\lambda_g - \lambda_m} + \frac{\lambda_g}{\lambda_g - \lambda_m} - 1 ,$$

где λ_g и λ_m постоянные распада основного и метастабильного состояния соотвественно.

По схеме распада In^{116} [16] ядро из метастабильного состоаания с высоким спином ($I_m = 5$) переходит в стабильное ядро Sn^{116} четырьмя β-группами, а основное состояние с низким значением спина ($I_g = 0;1$) одной β-группой. γ-переход между изомерными состояниями не имеется. Поэтому в случае постоянного потока и активности насыщения отношение сечений изомеров дается непосредственно отношением активностей.

Если поток нейтронов во время активации изменяется, соотношение между σ_g/σ_m и A_g/A_m сложнее, но несмотря на это, изменение потока может быть учтено с любой точностью [17, 18].

Параметры сложных кривых распада были определены методом "maximum likelihood" [19, 20].

Полученные значения отношений сечений изомеров при указанных выше энергиях нейтронов даны в таблице I.

Таблица 1.

Энергетическая зависимость σ_g/σ_m в реакциях $Rh^{103}(n,\gamma)Rh^{104,104m}$ и $In^{115}(n,\gamma)In^{116,116m}$ (В случае In $\sigma_m = \sigma_m^{54мин} + \sigma_m^{2,5сек}$).

E_n	σ_g/σ_m	
	Rh^{103}	In^{115}
термич.	11,53	
24 кэв	8,44	0,277
116 кэв	5,29	
2,5 Мэв	4,42	
3,1 Мэв		0,201
14,7 Мэв	3,28	0,194

Из наших измерений могут быть определены кроме данных выше отношений сечений и следующие новые сечения:

24 кэв

$Rh^{103}(n,\gamma)$ $\sigma_g = 1,69$ b[а/] $\sigma_{n\gamma} = \sigma_g + \sigma_m = 1,89$ b[а/]

$In^{115}(n,\gamma)$ $\sigma_g = 223$ mb[б/] $\sigma_{n\gamma} = 1028$ mb[б/]

2,5 Мэв

$Rh^{103}(n,\gamma)$, $Rh^{103}(n,\alpha)$ $\dfrac{\sigma_{n\gamma}}{\sigma_{n\alpha}} = 5,24$

3,1 Мэв

$In^{115}(n,\gamma)$ $\sigma_g = 18$ mb[в/] $\sigma_{n\gamma} = 108$ mb[в/]

14,7 Мэв

$Rh^{103}(n,\gamma)$ $\sigma_g = 10,6$ mb $\sigma_m = 3,2$ mb $\sigma_{n\gamma} = 13,8$ mb

$Rh^{103}(n,\alpha)$ $\sigma_{n\alpha} = 10,2$ mb

а/ Принимая результат $\sigma_m = 0,2$ b *Гамела* и *Гамермеша* [21].

б/ Принимая результат $\sigma_m = 805$ mb *Мэклина* и др. [22].

в/ Принимая результат $\sigma_m = 90$ mb *Кохэна* [23].

Интересно отметить, что в случае Rh нельзя пренебречь распадом γ-переходом по отношению эмиссии других частиц даже при высоких возбуждениях.

Для расчета отношения сечений изомеров в случае Br^{80} *Кац* и др. [24] ввели т.н. отношение каскадного разветвления, независимое от энергии возбуждения:

$$r_J = \frac{\text{число переходов на основное состояние}}{\text{число переходов на метастабильное состояние}} .$$

r_J обозначает частоту переходов промежуточного ядра с моментом количества движения J на основную и метастабильную уровни. Таким образом зная r_J и распределение моментов количества движения промежуточного ядра отношение сечений изомеров может быть расчитанно.

Распределение моментов количества движения J промежуточного ядра в зависимости от энергии E дается следующим выражением [25, 26]:

$$\sigma(J,E) = \pi\lambda^2 \sum_{S=|I-s|}^{I+s} \sum_{l=|J-S|}^{J+S} \frac{2J+1}{(2s+1)(2I+1)} T_l(E),$$

где λ длина волны *Де Бройля* падающего нейтрона, s спин нейтрона, I спин ядра-мишени, S спин канала, $T_l(E)$ проницаемость поверхности ядра для нейтронов с энергией E и орбитальным моментом l. Значения $T_l(E)$ в случае нейтронов могут быть точно рассчитанны [26, 17].

Нами была рассмотренна применимость отношения каскадного разветвления, характеризующего распада, в случае реакции $Rh^{103}(n,\gamma)Rh^{104}, {}^{104}m$. В таблице 2. даны измеренные и рассчитанные значения σ_g/σ_m, и значения $\sigma(J,E)$ и r_J.

Таблица 2.

Измеренные и расчитанные значения σ_g/σ_m, и значения $\sigma(J,E)$ и r_J.

E \ J	0	1	2	3	4	5	6	7	8	9	10	σ_g/σ_m	
												измеренное	расчитанное
термич.	0,2500	0,7500										11,53	12,3
24 Кэв	0,2274	0,7160	0,0566									8,44	10,1
116 Кэв	0,1792	0,6391	0,1744	0,0073								5,29	7,0
2,5 Мэв	0,0497	0,2733	0,3328	0,2376	0,0912	0,0151	0,0004					4,42	2,0
14,7 Мэв	0,0117	0,0700	0,1144	0,1540	0,1324	0,1865	0,1519	0,0880	0,0328	0,0073	0,0009	3,28	0,44
r_J	1/0	9/1	2/1	1/1	1/2	1/9	0/1	0/1	0/1	0/1	0/1		

Измеренные и рассчитанные отношения сечений изомеров удовлетворительно согласуются только при термических энергиях, в то время как расхождение становится все большее при высоких энергиях. Это означает, что отношение каскадного разветвления, введенное *Кацом* и др., не может считаться общедействующим законом.

4. Флуктуация отношения сечений изомеров в зависимости от энергии для реакции $Br^{81}(n,2n)Br^{80}$

Из-за статистической флуктуации сечения [27] можно ожидать, что при хорошем разрешении появляется флуктуация и в энергетической зависимости отношений сечений изомеров. Для исследований целесообразно выбрать реакцию с низким уровнем возбуждения конечного ядра, чтобы уменьшить усредняющее влияние γ-каскадов. Для этого реакция $Br^{81}(n,2n)Br^{80,80m}$ казалась подходящей. Энергетическая зависимость отношений сечений изомеров исследовалась методом активации при энергиях нейтронов $E_n = 13,5 \div 14,7$ Мэв и при разрешении $\Delta E_n \sim 100$ кэв. Нейтроны получились в реакции $D + T$ на ускорителе низкого напряжения (80 kV). Энергия изменялась, как это показывается на рис. 2., расположением мишени в различных направлениях. Нанося использованное в исследованиях LiBr на конусные поверхности разного угла раствора из фильтровальной бумаги, обеспечивалось весьма строгое определение направления.

Активность мишеней определялась сцинтилляционным γ-спектрометром [28, 29]. Применением γ-спектрометра с одной стороны удалось упростить обработку сложной кривой распада, с другой стороны исключить активность Se^{81}, происходящего из реакции (n,p) и имеющего период полураспада, равный периоду ядра Br^{80}.

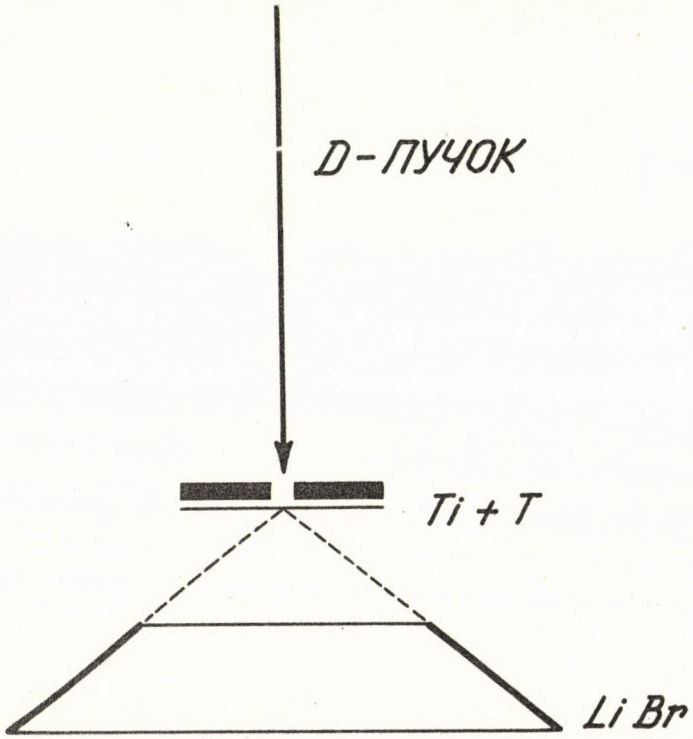

Рис. 2. Схема активации в случае реакции $Br^{81}(n,2n)Br^{80,80m}$.

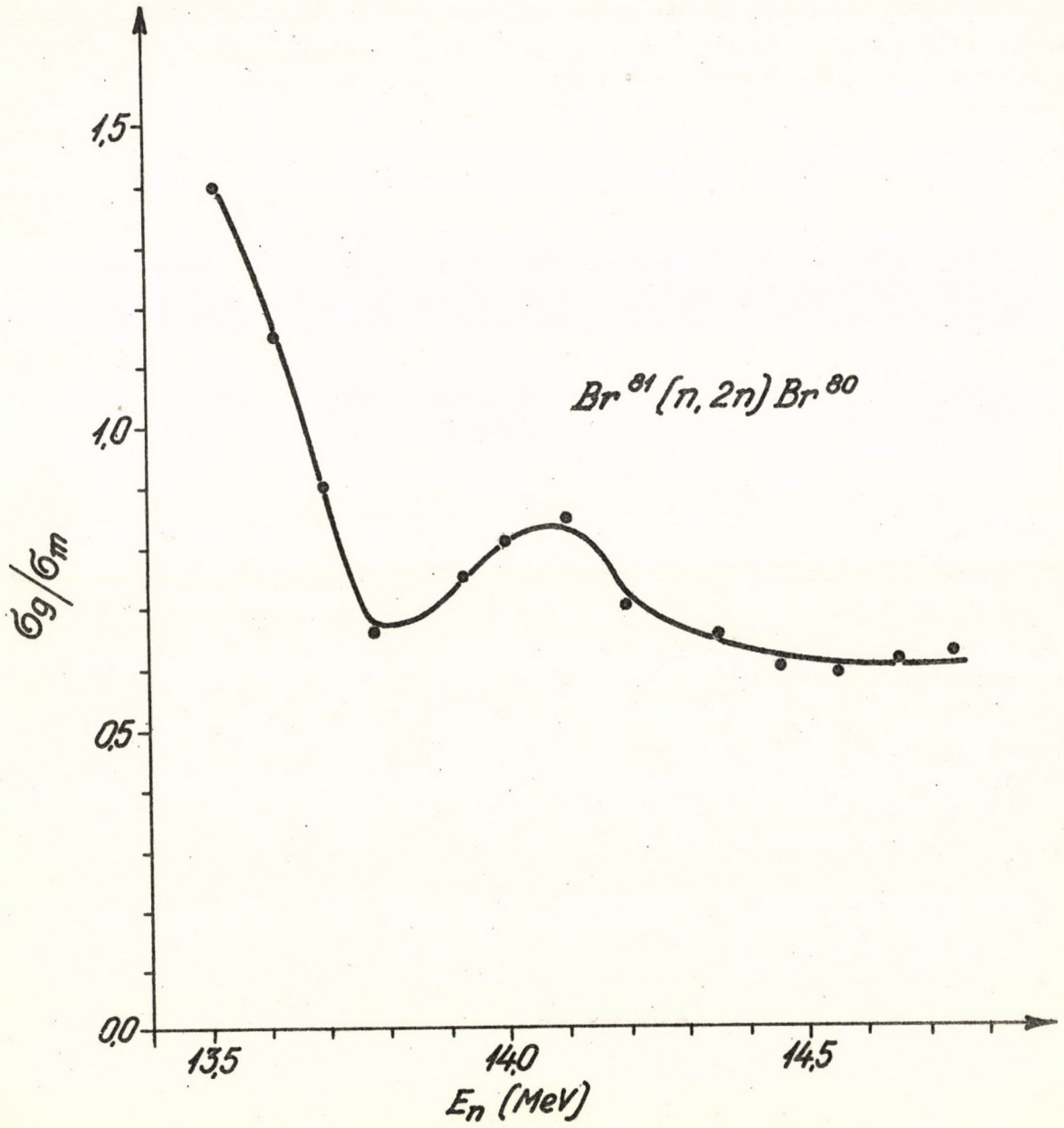

Рис. 3. Энергетическая зависимость отношений сечений изомеров при разрешении $\Delta E_n \sim 100$ кэв.

На рис. 3. показанны измеренные отношения сечений изомеров в зависимости от энергии нейтронов. Из кривой видно, что появляется, как это и ожидалось, значительная флуктуация в энергетической зависимости отношения сечений изомеров.

Для среднего значения отношений сечений изомеров в интервале энергий *13,5* ÷ ÷ *14,7* Мэв получилось значение

$$\overline{\frac{\sigma_g}{\sigma_m}} = 0,755,$$

хорошо согласующееся результатом 0,716 *Строхала* и др. [30].

В заключении авторы считают своим долгом выразить благодарность *Т. Балогу* (KLTE) и *Л. Ураи* (KFKI) за оказанную нам помощь в математической обработке сложных кривых распада, *Ч. Уйхейи* за изготовление стандартного источника и лаборанту *Л. Боднару* за участие в нумерических расчетах.

Литература

[1] *H.A. Bethe:* Revs. Modern Phys., *9*/1937/84.
[2] *C. Bloch:* Phys. Rev., *93*/1954/1094.
[3] *J.R. Huizenga - R. Vandenbosch:* Phys. Rev., *120*/1960/1305.
[4] *M.L. Sehgal:* Phys. Rev., *128*/1962/761.
[5] *C.T. Bishop:* ANL-6405 /1961/.
[6] *J. Wing:* ANL-6598 /1962/.
[7] *J.W. Meadows - R.M. Diamond - R.A. Sharp:* Phys. Rev., *102*/1956/190.
[8] *R. Vandenbosch - J.R. Huizenga:* Phys. Rev., *120*/1960/1313.
[9] *Csikai Gy. - Schadek J.:* ATOMKI Közl., *3*/1961/59.
[10] *Berecz I. - Papp I.:* ATOMKI Közl., *4*/1962/3.
[11] *Berecz I. - Bornemisza Gy-né. - Nagy J.:* Magy. Fiz. Folyóirat, *6*/1958/431.
[12] *Koltay E.:* Magy. Fiz. Folyóirat, *9*/1961/89.
[13] *П.И. Вацет - С.Г. Тонапетян - Г.А. Дорофеев:* Атомная Энергия, 7/1959/172.
[14] *R.G. Baker - L. Katz:* Nucleonics, *11*/1953/14 No. 2.
[15] *P. Brovetto - E. Chiavassa - G. Rosa - A. Pasquarelli:* Nucl. Instr. Meth., *14*/1961/302.
[16] *Landolt-Börnstein:* Group I. Vol. *I.* (Edited by A.M. Hellwege and K.H. Hellwege), Springer-Verlag, Berlin-Göttingen-Heidelberg, /1961/.
[17] *Csikai Gy. - Bacsó J. - Daróczy S.:* Magy. Fiz. Folyóirat, *11*/1963/7.
[18] *Bacsó J. - Daróczy S.:* ATOMKI Közl., *5*/1963/17.
[19] *Jánossy L. - Rupp E.:* KFKI Közl., *8*/1960/75.
[20] *Uray L.* (Частное сообщение).
[21] *V. Hummel - B. Hamermesh:* Phys. Rev., *82*/1951/67.
[22] *R.L. Macklin - N.H. Lazar - W.S. Lyon:* Phys. Rev., *107*/1957/504.
[23] *S.G. Cohen:* Nature, *161*/1948/475.
[24] *L. Katz - L. Pease - H. Moody:* Can. J. Phys., *30*/1952/476.
[25] *W. Hauser - H. Feshbach:* Phys. Rev., *87*/1952/366.
[26] *J.M. Blatt - V.F. Weisskopf:* Theoretical Nuclear Physics, John Wiley and Sons, Inc., New York, /1952/.
[27] *T. Ericson:* Adv. Phys., *9*/1960/425.
[28] *Máthé Gy. - Scharbert T.:* Mérés és Automatika, *8*/1959/1.
[29] *Máthé Gy.:* Magy. Fiz. Folyóirat, 7/1959/129.
[30] *P. Strohal - N. Cindro - B. Eman:* Nucl. Phys., *30*/1962/49.

Submitted to Nuclear Instruments for publication.

PROBLEMS AND RESULTS IN THEORETICAL AND EXPERIMENTAL INVESTIGATIONS ON ε/β^+ RATIO

D. Berényi

Institute of Nuclear Research of the Hungarian
Academy of Sciences, Debrecen, Hungary

The present state of the theory and the experiment concerning the electron capture to positron emission ratio is given. The experimental methods and procedures are reviewed too. Some application of the determination of the ratio and some open problems in connection with it are discussed especially in the case of forbidden transitions.

1. INTRODUCTION

Among the phenomena and characteristics of beta-decay (i.e. negative and positive beta-decay as well as electron capture) there are such which can obviously occur only in electron capture and positive beta-decay processes, respectively. These are the orbital capture ratios (K/L, L_I/L_{II} etc.) and the branching ratio of electron capture to positron emission (ε/β^+) in transitions of the decaying nucleus to the same level of the daughter nucleus. One can use these to determine parameters of nuclear levels and nuclear transitions but the relative probability of the capture of electron from the different atomic orbitals or also the relative probability of the electron capture and positron emission processes are interesting in themselves too, as phenomena, because they are not clarified in any respect especially in forbidden transitions.

In the present survey article the author tries to summarize the results and problems in connection with the capture to positron ratio especially for forbidden transitions for the above mentioned reasons. In the second section are reviewed the experimental methods and procedures of the determination of ε/β^+ ratio (first of all ε_K/β^+ ratio, as from the view-point of comparison with the theory, it is the most important). After that the theoretical calculations and experimental results as well as the comparison of these are discussed (Section 3) and finally some conclusions are drawn for existing problems and necessary farther measurements and calculations (Section 4).

2. EXPERIMENTAL METHODS

The individual methods for the determination of the capture to positron ratio are not universally valid. Partly they supplement one another, partly depend on the actual decay scheme [1, 2].

One of the simplest procedures is the comparison of the annihilation peak and the peak corresponding to X-ray radiation following K-capture in the scintillation γ-spectrum. In addition to the usual correction (energy distribution), fluorescence yield and internal conversion - if it is present - also have to be considered. Furthermore, also in case of an appropriate decay-scheme, the K-X-ray peak can be compared with a γ-peak [3]. It is likewise possible to determine the ε_K/β^+ ratio by measuring the area of the annihilation and an adequate γ-peak. Here of course, the usual corrections also have to be made. For the latter, one of the latest examples is the measurement of *Monaro* et al. for Zr^{88} [4]; while the former ones could rather be applied to nuclides of higher atomic number.

The proportional counter, as is well-known, is generally suitable for the spectroscopy of radiations with low energy. Under suitable conditions, the ε_K/β^+ ratio can be determined by applying a high pressure proportional counter with an internal source. In this way the peaks from the positrons and X-ray quanta, as well as the Auger electrons can be compared after the necessary corrections.

In magnetic β-spectrometers, the continuous positron spectrum can be compared with peaks corresponding to the Auger electrons. This method is applicable only at higher atomic numbers where the energy of Auger electrons is high enough to be reliably detected in the magnetic spectrometer. However, to determine the ε_K/β^+ ratio, here also in the same way as in the former methods, it is necessary to know the fluorescence yields. Theoretically it is possible to determine the ratio of electron capture to positron emission also by comparing the continuous β^+-spectrum with a suitable internal or external conversion line, if the internal conversion coefficient, i.e. if the cross-section of the photo or Compton effect is known.

The second and frequently used group of methods for determining the ε_K/β^+ ratio include procedures which apply the former apparatuses in coincidence. For the application, for instance, of a proportional counter and scintillation techniques in coincidence, some of the latest examples are [5] and [6]. The scintillation method combined with a magnetic spectrometer in coincidence is used in [7]. In the case of [8] three scintillation crystals are in coincidence, two of which detect the annihilation quanta.

Then it is possible to determine the ε_K/β^+ ratio by applying different methods and perhaps other samples to obtain separately the positron ratio and separately the capture (X-ray) ratio to a third radiation (β^--rays, γ-rays or conversion electrons) present in the disintegration. Examples in this case are [9-11].

Therefore, as we can see three main types of method used for the determination of ε_K/β^+ ratio can be distinguished. The first one determines the ratio of electron capture and positron emission by applying the same source and making measurements in the same apparatuses (scintillation counter, proportional counter, magnetic β-spectrometer). In the second one the same source for measurements in used but the apparatuses above are in coincidence. Finally, the branching ratio can be determined

by measuring separately the coefficient of electron capture for a given transition and separately the coefficient of positron disintegration referred to a third radiation so that different apparatuses and maybe different samples are used in the two separate measurements, and from that data on the ε_K/β^+ ratio can be calculated.

3. THEORETICAL CALCULATIONS AND EXPERIMENTAL RESULTS

3.1. Allowed transitions

The branching ratio of electron capture and positron emission can be obtained by dividing the probability for the two processes, i.e. by the Möller's formula and the Fermi's formula [1]. This way the capture to positron ratio for s-electrons

$$\frac{\varepsilon_s}{\beta^+} = \frac{\pi (W_0 + W_s)^2 g_s^2}{(1 + \gamma_0) \int_I^{W_0} W p q^2 F_0^+(Z, W)\, dW} \qquad /3.1/$$

In this formula the used notations are the following: W_0 is the total disintegration energy (in units $m_e c^2$) available for the transition (rest mass of electron is not included); W_s is the total energy of a K or L_I electron in units $m_e c^2$ (rest mass included); g_s is the large radial function of the electron; $\gamma_0 = (1 - \alpha^2 Z^2)^{1/2}$, where α is the fine structure constant; W is the total energy of positron in units $m_e c^2$; $p = (W^2 - 1)^{1/2}$, momentum of positron; $q = W_0 - W$, energy of the neutrino; $F_0^+(Z, W)$ is the Coulomb correction factor in normalized form, $F_0(Z = 0) = 1$.

The formula gives the electron capture from shells K and L_I if ε_K and ε_{L_I} respectively are substituted for ε_s, and at the same time g_K and g_{L_I} respectively are substituted for g_s.

It is not worthwhile here to consider the capture from other shells because with energies where positron emission also is possible ($W_0 > 1{,}02$ MeV), the capture takes place almost entirely from the s-orbits, and predominantly from the K-shell [12]. K-capture here is about ten-times more probable than L_I-capture, while L_{III}-capture is forbidden in allowed cases and so thus makes a negligible contribution to allowed transitions. The capture from the L_{II}-subshell is less probable at least by one, but at lower atomic numbers by two or three orders of magnitude than L_I-capture [2, 12].

Feenberg and *Trigg* [13] were the first to make calculations about ε_K/β^+ ratio, for allowed cases, and they gave the results diagrammatically. These workers used simple Coulomb wave-functions and ignored screening effects by electron-shells. In Zweifel's calculations that were carried out for six Z- and 18 energy-values, these effects has already been taken into consideration [14]. *Zweifel*'s values are interpolated and given in a graphical form in the *Wapstra*'s Nuclear Spectroscopy Tables [15].

There are several smaller corrections neglected by *Zweifel* in his calculations. Recently *Perlman* et al. [16] and *Depommier* et al. [17] have made calculations for the ε_K/β^+ ratio. The former have made their calculations mostly for the first forbidden transitions, but for allowed ones too. They are more accurate about the screening effect of the electron-shell both for positron emission and electron capture. Also they use a more precise value for function $F_0^+(Z, W)$ [18] and they take into consideration the finite size of nucleus. Furthermore, *Depommier* et al. performed the calculations with the supposition of the VA interaction. *Perlman* and *Depommier* do not give a Table like *Zweifel*'s. Partly they report formulas and partly the results of numerical calculations for some specific transitions.

In Table I. are assembled the pertaining data on the basis of the tables in [1] and [17] supplemented with a few recent results in calculated and measured ε_K/β^+ -values for allowed transitions.

As it can be seen, there is quite a good agreement between theoretical and experimental values. It is generally within 5 per cent. More significant discrepancy is noticeable only where Sc^{44} is concerned.

3.2. Forbidden transitions

In allowed transitions the ratio of electron capture to positron-emission is independent of the matrix-elements as they are cancelled in forming the ratio.

As to forbidden transitions, the case is far more complex and different, depending on whether unique or non-unique forbidden transitions are concerned.

3.2.1. Unique forbidden transitions

For unique forbidden transitions, $\Delta I = n + 1$, $\Delta\pi = (-1)^n$, the ratio is again independent of matrix-elements [17] inasmuch as, in this case also, the same nuclear matrix-element is involved in the expressions of probability for both electron capture and positive beta-decay [2, 12].

In unique first forbidden transitions, $\Delta I = 2$; $\Delta\pi = -1$, from the division of the two corresponding probability formulas, it follows that the ratio will increase by factor $2[(W_0 + 1)/(W_0 - 1)]$ as against the ratio in allowed transitions [12].

In the case of unique second forbidden transitions, $\Delta I = 3$; $\Delta\pi = +1$, it likewise follows, that here the ratio will increase to about the same extent as it did in the case of unique first forbidden transitions as compared to the allowed ones [12]. The comparison of experimental data available with numerical values calculated on the basis mentioned above are assembled on the basis of [1]. (Table II.).

Experimental data - as can be seen - are available only for the unique first forbidden transitions. Recently [21] positrons have successfully been demonstrated in the unique third forbidden decay of K^{40} and it has even proved possible to determine their spectrum and number per disintegration too but in this case, there is no experimental data on the ε_K disintegration rate to the Ar^{40} ground-state and so this on the ε_K/β^+ ratio.

Table I.

Measured and calculated values concerning transitions allowed for the ϵ_K/β^+ ratio

Nuclide transition	$\Delta I, \Delta\pi$	$E^{\beta^+}_{max}$	Measured values		Calculated values	
C^{11} $(3/2^- \longrightarrow 3/2^-)$	0, no	968	0,0019±0,0003	*Scobie* and *Lewis*[a]	0,0021	*Zweifel*[b]
F^{18} $(1^+ \longrightarrow 0^+)$	1, no	649	0,030±0,002	*Drever* et al.[c]	0,029 0,029	*Perlman* et al.[c] *Nguyen-Khac*[d]
Na^{22} $(3^+ \longrightarrow 2^+)$	1, no	541	0,103±0,006 0,122±0,010 0,102±0,008 0,112±0,004	*Sherr* and *Miller*[c] *Allen* et al.[c] *Konijn* et al.[c] *Ramaswamy*[a]	0,104 0,107	*Zweifel*[c] *Nguyen-Khac*[d]
Sc^{44} $(2^+ \longrightarrow 2^+)$	0, no	1467	0,067±0,016 0,021±0,019	*Blue* and *Bleuler*[c] *Konijn* et al.[c]	0,044 0,045 0,042	*Zweifel*[d] *Perlman* et al.[c] *Nguyen-Khac*[d]
V^{48} $(4^+ \longrightarrow 4^+)$	0, no	695	0,62±0,11 0,70±0,09 0,68±0,02 0,69±0,03	*Sterk*[d] *Bock*[c] *Konijn* et al.[c] *Konijn* et al.[c]	0,70 0,66 0,73	*Zweifel*[d] *Nguyen-Khac*[d] *Perlman* et al.[c]
Mn^{52} $(6^+ \longrightarrow 6^+)$	0, no	575	1,84±0,22 1,81±0,07 1,86±0,09	*Sehr*[c] *Konijn* et al.[c] *Konijn* et al.[c]	1,82 1,9 1,77	*Zweifel*[d] *Perlman* et al.[c] *Nguyen-Khac*[d]
Co^{58} $(2^+ \longrightarrow 2^+)$	0, no	472	5,4±0,2 6,1±0,8 5,2±0,16 5,13±0,2 5,08±0,17 4,83±0,1	*Cook* and *Tomnovec*[c] *Grace* et al.[c] *Konijn* et al.[c] *Ramaswamy*[d] *Ramaswamy*[f] *Kramer*[g]	5,0 5,2 4,9 4,87	*Zweifel*[d] *Perlman* et al.[c] *Nguyen-Khac*[c] *Nguyen-Khac*[d]
Cu^{61} $(3/2^- \longrightarrow 3/2^-)$	0, no	1205	0,18±0,03 0,25±0,03 0,22±0,03 0,27	*Huber* et al.[c] *Bouchez*[d] *Bouchez*[c] *Cook*[d]	0,29 0,29 0,28	*Zweifel*[d] *Perlman* et al.[c] *Nguyen-Khac*[c]
Cu^{64} $(1^+ \longrightarrow 0^+)$	1, no	657	1,75±0,2 2,6±0,3 2,32±0,28 1,81±0,2 2,07±0,2	*Huber* et al.[c] *Bouchez* and *Kayas*[c] *Reynolds*[c] *Plassman*[d] *Plassman*[d]	2,18 2,3 2,07	*Zweifel*[d] *Perlman* et al.[c] *Nguyen-Khac*[c]
Zn^{65} $(5/2^- \longrightarrow 3/2^-)$	1, no	325	28,0±3,2 32,5±6 26±3 30 25±2	*Perkins* and *Haynes*[c] *Sakai*[d] *Avignon*[c] *Perrin*[c] *Gleason*[c]	30 30,7	*Zweifel*[c] *Nguyen-Khac*[c]
Zr^{89} $(9/2^+ \longrightarrow 9/2^+)$	0, no	901	2,7 3,7 3,54±14	*Goldhaber* et al.[c] *Shore* et al.[c] *Monaro* et al.[h]	2,8 3,40	*Perlman* et al.[c] *Zweifel*[h]
Cd^{107} $(5/2^+ \longrightarrow 7/2^+)$	0, no	320	320±30	*Bradt* et al.[c]	325 310 331	*Zweifel*[d] *Perlman* et al.[c] *Nguyen-Khac*[c]
Sn^{111} $(7/2^+ \longrightarrow 9/2^+)$	1, no	1510	2,5±0,25	*McGinnis*[c]	1,5	*Perlman* et al.[c]
I^{128} $(1^+ \longrightarrow 0^+)$	1, no	245 /?/	1800±400	*Langhoff* et al.[i]		

a See reference [23]
b See reference [24]
c See reference [1]
d See reference [17]
e See reference [19]
f See reference [20]
g See reference [6]
h See reference [4]
i See reference [9]

Table II.

Measured and calculated values concerning transitions unique first forbidden for the ε_K/β^+ ratio ($\Delta I = 2$, yes)

Nuclide transition	$\Delta I, \Delta\pi$	$E^{\beta^+}_{max}$	Measured values	Calculated values		
				Allowed	Forbidden	Author
Rb^{84} ($2^- \rightarrow 0^+$)	2, yes	1700	2,06±0,36 *Welker*[a] 1,12±0,25 *Konijn*[c]	0,26 0,280±0,008	0,83 0,91±0,02	*Perlman* et al.[a] *Konijn*[c]
Sb^{122} ($2^- \rightarrow 0^+$)	2, yes	565	300±130 *Glaubman*[b] 300±50 *Perlman* et al.[a]	48,6 49	285 275±60	*Nguyen-Khac*[b] *Perlman* et al.[a]
I^{126} ($2^- \rightarrow 0^+$)	2, yes	1155	18±0,3 *Perlman* et al.[a]	4,6	17,3±1	*Perlman* et al.[a]

a See reference [1] b See reference [17] c See reference [33]

3.2.2. Non-unique forbidden transitions

3.2.2.1. First forbidden transitions. For the non-unique forbidden transitions, only the first forbidden disintegrations $\Delta I = 0, 1$; $\Delta\pi = -1$ have been analyzed theoretically [12, 16, 17, 22, 27] and only for these are - at least partly - experimental data available (cf. Table III. compiled on the basis of the corresponding table in ref. [1]). In these cases, according to *Brysk* and *Rose* as well as *Depommier* et al. no deviation is to be expected from the allowed ε_K/β^+ ratio or the discrepancy may be but extremely slight owing to the preponderance of Coulomb-terms [12, 17].

Experimental data however, for the $\Delta I = 1$, yes transitions are not available at all, for the $\Delta I = 0$, yes case some measured value in transitions $2^- \quad 2^+$ indicate a marked deviation from the allowed values [7], rising even to as high as 50 per cent. (Table III.) Attempts to elucidate this phenomenon have been made by *Perlman* et al. [16, 17] and recently by *Konijn* et al. [22] each following different courses. *Perlman* et al. suppose that in this transitions not only $\Delta I = 0$ and 1, but the spin change $\Delta I = 2$ also is involved to a considerable extent. Accordingly the ε_K/β^+ ratio takes the values actually allowed in the part of the transitions, in which $\Delta I = 0$, and 1, and the discrepancy being ascribable to the admixture of $\Delta I = 2$.

In the other view [22], the ratio of electron capture to positron emission generally deviates from that of the allowed transitions. In order to come to a suitable decision further experimental data are needed [7]. Measurements for Tl^{200} ($2^- \longrightarrow 2^+$) recently made by *Nooijen* et al. strongly point to the second interpretation [7].

3.2.2.2. Higher forbidden transitions. Concerning the higher non-unique forbidden transitions, e.g. the second forbidden transition $\Delta I = 2$, $\Delta\pi = +1$, the theory cannot state anything exact in the expression of ε_K/β^+

ratio owing to the presence of various unknown matrix-elements (cf. [16] for the cor - responding general formulae). One statement may, however, be safely made theoretically and it is that the value of the ε_K/β^+ ratio can be expected to increase in non-unique higher forbidden transitions as against allowed transitions, and the higher the order of forbiddenness, the greater deviation is to be expected [12]. Nevertheless it must be noted that evidence for this theoretical prediction exists only recently in the case of the $Cl^{36} \longrightarrow S^{36}$ transition [29-31]. This is the first experimental evidence that the value of ε_K/β^+ ratio increases in forbidden transitions of higher then order in comparison to that of the allowed ones.

Table III.

Measured and calculated values concerning transitions non-unique first forbidden for the ε_K/β^+ ratio (I = 0, yes)

Nuclide transition	$\Delta I, \Delta\pi$	$E^{\beta^+}_{max}$	Measured values		Calculated values		
					Allowed	Forbidden	Author
As^{74} ($2^- \longrightarrow 2^+$)	0, yes	920	1,5	*Perlman* et al.[a]	1,17	1,47	*Perlman* et al.[a]
			1,50±0,16	*Johansson* et al. and *Scobie*[c]	1,16±0,03	1,50±0,04	*Harmer* and *Perlman*[b]
					1,16±0,03	1,70	*Konijn* et al.[c]
						1,72	
Rb^{84} ($2^- \longrightarrow 2^+$)	0, yes	782	5,1±0,4	*Perlman* et al.[a]	3,4±0,3	4,2±0,4	*Perlman* et al.[a]
			5,72±0,12	*Konijn* et al.[d]	4,09	4,98	*Harmer* and
					3,3±0,3	4,2±0,4	*Perlman*[b]
						4,1±0,4	
					3,4±0,3	4,73	*Konijn* et al.[c]
						4,86	
I^{126} ($2^- \longrightarrow 2^+$)	0, yes	459	148	*Perlman* et al.[a]	122	143	*Perlman* et al.[a]
			145±4	*Harmer* and *Perlman*[b]	131±6	145±7	*Harmer* and *Perlman*[b]
					125±7	164	*Konijn* et al.[c]
						162	
Cs^{132} ($2^- \longrightarrow 2^+$)	0, yes	2150 (?)	0,003± ±0,0015	*Taylor* et al.[g]			
			0,006	*Taylor* et al.[g]			
Tl^{200} ($2^- \longrightarrow 2^+$)	0, yes	1068	110±10	*Konijn* et al.[c]		63,2	*Harmer* and *Perlman*[e]
			102±9	*Nooijen* et al.[f]	57±2	96	*Konijn* et al.[c]
						74	

a See reference [16]
b See reference [25]
c See reference [22]
d See reference [26]
e From reference [22]
f See reference [7]
g See reference [28]

4. CONCLUSIONS

Let us summarize the information we can obtain by experimentally determining the ε_K/β^+ ratio and the open questions or theoretical predictions not verified experimentally.

4.1. Allowed and unique forbidden transitions

As we can see in the case of allowed and unique forbidden transitions the nuclear matrix-elements disappear in the expression of the ε_K/β^+ ratio, if the Fierz interference terms are equal to zero. It means that the determination of the ε_K/β^+ ratio in these cases render a good test of the validity of the present β-disintegration theory if the present theory satisfactorily describes the phenomenon electron capture and positron emission. Recent experimental data agree very well with theoretical ones (cf. Section 3.1. and 3.2.1.).

As the theory may be regarded as justified concerning allowed and partly in unique forbidden transitions, the wave-functions of the captured electron and emitted positron also can be controlled by taking into account the finite size of nucleus and the screening effect of atomic shell [1].

With unique forbidden transitions, the branching increase according to theory in a calculated measure and so the measurement for ε_K/β^+ ratio may serve the purpose of identofying such transitions and to draw conclusions about the order of forbiddenness of it.

However it is worthwile to mention, that up till now there is no experimental evidence of increasing of the ε_K/β^+ ratio by the calculated factors for higher than first uniquely forbidden transitions. Furthermore, there are some more or less inaccurate data on the ε_K/β^+ ratio of allowed and uniquely first forbidden transitions which would be worth-while to controll (Sc^{44}, Sn^{111}; Rb^{84}; cf. Table I. and II.).

4.2. Non-unique forbidden transitions

As to non-unique forbidden transitions, the situation can be regarded much more perplexing.

First of all there are no experimental data available for the $\Delta I = 1$, yes-type of non-unique first forbidden transitions. Whereas in the case of $\Delta I = 0$, yes-types, at least at the measured $2^- \longrightarrow 2^+$ transitions, there appears a significant 20 - 25 per cent deviation from the corresponding allowed values (cf. Section 3.2.2.1. and Table III.). The reason for these deviations has not yet been clarified. Two interpretations have been suggested. Although one of the latest experimental data [7] points to one of them [22], yet the question cannot be regarded as settled. It must be noted that, at the same time, if the other view [16, 27] were valid, the presence of nuclear matrix-element $\Sigma |B_{ij}|^2$ and its extent could be demonstrated concerning non-unique first forbidden transitions more reliably than through studies of the

spectral shape according to the opinion of *Harmer* and *Perlman* [27]. Similarly *Perlman* et al. [16] consider experimental evidence lacking even for other non-unique first forbidden transitions differentiated according to shell-model (e.g. $\Delta I = 0$, $\Delta_j = 0$, i.e. $0 \longrightarrow 0$ transitions).

In the expression of ε_K/β^+ ratio for higher non-unique forbidden transitions, the unknown nuclear matrix-elements also are involved (see Section 3.2.2.2.). Consequently, theory cannot make a quantitative prediction for the numerical value of them only it shows an increasing tendency for higher forbiddenness (experimental evidence of it recenty in the case of Cl^{36}).

Such investigations, however, can give information on the nuclear matrix elements and help us to differentiate between unique and non-unique transitions becouse in the case of an actual order of forbiddenness transition the increasing factor in comparison to the corresponding allowed case is definite in the unique transition and practically indefinite in the non-unique one.

Reference

[1] *R. Bouchez* and *P. Depommier:* Reports on Prog. in Phys., *23*/1960/395.

[2] *P. Kramer:* Thesis. Amsterdam, 1961.

[3] *M. Goldhaber, - E. der Mateosian, - G. Scharff-Goldhaber, - A.W. Sunyar:* Phys. Rev., *83*/1951/661.

[4] *S. Monaro, - G.B. Vingiani, - R. Van Lieshout:* Physica, *27*/1961/985.

[5] *H.L. Hagedorn, - J. Konijn:* Physica, *23*/1957/1069.

[6] *P. Kramer, - A. de Beer, - J. Blok:* Physica, *28*/1962/587.

[7] *B. Van Nooijen, - H. Van Krugten, - W.J. Wiesehahn, - A.H. Wapstra:* Nuclear Physics, *31*/1962/406.

[8] *H.W. Taylor, - G.N. White, - R. McPherson:* Nuclear Physics, *41*/1963/221.

[9] *H. Langhoff, - P. Kilian, - A. Flammersfeld:* Zeits. f. Phys., *165*/1961/393.

[10] *D. Berényi:* Physics Letters, *2*/1962/332.

[11] *G. Fiedlander, - L. Yaffe:* Canad. Journ. Phys., *40*/1962/1249.

[12] *H. Brysk, - M.E. Rose:* Revs. Mod. Phys., *30*/1958/1169.

[13] *E. Feenberg, - G. Trigg:* Revs. Mod. Phys., *22*/1950/399.

[14] *P.F. Zweifel:* Phys. Rev., *96*/1954/1572; ibid. *107*/1957/329.

[15] *A.H. Wapstra, - G.J. Nijgh, - R. Van Lieshout:* Nuclear Spectroscopy Tables, North-Holland Publ. Co., Amsterdam, 1959.

[16] *M.L. Perlman, - J.P. Welker, - M. Wolfsberg:* Phys. Rev., *110*/1958/381.

[17] *P. Depommier, - U. Nguyen-Khac, - R. Bouchez:* Journ. de Phys. Radium, *21*/1960/456.

[18] *B.S. Dzelepov, - Zyryanova:* Effect of the Electrical Field of the Atom on the Beta-Decay. Publ. House of the Academy of USSR. Moscow-Leningrad, 1956. (In Russian).

[19] *M.K. Ramaswamy:* Indian Journ. Phys., *33*/1959/285.

[20] *M.K. Ramaswamy:* Indian Journ. Phys., *35*/1961/610.

[21] *D.W. Engelkemeir, - K.F. Flynn, - L.E. Glendenin:* Phys. Rev., *126*/1962/1818.

[22] *J. Konijn, - B. Van Nooijen, - A.H. Wapstra:* Nuclear Physics, *16*/1960/683.

[23] *J. Scobie, - G.M. Lewis:* Phil. Mag., 2/1957/1089.
[24] *J. Konijn, - B. Van Nooijen, - H.L. Hagedorn, - A.H. Wapstra:* Nucl. Phys., 9/1958-59/296.
[25] *D.S. Harmer, - M.L. Perlman:* Phys. Rev., 114/1959/1133.
[26] *J. Konijn, - H.L. Hagedorn, - H. Van Krugten, - J. Slobben:* Physica, 24/1958/931.
[27] *D.S. Harmer, - M.L. Perlman:* Phys. Rev., 122/1961/218.
[28] *H.W. Taylor, - G.N. Whyte, - R. McPherson:* Nuclear Physics, 41/1963/221.
[29] *D. Berényi:* Physics Letters, 2/1962/332.
[30] *P.W. Dougan, - K.W.D. Ledingham, - R.W.P. Drever:* Phil. Mag., 7/1962/1223.
[31] *D. Berényi:* Acta Phys. Hung., to be published.
[32] *B.E. Joshi, - G.M. Lewis:* Proc. Phys. Soc., 78/1961/1056.
[33] *J. Konijn:* Thesis. Delft. 1958.

EXPECTED α-DECAY DATA OF THE RARE EARTH NUCLIDES ON THE BASIS OF DIFFERENT SYSTEMATICS

T. Fényes

Institute of Nuclear Research of the Hungarian Academy of Sciences, Debrecen, Hungary

and

Z. Bődy

Institute for Experimental Physics of the L. Kossuth University, Debrecen, Hungary

This work summarizes the α-decay data of rare earth nuclides. The presently existing experimentally measured α- and β-decay energies allow the computation of the decay energy of some 30 further nuclides. By plotting the α-decay energy vs. atomic number, the expected α-decay energy of nuclides, the α-activity of which has not yet been detected experimentally, has been estimated. The estimation of the α-decay energies for the above nuclides on the basis of the available mass data as well as p and n separation energies has also been performed. The expected α-partial half-lives were also estimated from the gained α-decay energies using a semiempirical relation (see [15], p. 6) expressing explicitly the dependence of the half-life on the atomic number. Finally, some questions about the possibility of experimental detection of the α-activities, having not yet been measured, are discussed.

1. Introduction

It is known that for nuclides having mass number greater than about 140 α-decay is allowed energetically [1], but in most cases the half-lives are so high that the disintegrations have not yet been detected experimentally.

The probability of the α-decay in the region of great mass numbers is high especially for nuclides containing protons or neutrons of magic number plus 2, 3,... [2], because the binding energy of nucleons just above a closed shell is small and so the energy loss of the α-particles due to the binding energy is small. In the medium heavy region those are the nuclides of neutron number 84, 85,..... etc.

It is known too that among the nuclides of the same atomic number (far from magic numbers) the smaller is the number of neutrons in the nucleus, the greater is the disintegration energy [2], as the repulsing effect of protons in that case has relatively more influence.

Starting from these points the α-radiation of many neutron deficient rare earth nuclides has been experimentally detected - especially during the last 14 years. A detailed discussion of the literature up to 1959 can be found in paper [3].

The aim of this work is to summarize up to the middle of 1962 the data of α- and β-decays of the rare earth nuclides recently measured and computed from mass data, to complete them with disintegration energies calculated from α - β decay cycles and draw conclusions on the α-decay energy of the rare earth nuclides whose α-decay has not yet been observed. The disintegration energies mentioned above were computed also by means of energy cycles composed by using known α-decay and proton (neutron) separation energies. Conclusions have also been drawn on the expected partial half-lives from the disintegration energies, using the semiempirical formula discussed in [15].

2. Summary of experimental α-decay data

See table I.

The sources of the data are indicated in the last column. We have sometimes used the data of works [4] and [10], but have not referred to them. Paper [3] is a comprehensive work containing further references.

Table I.

Data of α-active rare earth nuclides. The total decay energy was gained from the expression

$$Q = E + \frac{m}{M} E + (65,3\, Z^{7/6} - 80\, Z^{2/6})\, 10^{-6},$$

where Q total decay energy (MeV),
E kinetic energy of α-particle (MeV),
m mass of α-particle,
M mass of daughter nucleus,
Z atomic number of parent nucleus.

The first member of the expression gives the kinetic energy of the α-particle, the second the kinetic energy of the recoiled daughter nucleus, the third the correction for electron screening.

Nuclide	Mass number (A)	α-particle energy (MeV). In brackett: the total alpha-decay energy (MeV)	Method of detection	Total half-life	Other decay modes observed	α/total decay ratio	α-partial half-life (T_α)	Method of measuring T_α	Production (bombarding energy)	References
$_{60}Nd$	144	1,90 ± 0,1	nuclear emulsion		natural β-stable		≈1,5 10^{15} years	from decay rate of a given number of atoms	natural 23,83 %	[3]
		1,83 ± 0,03 (1,902)	ion.chamber				(2,4 ± 0,3). 10^{15} years	- " -		[5]
$_{61}Pm$	145	2,24 ± 0,04 (2,32)	ion.chamber	17,7 ± 0,4 years	e^--capture	(2,8 ± 0,6) 10^{-9}	(6,3 ± 1,4).10^9 years	$\frac{\alpha}{\text{x-ray}}$ ratio	Sm^{144} (n, γ) Sm^{145} $Sm^{145} \xrightarrow[\text{capture}]{e^-} Pm^{145}$ with thermal neutrons	[18]
$_{62}Sm$	146	2,55 ± 0,05 (2,64)	nuclear emulsion		β-stable		≈5.10^7 years	estimated from reaction yield	Nd^{143} (α, n)	[3]
							<3.10^8 years		Gd^{150} (>10^5 years) $\xrightarrow{\alpha}$	[5]
	147	2,18 ± 0,02	ion.chamber		natural β-stable		~1,3.10^{11} years	from decay rate of a given number of atoms	natural 15,09 % Pm^{147} (2,6 years) $\xrightarrow{\beta^-}$	[3]
		2,23 ± 0,02	- " -				(1,15 ± 0,05). 10^{11} years	- " -	U^{235} (n, fission)	[5]
		2,20 ± 0,02	- " -				(1,17 ± 0,05). 10^{11} years	- " -		[7]
		2,19 ± 0,01	- " -							[6]
		2,21 ± 0,01 mean (2,293)					(1,18 ± 0,05). 10^{11} years mean			[7] see also [26]
	148	2,14 ± 0,03 (2,220)	ion.chamber		natural β-stable		(1,2 ± 0,3).10^{13} years	- " -	natural	[7]
							>2.10^{14} years		(11,35 ± 0,09) %	[5]
	149	1,84 ± 0,05	ion.chamber		natural β-stable		(4 ± 2).10^{14} years	- " -	natural	[7]
		(1,91)					>1.10^{15} years		(13,96 ± 0,10) %	[5]
$_{63}Eu$	147	2,88 ± 0,10 (2,98)	ion.chamber	24 ± 2 days	e^--capture	≈10^{-5}	4,4.10^3 years ≈6.10^3 (within a multiplying factor 3)	$\frac{\alpha}{\text{x-ray}}$ ratio	Sm^{147} (p,n) 8,5 MeV Sm^{147} (d,2n) 19 " Sm^{148} (d,3n) 19 "	[3] [22]
		2,91 ± 0,01 (3,01)	ion.chamber			(2,2 ± 0,6). 10^{-5}		$\frac{\alpha}{\text{x-ray}}$ ratio	Sm^{147} (p,n) 9,5 MeV	[26]
$_{64}Gd$	148	3,16 ± 0,10 (3,27)	ion.chamber	>35 years ~130 years	β-stable (?)	>25 %	≈1,3.10^2 years (within a multiplying factor 3)	estimated from reaction yield	Sm^{147} (α, 3n) 36 MeV Eu^{151} (p, 4n) 32 "	[3] [22]
		3,18 ± 0,01 (3,29)	ion.chamber				84 ± 9 years	from decay rate of a given number of atoms	Eu(p, xn) 100 MeV	[26]
	149	3,00 ± 0,15 (3,11)	ion.chamber	9,0 ± 1 days	e^--capture	7.10^{-6}	≈4.10^3 years (within a multiplying factor 3)	$\frac{\alpha}{\text{x-ray}}$ ratio	Sm^{147} (α, 2n) 30 MeV Tb^{149} (4,1 h) e^--capture	[22] [3]
	150	2,70 ± 0,15 (2,80)	ion.chamber	≈3.10^5 years	β-stable		≈3.10^5 years	from decay rate of a given number of atoms	Eu^{151} (d, 3n) 19 MeV Eu^{150} (13,7 h) β-	[3]
		2,53 ± 0,05 (2,62) 2,55 ± 0,05 mean of the first two data (2,64)	ion.chamber				3.10^6 years	- " -	Eu^{151} (γ, n) Eu^{150} Eu^{150} (13,7 h) β^-	[19] preliminary report
		2,73 ± 0,01 (2,83)	ion.chamber				(2,1 ± 0,3).10^6 years	- " -	Sm^{150} (p,n) 9,5 MeV Eu^{150} (13,7 h) β^-	[26]
	152	1,7	nuclear emulsion				≈10^{15} years		natural 0,2 %	[23]
		2,14 ± 0,03 (2,22)	ion.chamber		natural β-stable		(1,08 ± 0,08) 10^{14} years	- " -		[5]

Nuclide	Mass number (A)	α-particle energy (MeV) In brackett: the total alpha-decay energy (MeV)	Method of detection	Total half-life	Other decay modes observed	α/total decay ratio	α-partial half-life (T_α)	Method of measuring T_α	Production (bombarding energy)	References
$_{65}Tb$	149	4,0				0,1				
		3,95 ± 0,02 (4,08)	α-spectroscope	(4,10 ± 0,05) hours	β^+	0,16 ± 0,04	36 ± 7 hours	$\frac{\alpha}{\text{total decay ratio}}$	Eu^{151} (α, 6n) 60 MeV Gd(p, xn) 32-200 -"- Bi(p, fission)	[21] [3]
	149^m m=metastable	3,99 ± 0,03	ion.chamber	(4,3 ± 0,2) minutes	e^--capture and β^+	-	-	-	La^{139} (O^{16}, 6n) Tb^{149m} 80-140 MeV linear accelerator	[17]
	151	3,44 ± 0,1 (3,55)	ion.chamber	19 ± 1 hours 17,5 ± 0,7 hours	e^--capture	3.10^{-6}	$7,4.10^2$ years	$\frac{\alpha}{\text{x-ray ratio}}$	Gd(p, xn) 100 MeV Eu^{151} (α, 4n) 45 MeV	[3] [21]
	152			17,4 + 0,3 hours (4 ± 0,5)^m minutes	β^+-stable e^--capture (β^+, e^--capture)^m	$\frac{\alpha}{\text{x-ray(K) ratio}} \approx$ $\approx (2.10^{-5})^m$			Eu^{151} (α, 3n) 44 MeV Gd^{152} (p, n) 11 MeV (m = from metastable state)	[8] [21]
$_{66}Dy$	150	4,21 ± 0,06 (4,35)	ion.chamber	7 ± 2 minutes	e^--capture and β^+				Tb^{159} (p, xn) 100 MeV	[3]
	151	4,06 ± 0,04 (4,19)	ion.chamber	19 ± 4 minutes	e^--capture and β^+					[3]
	152	3,66 ± 0,05 (3,78)	ion.chamber	(2,3 ± 0,2) hours	e^--capture and β^+		≈1,45 years	estimated from reaction yield		[3]
	153	3,48 ± 0,05 (3,59)	ion.chamber	5 ± 0,5 hours	indirect proof for e^--capture		≈13,4 years	- " -		[3]
	154	3,35 ± 0,05 (?)	ion.chamber	13 ± 2 (?) hours	no observed				Gd(α, ...)	[3]
		2,85 ± 0,05 (2,95)	ion.chamber	>10 years, if exists β^+	no observed		≈10^6 years, (within a multiplying factor 3)	- " -	Gd(α, ...) 48 MeV from a sample enriched in Gd^{154}	[9]
$_{67}Ho$	151	4,51 ± 0,02 (4,63)	ion.chamber	35,6 ± 0,4 sec	e^--capture, β^+	0,20 ± 0,05		growth of daughter	Pr^{141} (O^{16}, 6n) 75-137 MeV	[25]
	151m	4,60 ± 0,02 (4,73)	- " -	42 ± 4 sec	- " -	~0,28 (within a factor of 2)		excitation function	- " -	[25]
	152 g or m	4,45 ± 0,02 (4,57)	- " -	52,3 ± 0,5 sec	- " -	0,19 ± 0,05		- " -	Pr^{141} (O^{16}, 5n) 75-137 MeV	[25]
	152 g or m	4,38 ± 0,02 (4,50)	- " -	2,36 ± 0,16 min	- " -	~0,30 (within a factor of 2)		- " -	- " -	[25]
	153	3,92 ± 0,03 (4,03)	- " -	9 ± 2 min	- " -	$(3 \pm 2).10^{-3}$		- " -	Pr^{141} (O^{16}, 4n) 75-137 MeV	[25]
$_{68}Er$	152	4,80 ± 0,02 (4,95)	solid state ion.chamber	10,7 ± 0,5 sec	e^--capture, β^+	$0,90^{+0,05}_{-0,20}$		detection of daughter	Nd^{142} (O^{16}, 6n) 75-151 MeV	[27]
	153	4,67 ± 0,02 (4,82)	- " -	36 ± 2 sec	- " -	$0,95^{+0,05}_{-0,20}$		excitation function	Nd^{142} (O^{16}, 5n) 75-151 MeV	[27]
	154	4,15 ± 0,02 (4,28)	- " -	4,5 ± 1,0 min	-	-		-	Nd^{142} (O^{18}, 4n) 75-151 MeV	[27]
$_{69}Tm$	153	5,11 (5,27)		1,12 sec					Nd^{142} (F^{19}, ...) 190 MeV	[28]
	154	5,04 (5,20)		3,10 sec					- " -	[28]

3. β - d e c a y d a t a

The disintegration energy values of the $\beta^{\pm}$-decays (including electron captures) are contained in tables II, III, IV, V concerning the α - β decay cycles. The data are taken from [10] and [11], as well as from the recent papers (up to about the middle of 1962). When the latter case holds, the source is indicated in the tables. The *Everling, Gove, Lieshout* systematics [13] recently published shows the $\beta^{\pm}$-decay and e^{-}-capture energies vs. mass number for even and odd nuclides respectively. This systematics in some cases makes it possible to estimate the energy released in $\beta^{\pm}$-decay (electron capture) processes, which have not been measured experimentally.

4. C o m p u t a t i o n o f α a n d β d e c a y e n e r g i e s b y m e a n s o f c l o s e d d e c a y c y c l e s

Tables II, III, IV, V allow to compute new energy values from known decay cycles.

The alpha disintegration energies computed from closed decay cycles, containing only experimentally measured disintegration energies, are presented in table VI.

The β-decay energies computed from α - β decay cycles are shown in table VII. Throughout the calculations cycles were used containing only experimental data and occasionally single inter- or extrapolated α-decay energy value from fig. 1.

5. D e p e n d e n c e o f α - d e c a y e n e r g y o n m a s s n u m b e r

Figure 1. shows the decay energies (Q_α) vs. mass number (A).

In the systematics the curves Z = const. and N = const. are drawn in majority through the measured points within the limits of error in order to get a better agreement with the general tendency of the curves. Linearity or at least quasi linearity was accepted as a general tendency, supported by analogy with the behaviour of the corresponding curves in the region of heavy nuclides (far from magic numbers).

In one single case - that of Nd^{149} - the curves are drawn beyond the limits of error. This was suggested by experimental evidences. The decay cycle - from which the β^--decay energy of Nd^{149} was computed - contains the β^--decay energy of Ce^{145}. We accepted the value 2,0 ± 0,1 MeV for this energy given in [10] and [11], while paper [20] gives 2,6 ± |≤0,5| MeV for it. Therefore it is probable that the α-decay energy of Nd^{149} is lower than 0,81 MeV.

The effect of the magic number N = 82 is evident from fig. 1. For a given atomic number the α-decay energy increases gradually as the number of neutrons decreases down to N = 84 and then there is a sharp cut off. See cases of Pr_{83}^{142}, Nd_{83}^{143}, Sm_{83}^{145}, Eu_{83}^{146} and Eu_{82}^{145}, Gd_{82}^{146} respectively.

It is also clear that passing on from atomic number 64 to 65 the α-decay energy increases more rapidly than it generally does, this fact is related to a closed

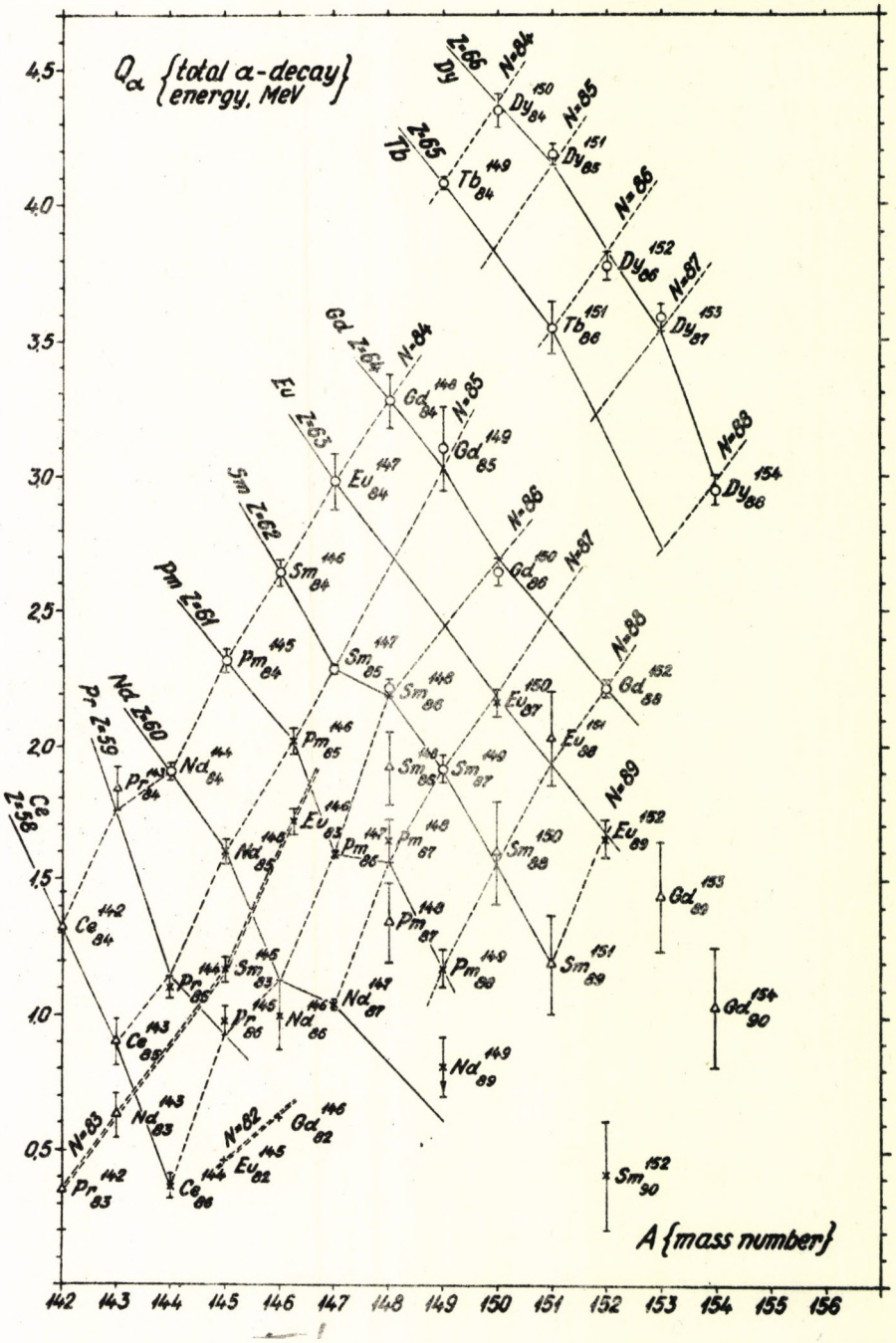

Figure 1. The total α-decay energy (Q_α) in function of the mass number of the parent nuclide. Table of symbols:

- o experimentally measured value,
- x value computed from experimental data on the basis of α - β decay cycles (only those are presented which have an error ≤200 keV),
- Δ value gained from mass data (see [11]), (also only those which have an error ≤200 keV).
- \+ Q_α computed from α - β decay cycle containing also an inter- or extrapolated value gained from β-systematics [13] besides the experimental data.

——— connects the values belonging to the same atomic number,

------ connects the values belonging to the same neutron number.

Tables II, III, IV, V.

α - β decay cycles in the rare earth region. Explanation of the symbols written after decay energies:

e experimental value,
ecc value computed from decay cycle containing only experimental data,
m value gained from mass data having an error ≤200 keV,
mcc value computed from decay cycle containing also a decay energy calculated from mass data besides the experimental ones,
i inter- or extrapolated value on the basis of figure 1.
icc value computed from decay cycle containing also an inter- or extrapolated value on the basis of figure 1. or [13] besides the experimental data.

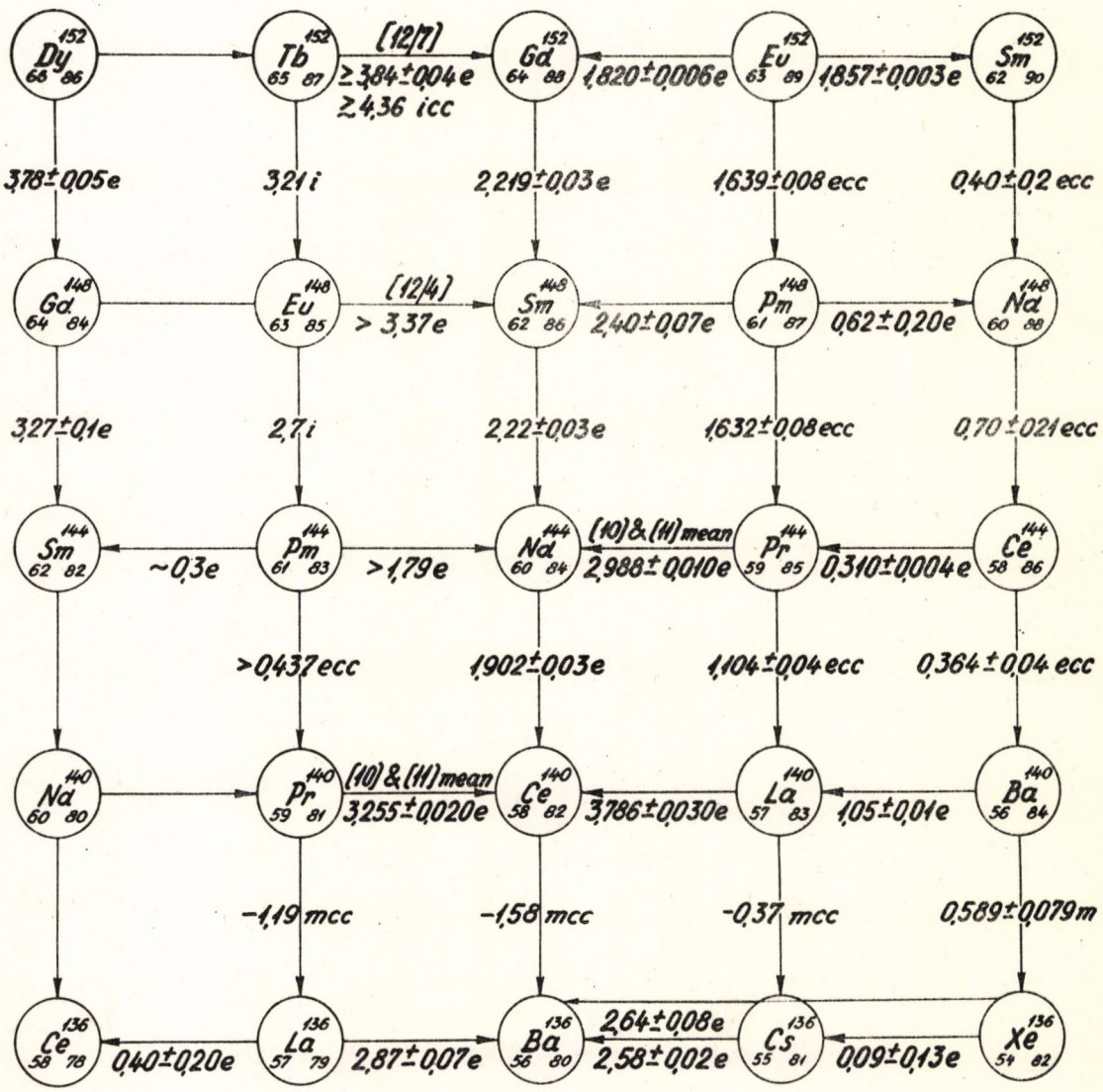

Table III.

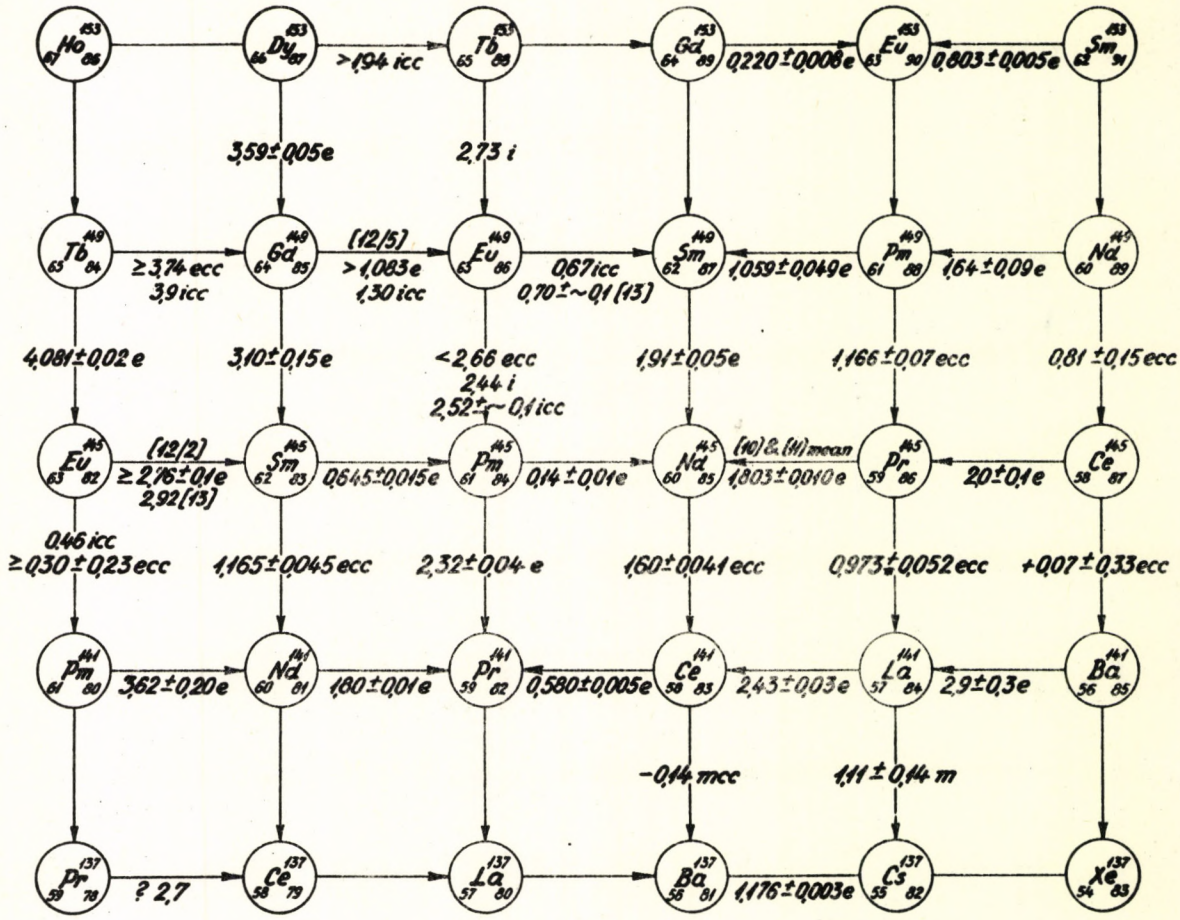

Table IV.

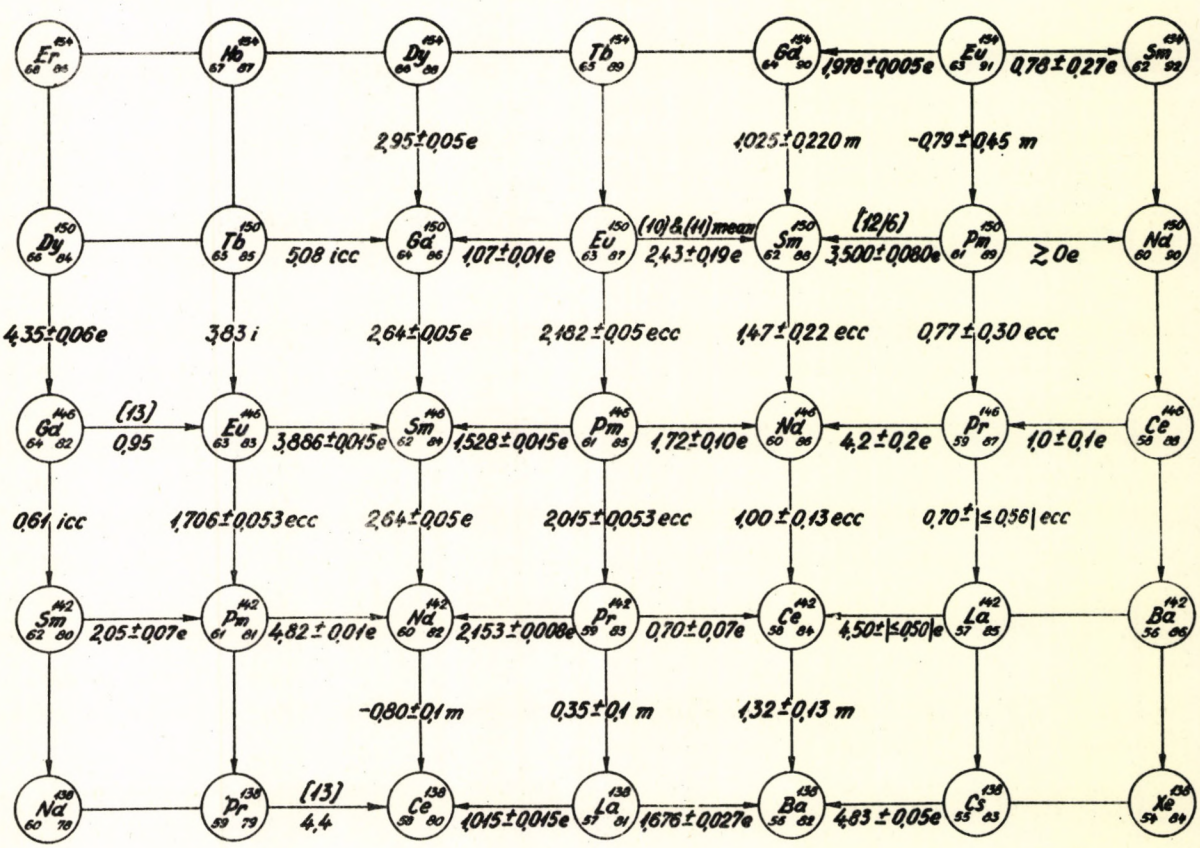

Table V.

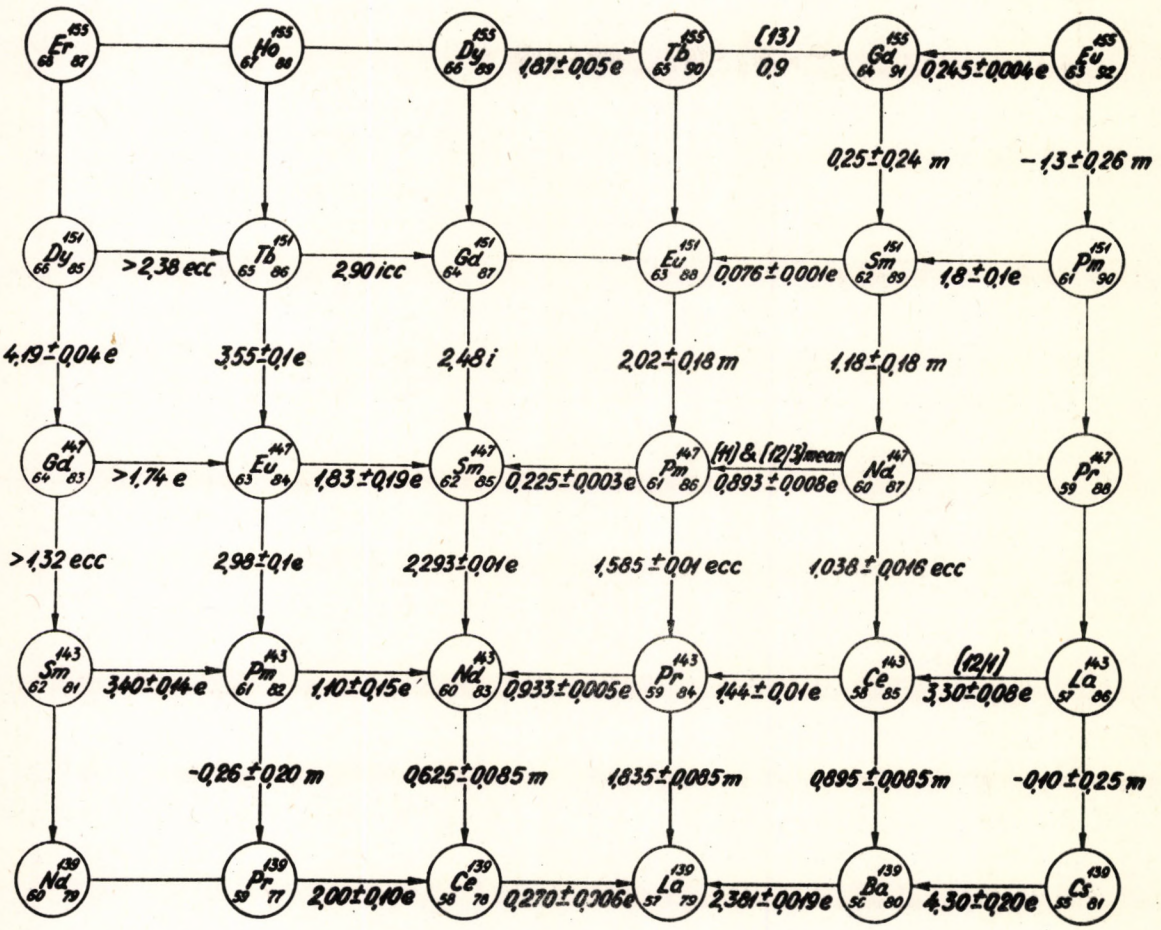

subshell at Z = 64 predicted by the independent particle model. (See for example [14]).

It is surprising that the decay energies of Sm^{152}, Gd^{153} and Gd^{154} are considerably lower than one might expect them to be on the basis of the general tendency. It seems that the disintegration energy decreases essentially in many cases as the neutron number increases from 88 to 90. This effect has already been remarked by *Toth* and *Rasmussen* [3] and the new data support that positively. It is to be noted that *Macfarlane* [24] found 1,5 MeV for the α-decay energy of Dy^{156} having calculated it from the Cameron mass formula. This also confirms the effect mentioned above.

From Fig. 1. some inter- and extrapolated energy data can be got for nuclides, the α-decay of which has not yet been observed or if it has been, the value of α-decay energy has not been measured. The data gained by this method are presented in the second column of table X. In the second place of the same column values of α-decay energies computed from mass data as given by [11] as well as in the third place α-decay energies calculated on the basis of closed decay cycles from proton (neutron) separation energies are also set out. The proton and neutron separation energies are given in [20]. "Decay cycles" constructed by taking separation energy data into account can be found in tables VIII. and IX. The last method of computation was carried out only in cases where we gained an energy value also by other methods*. Finally there are data in table X. calculated from α - β decay cycles too.

+ This way of computation was not carried out for other nuclides because of the great errors in separation energies (although these errors seem to be overestimated in many cases).

Table VI.

α-decay energies computed only from experimental data on the basis of α - β decay cycles as well as some data gained from other sources for the purpose of comparison.

Nuclide	Expected α-decay energy		Deviation of the data of 2nd column from the lines in figure 1. (MeV)
	from α-β cycle Q_α (MeV)	from mass data Q_α (MeV) See [11]	
Ce^{144}	0,364 ± 0,04	0,345 ± 0,09	0,0
Ce^{145}	0,07 ± 0,33	-0,095 ± 0,34	- -
Pr^{144}	1,104 ± 0,04	1,075 ± 0,084	-0,04
Pr^{145}	0,973 ± 0,052	0,815 ± 0,16	+0,052
Pr^{146}	0,7 ± |≤0,54|	- -	- -
Nd^{145}	1,60 ± 0,041	1,435 ± 0,16	0 0
Nd^{146}	1,00 ± 0,13	0,975 ± 0,17	-0,12
Nd^{147}	1,038 ± 0,016	0,975 ± 0,084	0,0
Nd^{148}	0,70 ± 0,21	0,415 ± 0,16	- -
Nd^{149}	0,81 ± 0,15	0,925 ± 0,235	+0,2
Pm^{144}	/~0,647/ >0,437	- -	- -
Pm^{146}	2,015 ± 0,053	1,995 ± 0,1	0,0
Pm^{147}	1,585 ± 0,01	1,515 ± 0,084	0,0
Pm^{148}	1,632 ± 0,08	1,335 ± 0,15	+0,075
Pm^{149}	1,166 ± 0,07	1,275 ± 0,2	0,0
Pm^{150}	0,77 ± 0,3	1,21 ± 0,49	- -
Sm^{145}	1,165 ± 0,045	- -	0,0
Sm^{150}	1,47 ± 0,22	1,595 ± 0,19	- -
Sm^{152}	0,40 ± 0,2	0,365 ± 0,18	- -
Eu^{145}	≥0,30 ± 0,23	- -	- -
Eu^{146}	1,706 ± 0,053	- -	0,0
Eu^{149}	<2,66	- -	- -
Eu^{150}	2,182 ± 0,05	2,305 ± 0,17	-0,03
Eu^{152}	1,639 ± 0,08	1,615 ± 0,175	-0,03
Gd^{147}	>1,32	- -	- -

Table VII.

Electron capture and β^+-decay energies computed from closed decay cycles

Nuclide	Type of decay	Q_β from decay cycles based on experimental data only (MeV)	Q_β from decay cycles containing beside the experimental data a single inter- or extrapolated Q_α (MeV)	Q_β from systematics [13] (MeV)
Eu^{149}	e^--capture or β^+		0,67	0,70
Gd^{149}	- " -		1,30	- -
Tb^{149}	- " -	≥3,74	3,9	- -
Tb^{150}	- " -		5,08	- -
Tb^{151}	- " -		2,90	- -
Tb^{152}	- " -		>4,36++	- -
Dy^{151}	- " -	>2,38		- -
Dy^{153}	- " -		1,94	- -

6. Dependence of half-life on the disintegration energy

It is known that the connection between half-life and decay energy for the ground state transition of even-even nuclides is given by the equation

$$\log T_\alpha = A + \frac{B}{\sqrt{Q_\alpha}} \quad , \qquad /1/$$

where the coefficients A and B are functions of atomic number only. For this reason in the region of heavy nuclei they usually connect the points belonging to the same Z when plotting the function $T_\alpha = f(Q_\alpha)$. This method of plotting does not seem to be suitable in the medium heavy region because there are only a few isotopes belonging to the same atomic number and having known α-partial half-life. (Even the known half-life values are not too reliable.)

Recently *Taagepera* and *Nurmia* [15] suggested an approximate formula, derived from the α-decay theory of quantum mechanics, which gives explicitly the Z dependence of the coefficients A and B. According to this formula for the transition between the

++ The decay energy of Eu^{148} in systematics [13] is about 3,4 MeV, while the experimental value is >3,37 MeV. It seems therefore that the true value of the decay energy of Tb^{152} does not exceed the calculated one very much, they are probably equal.

Table VIII.

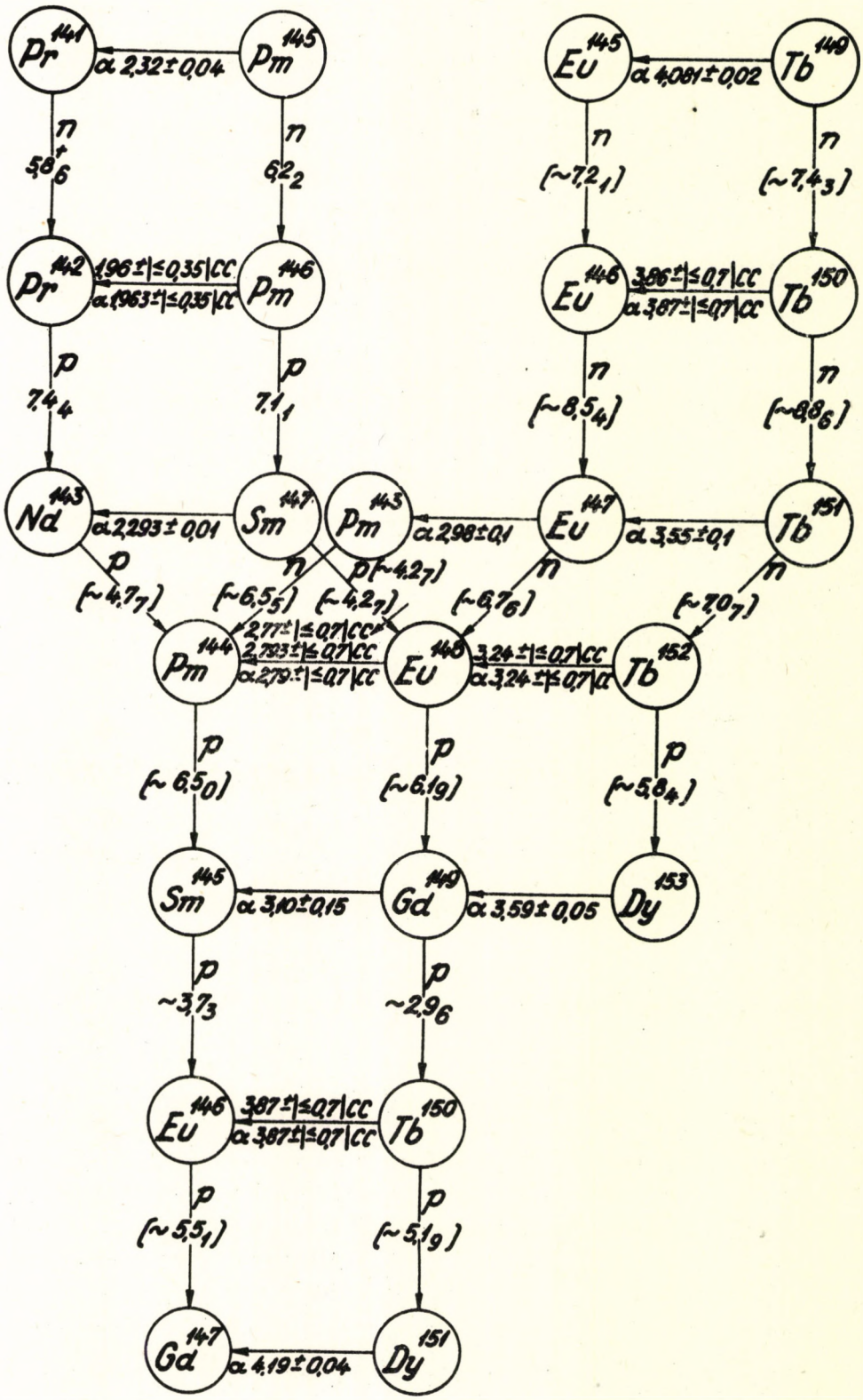
Pr 141
α 2,32±0,04
Pm 145
n
5,8 t 6
n
6,2 2
Pr 142
1,96±|≤0,35|cc
α 1,963±|≤0,35|cc
Pm 146
p
7,4 4
p
7,1 1
Nd 143
α 2,293±0,01
Sm 147
Pm 143
α 2,98±0,1
Eu 147
α 3,55±0,1
Tb 151
p
(~4,7 7)
n
(~6,5 5)
p (~4,2 7)
n
(~6,7 6)
n
(~7,0 7)
Pm 144
2,77±|≤0,7|cc
2,783±|≤0,7|cc
α 2,79±|≤0,7|cc
Eu 148
3,24±|≤0,7|cc
α 3,24±|≤0,7|α
Tb 152
p
(~6,5 0)
p
(~6,1 9)
p
(~5,8 4)
Sm 145
α 3,10±0,15
Gd 149
α 3,59±0,05
Dy 153
p
~3,7 3
p
~2,9 6
Eu 146
3,87±|≤0,7|cc
α 3,87±|≤0,7|cc
Tb 150
p
(~5,5 1)
p
(~5,1 9)
Gd 147
α 4,19±0,04
Dy 151
Eu 145
α 4,081±0,02
Tb 149
n
(~7,2 1)
n
(~7,4 3)
Eu 146
3,86±|≤0,7|cc
α 3,87±|≤0,7|cc
Tb 150
n
(~8,5 4)
n
(~8,8 6)

Table VIII. and IX.

Computation of α-decay energies using proton and neutron separation energies [20] on the basis of closed decay cycles.
Table of symbols:

*	experimental value,
+	experimental value corrected within the error,
( )	estimated value,
	a value without mark: computed value,
cc	value computed from cycle.

Errors: the last numeral written below: 0,04< ≤0,25,
- " - and ~ : 0,25< ≤0,50.

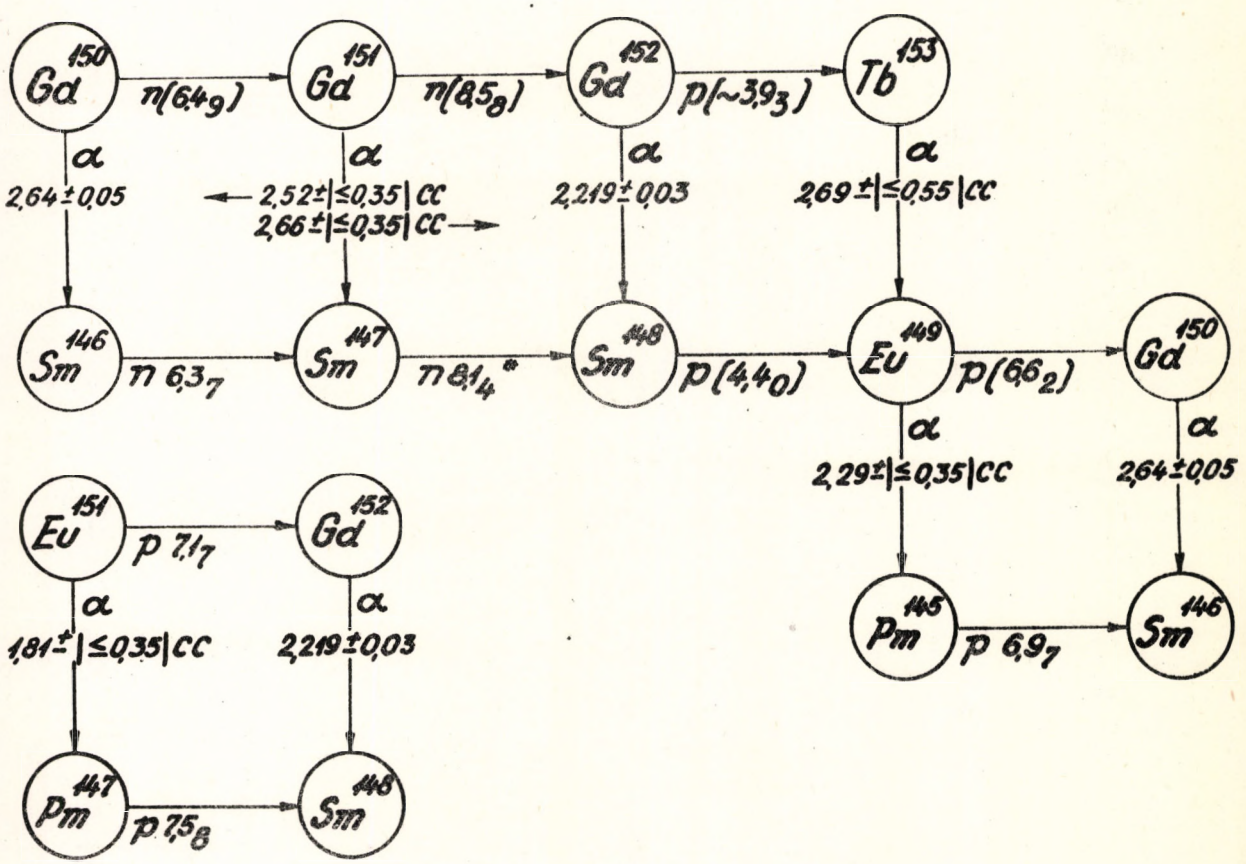

ground states of even-even nuclei we have

$$\log T_\alpha = C + D\,[\frac{Z_d}{\sqrt{E}} - Z_d^{2/3}], \qquad /2/$$

where C and D are constants independent of the atomic number,.

T_α = partial half-life of α-decay,
Z_d = atomic number of daughter nucleus,
E = kinetic energy of α-particle.

In figure 2. there are presented the values of Q_α and T_α known for rare

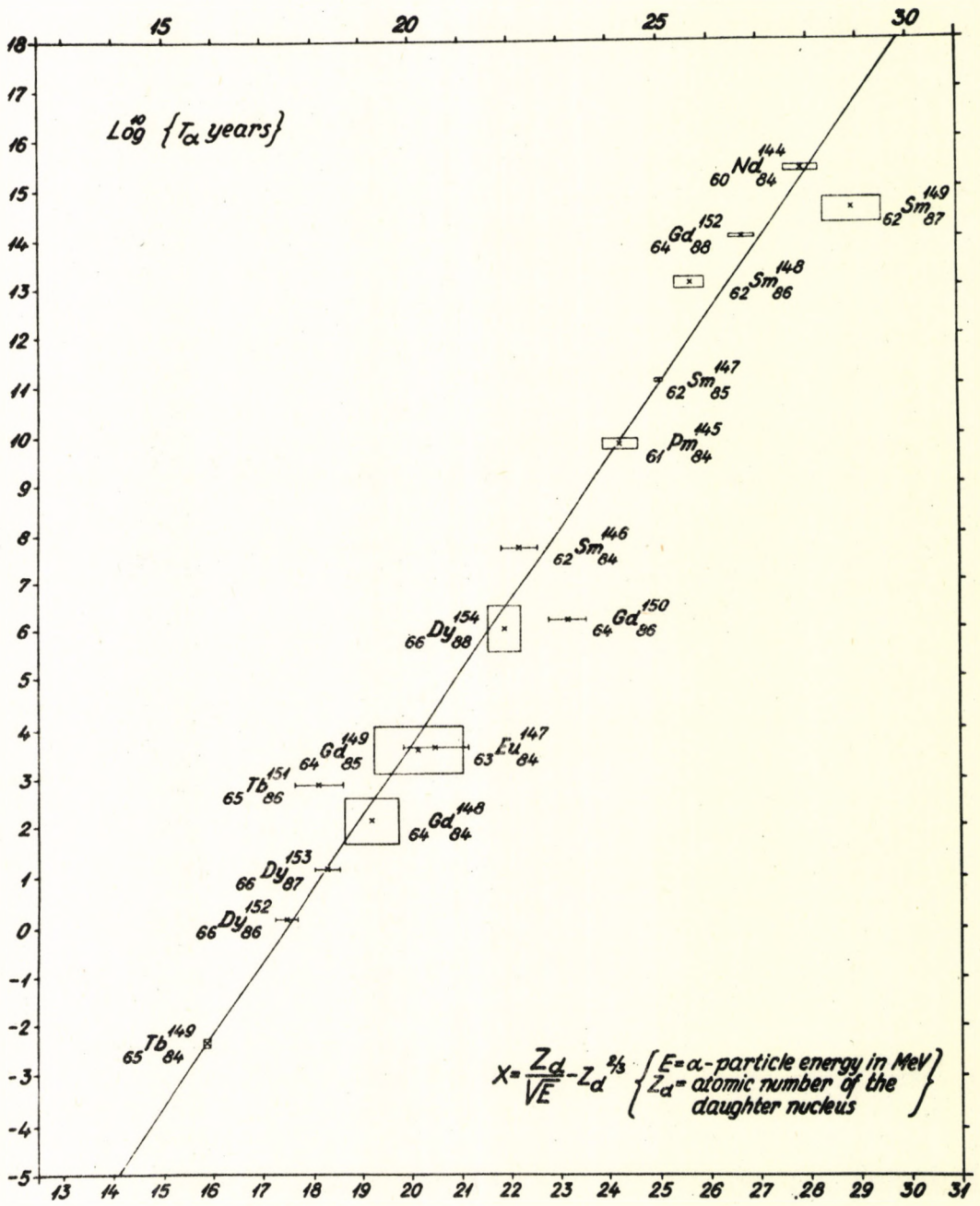

Figure 2. Relation between the logarithm of α partial half-life and α particle kinetic energy of rare earth nuclides. Z_d is the atomic number of daughter nucleus. The straight line connects the data of even-even nuclides (see formula [2]). Only experimentally measured data are presented in the figure.

earth nuclides, and the points representing the data of even-even nuclides are connected by a straight line.

There are four nuclides whose data deviate considerably from this line: Sm^{148}, Sm^{149}, Gd^{150} and Tb^{151}.

As for the data of Sm^{148} we refer to paper [7]. The kinetic energy of the α-particle - given by this paper - seems to us for some reason too high. First, it does not fit the decay systematics of figure 1., second, it is much greater than the value gained from mass data, third, the Q_α of Pm^{148} calculated from the closed decay cycle containing Q_α of Sm^{148} is also higher than Q_α of Pm^{148} computed from mass data and it does not fit the systematics too. If we had decreased the Q_α value of Sm^{148} then X would be increased and so the fit would be better, although - according to reference [5] - T_α is also greater than that of [7], to be more exact $T_\alpha > 2.10^{14}$ years.

We took 4.10^{14} years for the partial half-life of Sm^{149} as given in [7]. If $T_\alpha > 1.10^{15}$ years had been accepted - given by [5] - the fit would have been better.

The kinetic energy of Gd^{150} according to reference [3] is $2,7 \pm 0,15$ MeV, while according to ref. [19] this is $2,53 \pm 0,05$ MeV. The value we accepted was the mean of these weighted by the reciprocal square of errors. Ref. [3] gives $T_\alpha \approx 3.10^5$ years and [19] gives $T_\alpha = 3.10^6$ years. There is no reference to the errors in either paper but in both cases the half-lives are probably approximate ones as indicated by symbol $\approx$ in paper [3], and by the remark of [19], which is only a preliminary report, that the more exact results will be published later.

As for the case of Tb^{151} the α-decay is likely hindered which is the more probable because the number of protons in this nucleus is odd. The logarithmic hindrance factor H will then be in the case of Tb^{151}

$$H = log^{10} \frac{T_{experimental}}{T_{predicted}} = 2,88 - 0,92 = 1,96 ,$$

where $T_{predicted}$ is the value given by the straight line in figure 2.

The data of the other nuclides either fit the straight line within the limits of error or their H value is lower than 0,8.

Heavy even-even nuclides containing protons or neutrons of magic number +2 or a little more, exhibit higher half-life than indicated by the general tendency. (See e.g. Po^{214}_{130}, Po^{212}_{128} in [16]). This fact is probably connected with the sharp change in nuclear radius taking place by the process of α-decay. We disregarded this effect in the medium heavy region when plotting the line of fig. 2. for two causes. First, in the region of the rare earth there is but one single neutron magic number, 82, influencing the α-decay, the number of protons is not magic and a smaller diviation from the general tendency in the nuclear radius and half-life can be expected than in the case of the Po isotopes mentioned above. Second, the known energy and half-life data in the rare earth region are not precise enough to get an altering beyond the limits of error, when taking into account this effect.

It can be seen from table I. that Dy^{150} and Dy^{151} have experimentally measured decay energies but their α-partial half-lives are unknown. We computed also

these half-lives on the basis of fig. 2., and of data [3]. The results are presented at the end of table X.

Basing on the line in fig. 2. we estimated, what α-partial half-lives are to be expected for rare earth nuclides, the α-decay of which has not yet been observed or, if it has been, the α-decay energy or the partial half-life has not measured. The results can be seen in table X.

The supposition of an essential hindrance not arising by α-decay is justifiable but for transitions between the ground states of even-even nuclei. For nuclides of odd mass number the only thing to be expected is that H does not surpass the value 1,5. This suggestion is based on analogy between heavy nuclides having a proton number 82 + 2, 3, 4, 5 (and neutron number >127) and nuclides having a neutron number 82 + + 2, 3, 4, 5 (and proton number also far from the magic). Indeed, using data measured spectrometrically the logarithmic hindrance factor does not surpass the value 1,5 and in most cases it is even below 1. See [2], p. 122. This suggestion is supported by the work [15] of *Taagepera* and *Nurmia* too, who concluded, on the basis of generally accepted and rather precise-looking experimental data, that for nuclei far from magic numbers the value of H rarely surpasses 1,2.

Here "nucleus far from magic number" means such nucleus the proton and neutron number of which are beyond the environment ±1 of any magic number.

Paper [15] presents the mean logarithmic hindrance factors (H) of 71 nuclides whose Z and N are far from the magic numbers in the above sense. Taking $H = 0$ for even-even nuclides we get

	mean H	
Z odd, N even	0,38	
Z even, N odd	0,16	/3/
Z odd, N odd	0,69	

Column 5. of table X. shows the α-partial half-lives for each type of nuclides gained by supposing hindrance [3].

It is to be noted that for nuclides presented in table X. there are no known spin values except in a few cases.

In column 5. of table X. the errors of the predicted α-partial half-lives arise from three sources.

First, there is a contribution from the error of the approximate decay energy. For example in the case of Eu^{148} attributing an error ±0,1 MeV to the value Q_α

Table X.

The expected parameters of α-activity from atomic number 60 to 66 and from neutron number 84 to 88*. In this table are presented only those nuclides having an expected α-decay energy greater than 1,8 MeV+ and the α-partial half-life and α-decay energy of which has not yet been measured experimentally (except the cases of Dy^{150} and Dy^{151} where the α-decay energies are known).

* Beyond this region the estimation is rather uncertain.

\+ At present this value seems to be the lowest limit of detectability.

1.	2.	3.	4.	5.
Nuclide	Ground of calculation of energy data	The expected: total energy of α-decay Q_α (MeV)	The expected: log T_α taking into account no hindrance (T_α in years)	The expected: T_α partial half-life (in years) taking into account average hindrance given by [3]
$_{65}Tb^{150}_{85}$	fig. 1.	3,83 ± /~0,1/	-0,87	6,7 10^{-1}
	mass data			
	separation energy	3,87 ± |≤0,7|	-1,15	3,5 10^{-1}
	α – β cycle			
$_{65}Tb^{152}_{87}$	fig. 1.	3,22 ± /~0,1/	3,42	1,3 10^{4}
	mass data			
	separation energy	3,24 ± |≤0,7|	3,28	0,93 10^{4}
	α – β cycle			
$_{65}Tb^{153}_{88}$	fig. 1.	2,73 ± /~0,1/	7,95	2,1 10^{8}
	mass data			
	separation energy	2,69 ± |≤0,55|	8,35	5,4 10^{8}
	α – β cycle			
$_{64}Gd^{151}_{87}$	fig. 1.	2,48 ± /~0,1/	10,1	170 10^{8}
	mass data			
	separation energy	2,59 ± |≤0,35|	8,8	9,1 10^{8}
	α – β cycle			
$_{63}Eu^{148}_{85}$	fig. 1.	2,69 ± /~0,1/	7,1	56 10^{8}
	mass data			
	separation energy	2,78 ± |≤0,7|	6,14	6,8 10^{8}
	α – β cycle			
$_{63}Eu^{149}_{86}$	fig. 1.	2,44 ± /~0,1/	9,9	17 10^{9}
	mass data			
	separation energy	2,29 ± |≤0,35|	11,8	1400 10^{9}
	α – β cycle			
	(See [13], Q_β interpol.)	2,52 ± /~0,1/	8,91	2 10^{9}
$_{63}Eu^{150}_{87}$	fig. 1.	2,19 ± /~0,1/	13,1	66 10^{12}
	mass data	2,305 ± 0,17	11,5	1,7 10^{12}
	separation energy			
	α – β cycle	2,182 ± 0,05	13,2	78 10^{12}
$_{63}Eu^{151}_{88}$	fig. 1.	1,93 ± /~0,1/	17,2	360 10^{15}
	mass data	2,025 ± 0,180	15,6	9,1 10^{15}
	separation energy	1,81 ± |≤0,35|	19,3	46000 10^{15}
	α – β cycle			
$_{61}Pm^{146}_{85}$	fig. 1.			
	mass data	1,995 ± 0,1	14,5	14 10^{14}
	separation energy	1,96 ± |≤0,35|	15,0	49 10^{14}
	α – β cycle	2,015 ± 0,053	14,2	6,9 10^{14}
$_{66}Dy^{150}_{84}$	experimental	4,35 ± 0,06	-3,36	4,37 10^{-4}
$_{66}Dy^{151}_{85}$	experimental	4,19 ± 0,04	-2,54	4,17 10^{-3}

taken from figure 1., we get $\Delta log^{10} T_\alpha = \pm 1,1$, i.e. an error a little more than an order of magnitude. This error is decreased because of the possibility of computing T_α from Q_α values got by different methods.

Second, the estimation of T_α is influenced by the uncertainty in drawing the straight line of fig. 2. through the experimental points for even-even nuclides. The experimental data deviate from this line not more than by a value $\Delta log\ T_\alpha = \pm 0,8$ apart from the four nuclides mentioned above (Sm^{148}, Sm^{149}, Gd^{150}, Tb^{151}) which cases are more or less explainable.

Finally, a hindrance fluctuation can take place in the case of nuclides of table X., although the mean hindrance was taken into account by [3]. The mean hindrance is of course of an approximate character, nevertheless, it is probable that the error because of the hindrance is $\Delta log^{10} T_\alpha < 1,2$.

If all these are taken into account we have an error $\approx (\pm 1,5)$ for the values $log^{10} T_{\alpha mean}$.

7. Concluding remarks

Although some advances have been made in the α-spectroscopy of neutron deficient rare earth nuclides (the α-spectrum of some 27 nuclides were measured) still many nuclides exist the disintegration energy and half-life of which are in the measurable region, but their α-decay have not been detected.

One of the main difficulties - if one uses an ionization pulse chamber - is the fact that the value of the branching ratio ($\frac{\alpha}{\text{total}}$ decay ratio) is very small in many cases. The expected value of the branching ratio is $\lesssim 10^{-9}$ for the majority of nuclides in table X. which makes difficult, and in some cases, even impossible to carry out measurements by means of an ionization chamber.

A significant development can be expected in this region by using electromagnetic "giant" spectrometer where the electron capture or β^+-decay have but a very small disturbing effect. If the source area is some cm^2, the effective solid angle is about 10^{-3} of 4π and the source thickness is some-fold 10 $\mu g/cm^2$, then up to $T_\alpha \approx 10^{10}$ years the α-partial half-life is measurable. It can be seen from table X. that many α-partial half-lives are below the above mentioned limit.

Remark

Reports on Ho [25], Er [27], Tm [28] and some Eu and Gd [26] isotopes were brought to our knowledge only after despatching the paper for publication. The data of [25], [26], [27] and [28] are presented in table I., but otherwise were not put into use.

The authors are very much indebted to *Professor A. Szalay* for interest in this work.

References

[1] *T.P. Kohman:* Phys. Rev., *76*/1949/448.

[2] Experimental Nuclear Physics, editor Segré, *III.* Vol., 1959, p. 65. New York, J. Wiley & Sons.

[3] *K.S. Toth - J.O. Rasmussen:* Nucl. Phys., *16*/1960/474.

[4] *W. Kunz - J. Schintlmeister:* Tabellen der Atomkerne, Berlin, Akad. Verlag, 1959.

[5] *R.D. Macfarlane - T.P. Kohman:* Phys. Rev., *121*/1961/1758.

[6] *Воробьев - Комар - Королев - Солякин:* ЖЭТФ, *37*/1959/546.

[7] *M. Karras:* Annales Acad. Sci. Fennicae, Ser. A., *VI.* Physica, No. 65, 1960.

[8] *Olkowsky - Gratot - Le Pape - Cohen:* Nuclear Phys., *12*/1959/159.

[9] *R.D. Macfarlane:* J. Inorg. Nucl. Chem., *19*/1961/9.

[10] *Landolt-Börnstein:* New Series, Group I. Vol. *1*, Springer, Berlin, 1961.

[11] *König - Mattauch - Wapstra:* Nuclear Phys., *31*/1962/18.

[12/1] *Fritze - Kennett - Prestwich:* Can. J. Phys., *39*/1961/662.

[12/2] *Ю.А. Александров - М.К. Никитин:* Изв. АН СССР, сер. физ. *25*/1961/1176.

[12/3] *R.P. Sharma* et al.*:* Phys. Rev., *125*/1962/2071.

[12/4] *K. Sugiyama:* J. Phys. Soc. Japan, *17*/1962/264.

[12/5] *Prask - Reidy - Funk - Mihelich:* Nucl. Phys., *36*/1962/441.

[12/6] *N.B. Gove:* Bull. Am. Phys. Soc., Ser. *II.*, 7/1962/352, XA8.

[12/7] *Громов - Джелепов - Желев - Кудрявцева:* Изв. АН СССР, сер. физ. *25*/1961/1084.

[13] *Everling - Gove - Lieshout:* Beta-Disintegration Energy Charts, Nuclear Data Sheets, NAS-NRC 61-3-142, 1962.

[14] *Nijgh - Wapstra - Lieshout:* Nuclear Spectroscopy Tables, North Holland, Amsterdam, 1959, p. 111.

[15] *R. Taagepera - M. Nurmia:* Ann. Acad. Sci. Fennicae, Ser. A., VI. Physica, No. *78*/1961/1.

[16] *И. Перлман - Дж. Расмуссен:* Альфа-радиоактивность, Москва, 1959, Изд. Иностранной Лит., p. 72.

[17] *R.D. Macfarlane:* Phys. Rev., *126*/1962/274.

[18] *Nurmia - Kauranen - Siivola:* Phys. Rev., *127*/1962/943.

[19] *T. Doke:* Canad. J. Phys., *40*/1962/607.

[20] *M. Yamada - Z. Matumoto:* J. Phys. Soc. Japan, *16*/1961/1497.

[21] *Toth - Björnholm - Jörgensen - Nielsen - Skilbreid - Svanheden:* J. Inorg. Nucl. Chem., *14*/1960/ 1.

[22] *Rasmussen - Thompson - Ghiorso:* Phys. Rev., *89*/1953/33.

[23] *W. Riezler - G. Kauw:* Z. Naturforsch., *14a*/1959/196.

[24] *R.D. Macfarlane:* Natural Alpha Radioactivity in Medium-Heavy Elements (Thesis), NYO-7687, 1959. p. 148. Carnegie Institute of Technology, Pittsburg, Pennsylvania.

[25] *R.D. Macfarlane - R.D. Griffioen:* Phys. Rev., *130*/1963/1491.

[26] *A. Siivola:* Ann. Acad. Sci. Fennicae, Ser. A., VI. Physica, No *109*/1962/1.

[27] *R.D. Macfarlane:* Private communication.

[28] *R.D. Macfarlane:* Bull. Am. Phys. Soc., Ser. II., *8*, No. 4. /1963/387, X5.

A METHOD OF ELIMINATING SUPERPOSED PULSES IN NUCLEAR SPECTROSCOPY AND INVESTIGATIONS ON THE DECAY SCHEME OF Cr-51

Gy. Máthé

Institute of Nuclear Research of the Hungarian
Academy of Sciences, Debrecen, Hungary

1. Introduction

Last year, the Cr-51 nuclid was examined from the viewpoint of nuclear spectroscopy. Its decay scheme had not been fully elucidated in the literature. The problem was as follows.

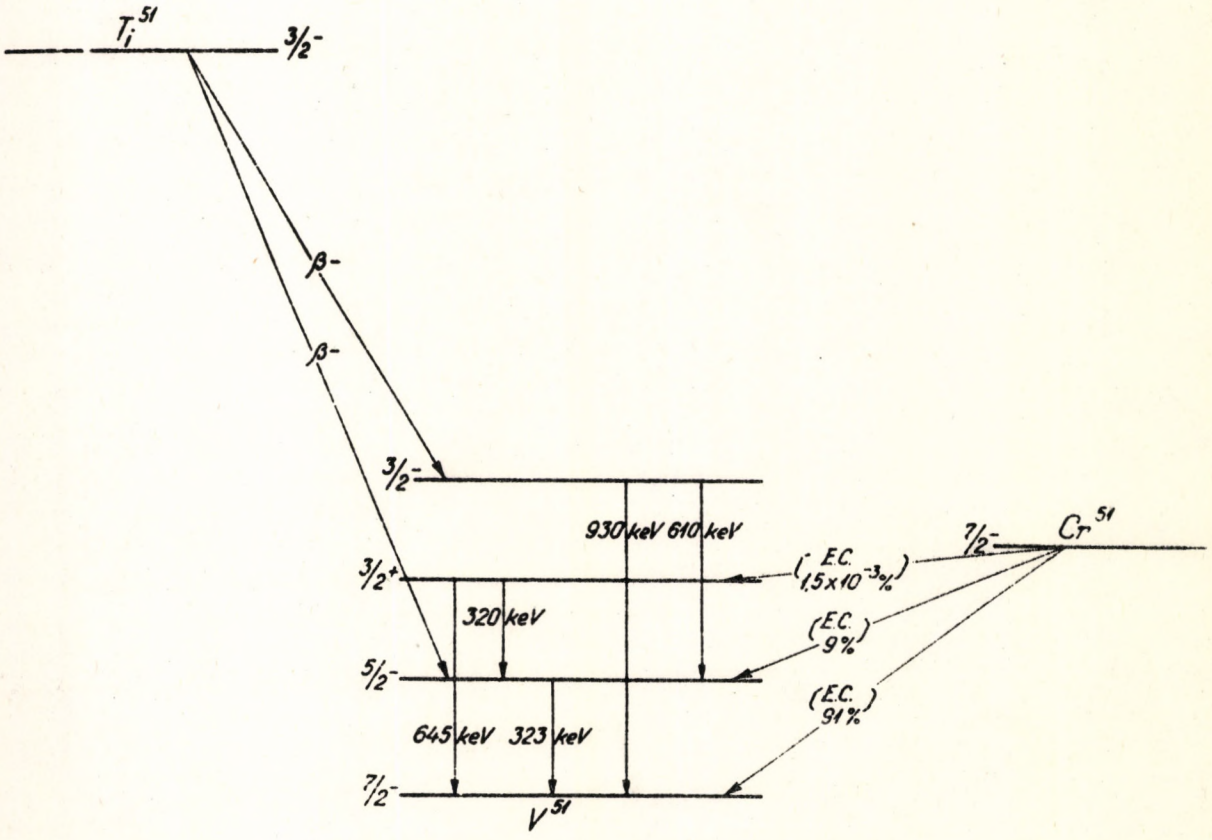

Fig. 1. Decay scheme of Cr-51 (after *Ofer* and *Wiener*)

Several authors investigated the decay scheme of Cr-51 and found an excited level about 646 keV in addition to the familiar one of V-51 at 323 keV [1-4]. According to some of the authors, the nucleus returns from this level to ground level with an intensity of $2,6.10^{-4}$ cross-over transitions per decay [1], other authors claim this value to be 5.10^{-6} [2]. The latter authors have found an additional cascade transition from this level. However, the coincidence spectrum published by them is not unambiguous; this fact was admitted by the authors themselves.

2. Experimental methods

To clear up the problems, a single spectrum of Cr-51 was taken by the scintillation method.

Unfortunately, the spectrum visible in the higher energy ranges is not due to 645 keV gammas but to pulses coming from 323 keV gammas that arrived in a quick succession; as a result, their amplitudes were added together. This effect can be reduced through the use of a source of lower intensity.

In the case of Cr-51 this did not work because at lower source intensities undue long measurement periods were obtained.

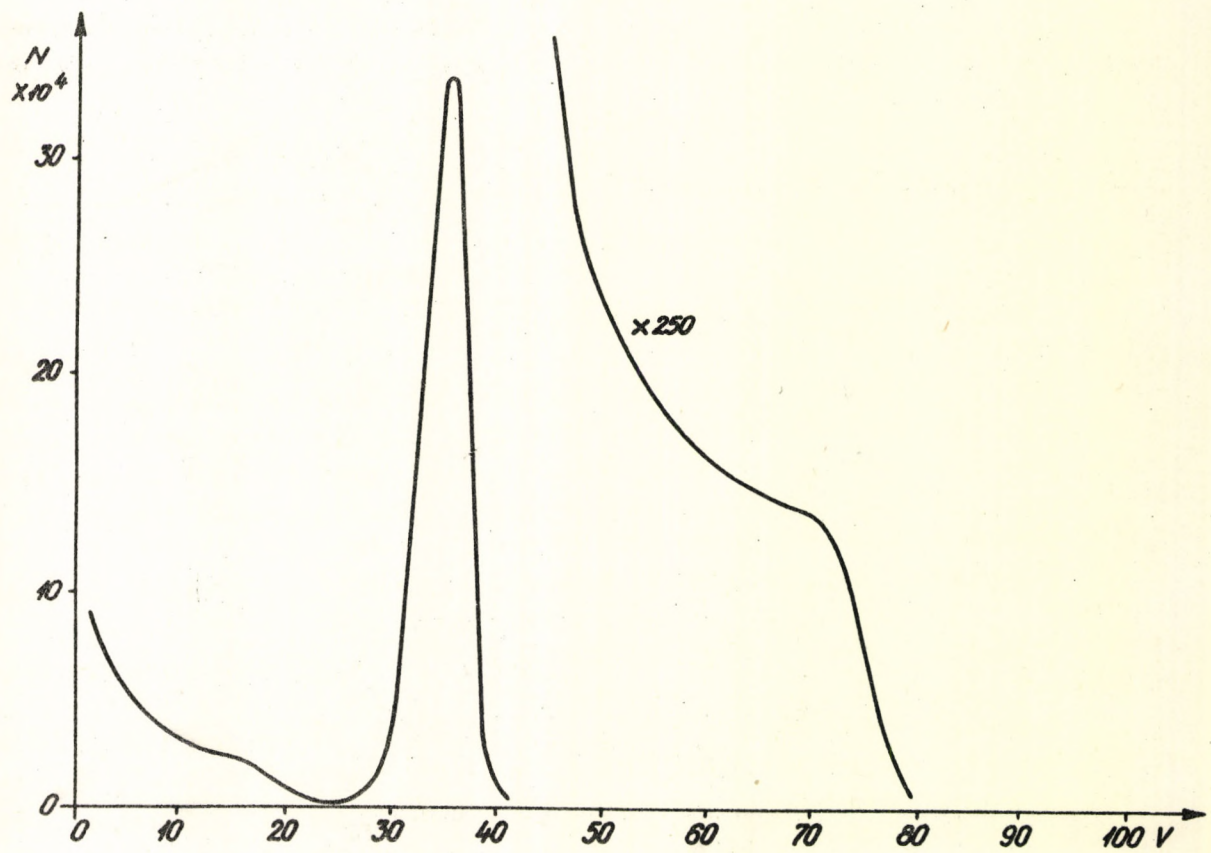

Fig. 2. Scintillation spectrum of Cr-51.

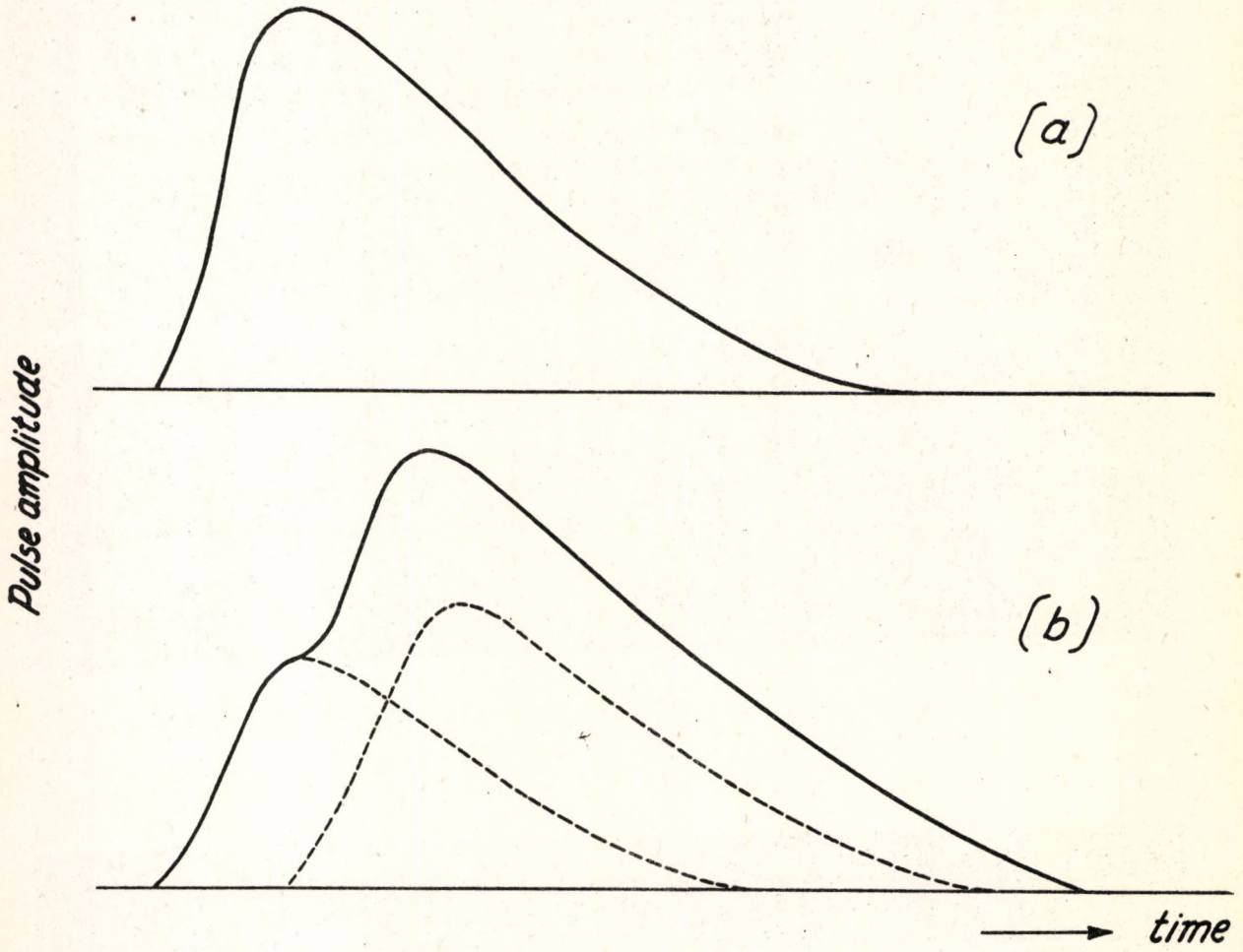

Fig. 3. The scintillation pulse wave-forms, a./ Normal pulse; b./ Pulses superposed within the rise-time.

The problem could be solved in a different way along the following concept: The electric pulses due to the absorption of a single particle are of normal course. The pulse includes a leading portion determined by the decay time of the scintillator and an exponential trailing portion determined by the integrating time constant of the RC component in the multiplier plate circuit. (see Fig. 3/a.)

On the other hand, pulses due to the absorption of two or more particles are distorted (see Fig. 3/b.).

To eliminate those distorted pulses, the following pulse-shape discrimination has been carried out.

The pulses were differentiated by a suitable RC circuit and their phases were inverted. In the cases of normal pulses, each differentiated pulse crosses the time axis at a well defined moment - irrespective of its amplitude (see Fig. 4). In contrast to this, that crossing point always lags with distorted pulses (see Fig. 5).

If a suitable delay is applied, than coincidence can be made between the leading edge and the crossing point of the pulse; consequently, the coincidence device will count only pulses of pre-determined shape - preferably the normal ones.

The following electronic system has been employed for the measurements.

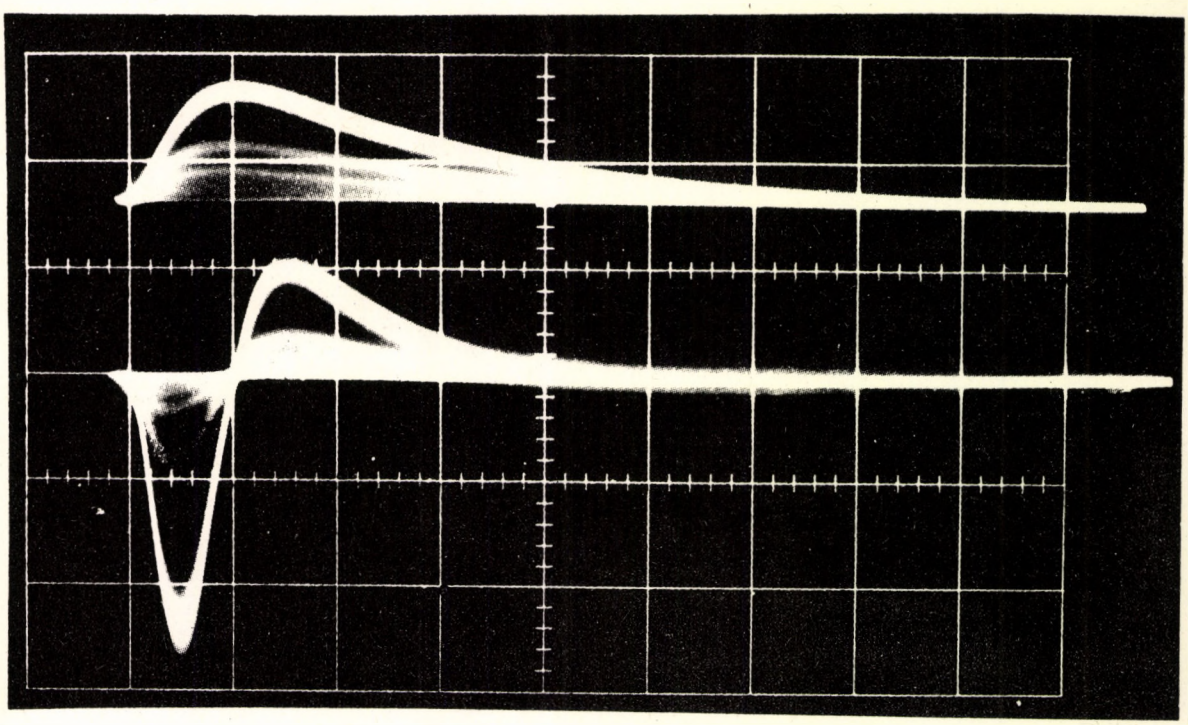

Fig. 4. The normal pulse wave-forms and their differentiated shapes after reversal of signs.

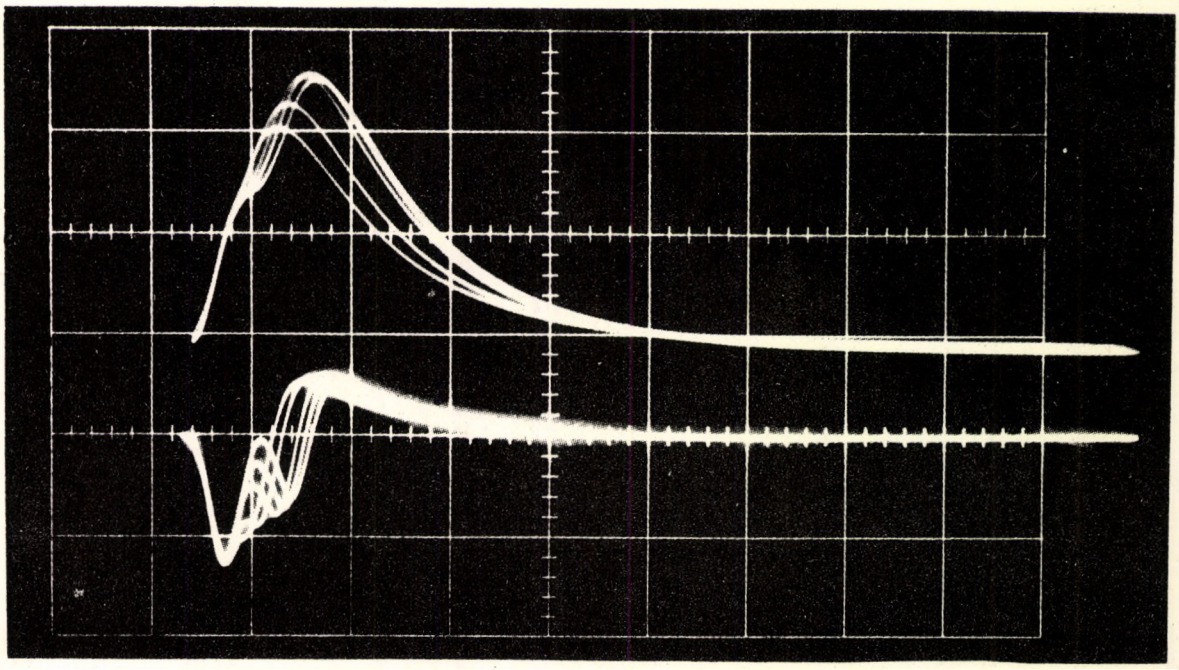

Fig. 5. The superposed pulses wave-forms, and their differenciated shapes after reversal of signs.

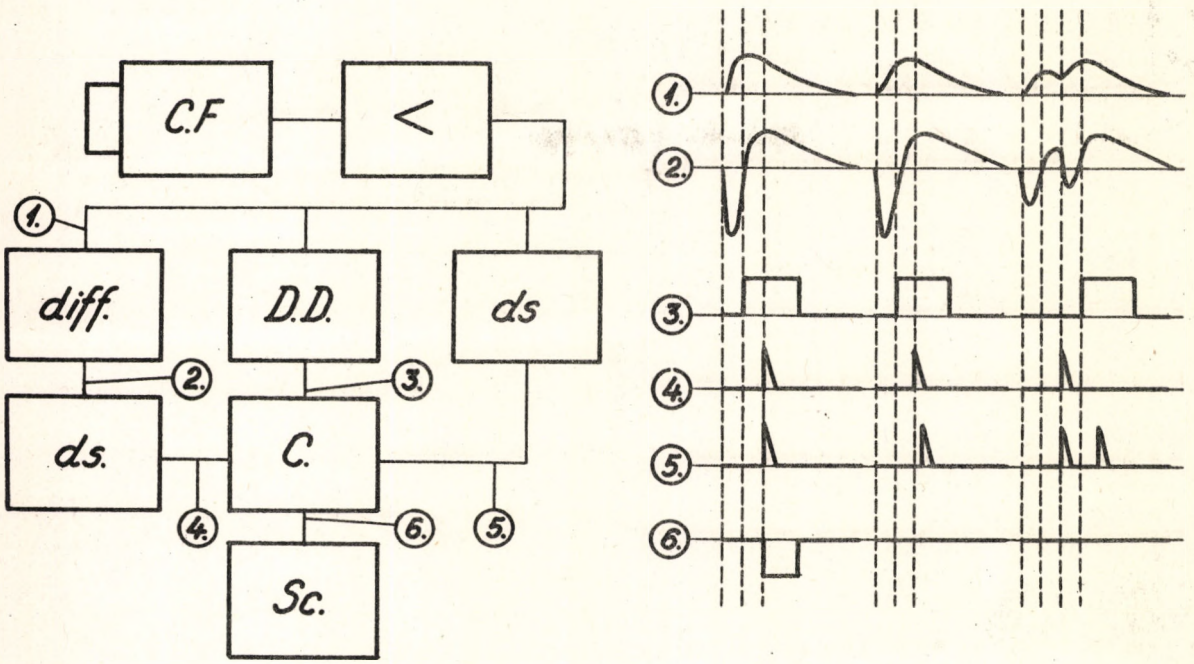

Fig. 6. Block-scheme of the apparatus eliminating pulses arising from superposition, with wave-forms for each point.

The pulses coming from the detector are amplified and then conducted in three different directions. In the middle, they are selected for amplitudes by means of a differential discriminator. In the left-hand arm they are differentiated and their signs inverted. Subsequently using the method known in the fast coincidence technique, the positive part of the pulses are delayed at the place marked "d_s" by a few times 10^{-7} seconds and they are shaped to fit the coincidence circuit. In the right-hand arm, the original pulses are delayed in "d_s" and shaped. Care should be taken to adjust the delays so, that the signals should arrive simultaneously at the fast part of the coincidence circuit, when normal pulses are concerned. Passing under the gate signal of the differential discriminator, the pulses of the fast part deliver pulses for the scaler.

The coincidence circuit employed had a resolving time of 3.10^{-8} sec. When two pulses arrive within 3.10^{-8} seconds, the unit will count them as a single normal pulse. If, however, additional delay is employed in the right-hand arm, the pulses arriving accidentally during the time of resolution of the coincidence circuit can be counted and taken into account - similar to the accidental coincidence numbers.

It should be noted that the "accidental coincidence" spectrum obtained in this way is displaced along the discriminator scale towards lower energies. This is due to the application of delay in which pulses are selected with their component pulses starting at different times; the resultant pulse will thus be smaller than the sum of the two initial pulses.

The extent of the displacement of the "accidental coincidence" spectrum can be determined by means of standard preparates (here Hg-203) in which there is no gamma-transition in the higher energy levels.

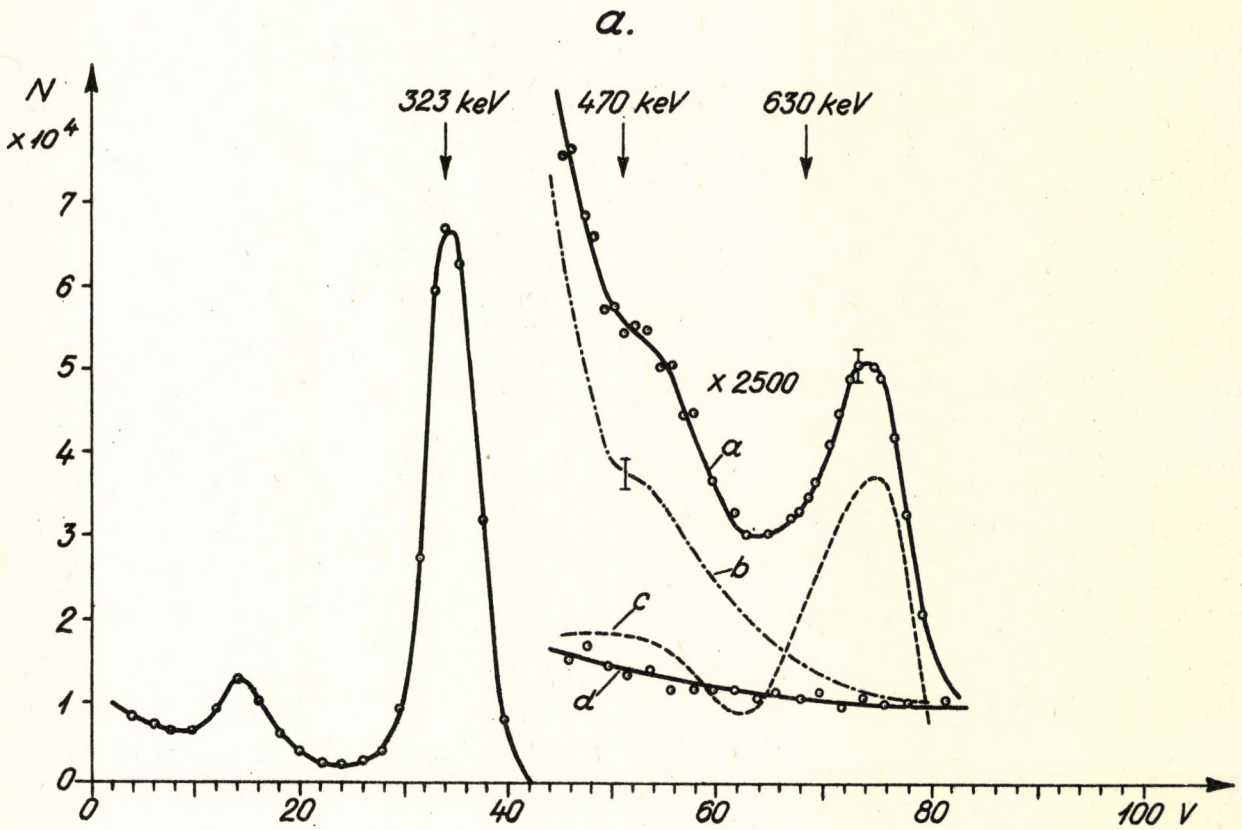

Fig. 7. Spectra of Cr-51 taken by the apparatus eliminating superposition of pulses. Curve a is the uncorrected spectrum, b is the spectrum corrected for superposition, c is the spectrum of superimposed pulses arriving within 3.10^{-8} sec, and d is the background effect. (a) collimated spectrum, (b) summing spectrum.

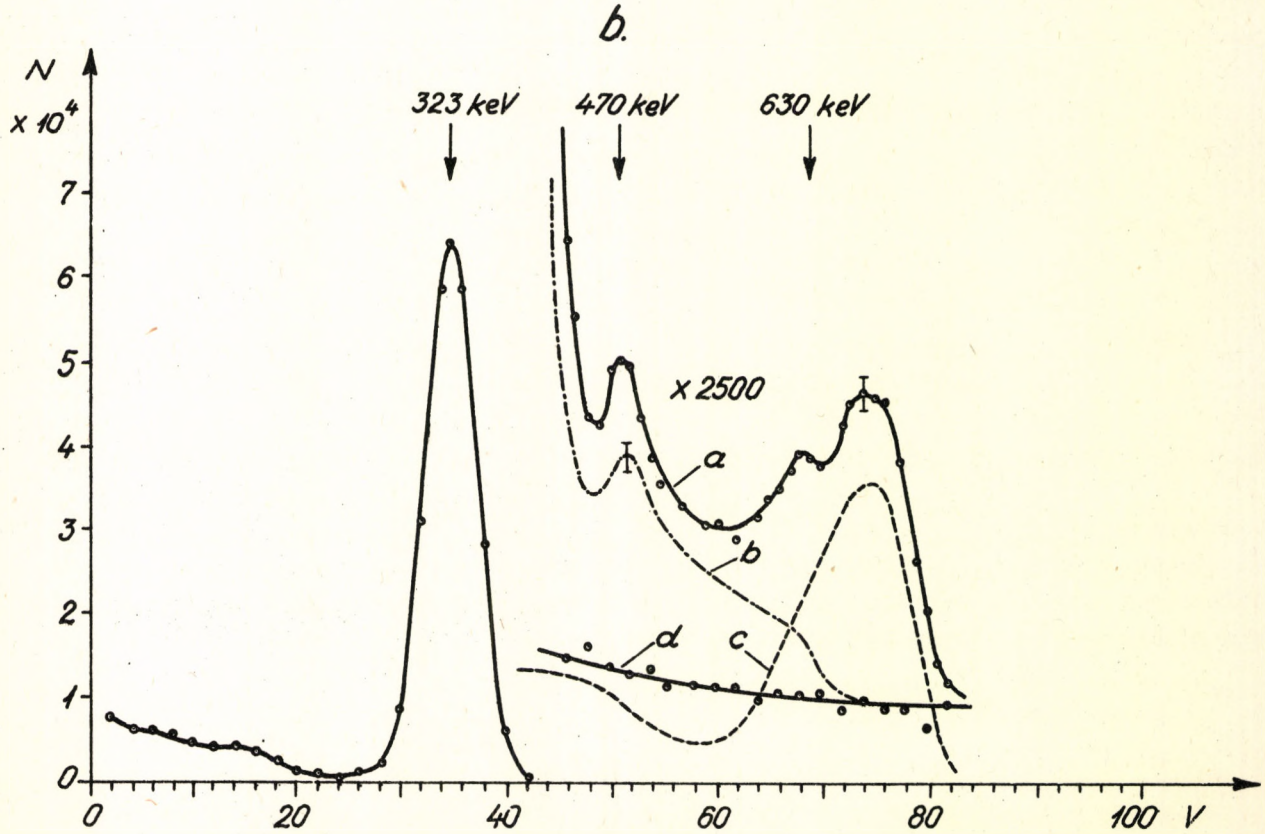

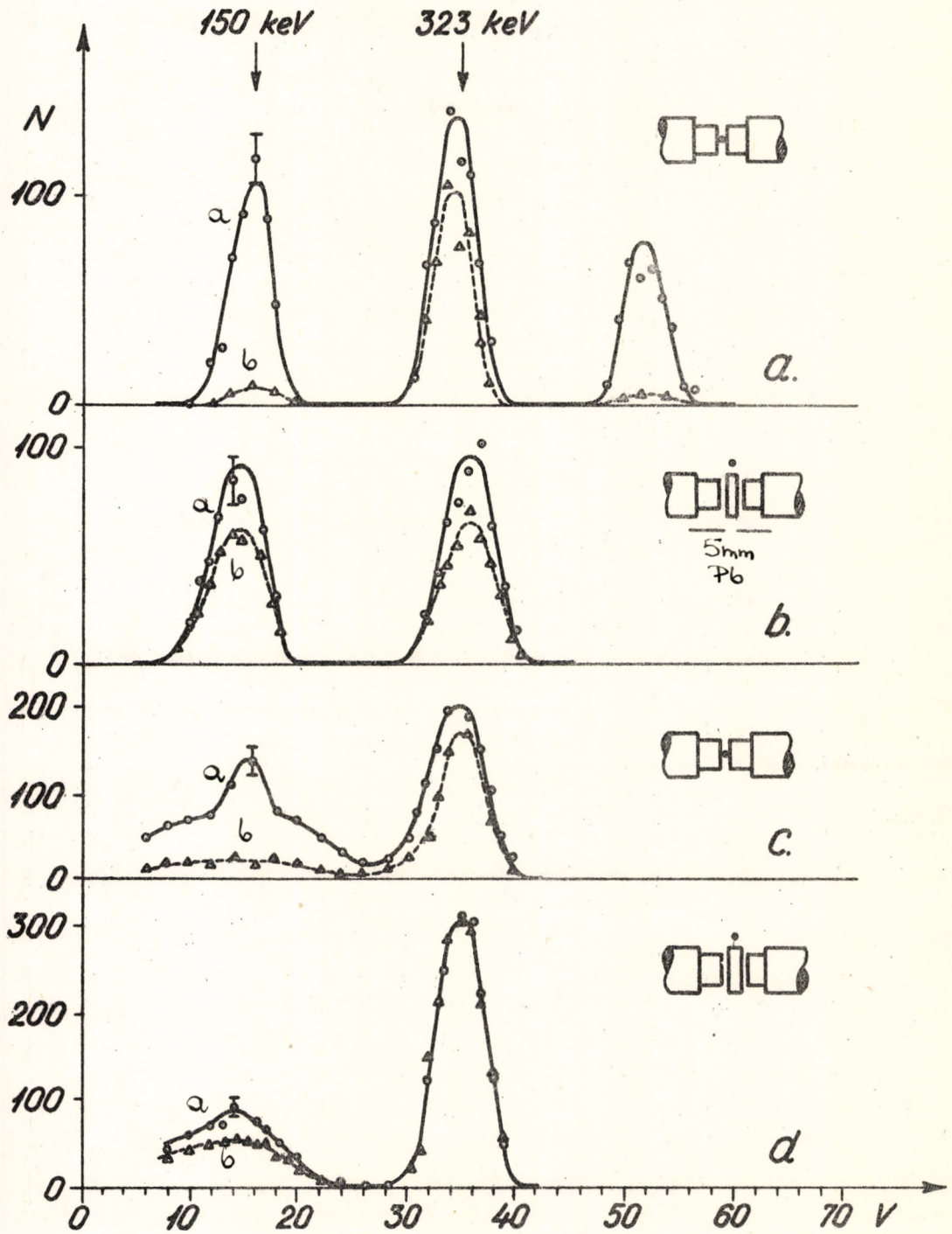

Fig. 8. Coincidence spectra. Sum coincidence spectra. (a) the sum channel is set at 630 keV with no anti-Compton shield. (b) The sum channel is set at 470 keV with anti-Compton shield. Normal coincidence spectra in coincidence with the 323 keV line. (c) without and (d) with an anti-Compton shield. The solid curve disignates the uncorrected results and the dotted curve shows the chance-coincidences.

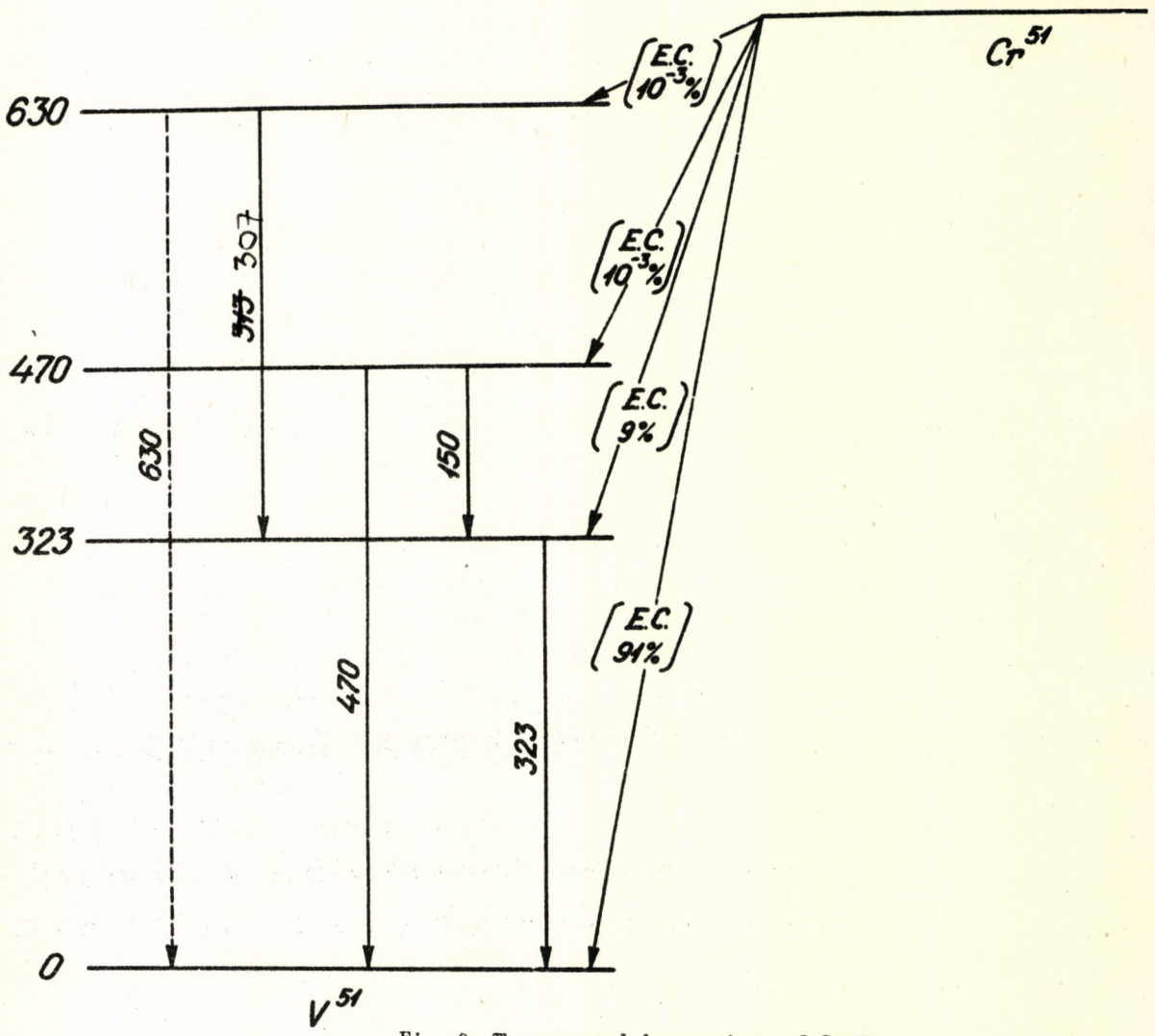

Fig. 9. The proposed decay-scheme of Cr-51.

3. Results

The equipment described above was used to take the collimated and summing spectra of Cr-51 (7/a. and 7/b. respectively).

In the spectra, the curves "a" indicate the amplitude distributions without any correction applied. Curve "d" represents the background, and curve "c" stands for the superposed pulses arrived accidentally within 3.10^{-8} sec. Curve "b" is the difference between curves "a" and "c".

On ground of an analysis of the two spectra, it may be claimed that there is a cascade transition from the 630 keV level. Its intensity is $1,0 \pm 0,4.10^{-5}$ per disintegration. Presumably, there is no cross-over transition from this level; if yet, it cannot have an intensity above 7.10^{-8} per disintegration. A new cascade transition has been found at 470 keV; and parallel with it a cross-over transition also exist. The cascade transition has an intensity of $7,6 \pm 1,3.10^{-8}$, that of the cross-over transition is 3 ± 2.10^{-8}.

The Cr-51 was examined by normal as well as sumcoincidence methods. The coincidence spectra and the measuring geometry employed are shown in Fig. 8.

The curves "a" are representing the results of measurements without correction; curves "b" are the accidental coincidences; 8a and 8b are sum coincidences, while 8c and 8d are normal coincidence measurements. On the basis of an analysis of the single and coincidence spectra, the disintegration scheme of Cr-51 is established as follows (see Fig. 9).

Apart from the familiar excited condition at 323 keV, there is an additional level at 630 keV; hence, the nucleus returns to ground level through a cascade transition of 323 - 307 keV.

A new level needs to be assumed at 470 keV from where the nucleus returns to ground level partly through cross-over, partly through a cascade transition of 323 - - 147 keV.

At present, a new application of the above pulse-shape discrimination is being studied in co-operation with *Mr. Bálint Schlenk*. It is intended to separate charged particles, making use of the fact that in certain scintillators the decay time of the light pulse is a function of the particle mass.

Reference

[1] *Bisi - Germagnoli - Zappa:* Nuovo Cim., *2*/1955/1052.

[2] *S. Ofer - R. Wiener:* Phys. Rev., *107*/1957/1639.

[3] *L. Bambe - L. Pelekis:* Chem. Abst., *52*/1958/ no. 5153 d.

[4] *F.C. Chang:* Thesis, University of Michigen /1958/. Dissertation. Abstr. *19* /1958/1418.

SILICON JUNCTION DETECTOR IN A MAGNETIC BETA-RAY SPECTROMETER

By D. Berényi and T. Fényes

Institute of Nuclear Research of the Hungarian
Academy of Sciences, Debrecen, Hungary

We put the silicon junction detector in the focus of a toroid sector type beta--ray spectrometer. In the magnetic beta-ray spectrometer using Co^{60} and Cs^{137} sources we investigated the relative detection efficiency of the semiconductor detector, its pulse height - energy linearity, and the alteration of the full width at half-maximum of the total absorption peak as a function of energy, concentrating our attention mainly to the region of the minimum detectable energy.

Semiconductor counters may be applied as detectors in magnetic beta-ray spectrometers as well as counter tubes or scintillation counters. Their great advantage against the scintillation counters is their insensitivness to the presence of magnetic field, and at the same time with their aid one can discriminate energy, and this fact is a great advantage over the G.M. tubes.

We have to mention the relative simplicity and handiness of the semiconductor detectors, in these respects they surpass not only the formerly mentioned type of detectors but the proportional counters too.

In a toroid-sector type beta-ray spectrometer [1, 2] we used silicon junction detector for counting beta particles. The crystal consists of a p type Si semiconductor, its electrical resistivity being $>10^4$ Ω.cm. The sensitive area of the detector is 5 mm^2. The depth of the frontal n layer 0,2 μ. We operate the detector at a bias of 15 V. In this case the barrier depth is about 120 μ and this correspondes to the range of ~150 keV electrons. As for the arrangement see Fig. 1.

The area covered by the focused electron beam was considerably larger then the sensitive area of the detector.

The preamplifier connected to the detector has a cascode input stage and in many respects similar to that suggested by *Cottini* and his collaborators [3]. The characteristic maximal R.C. integrating time constant of the amplifier system is equal to the minimal differenciating time constant and both have a value of 0,7 μsec.

First we examine the alteration of the relative detection efficiency with special respect to low electron energies.

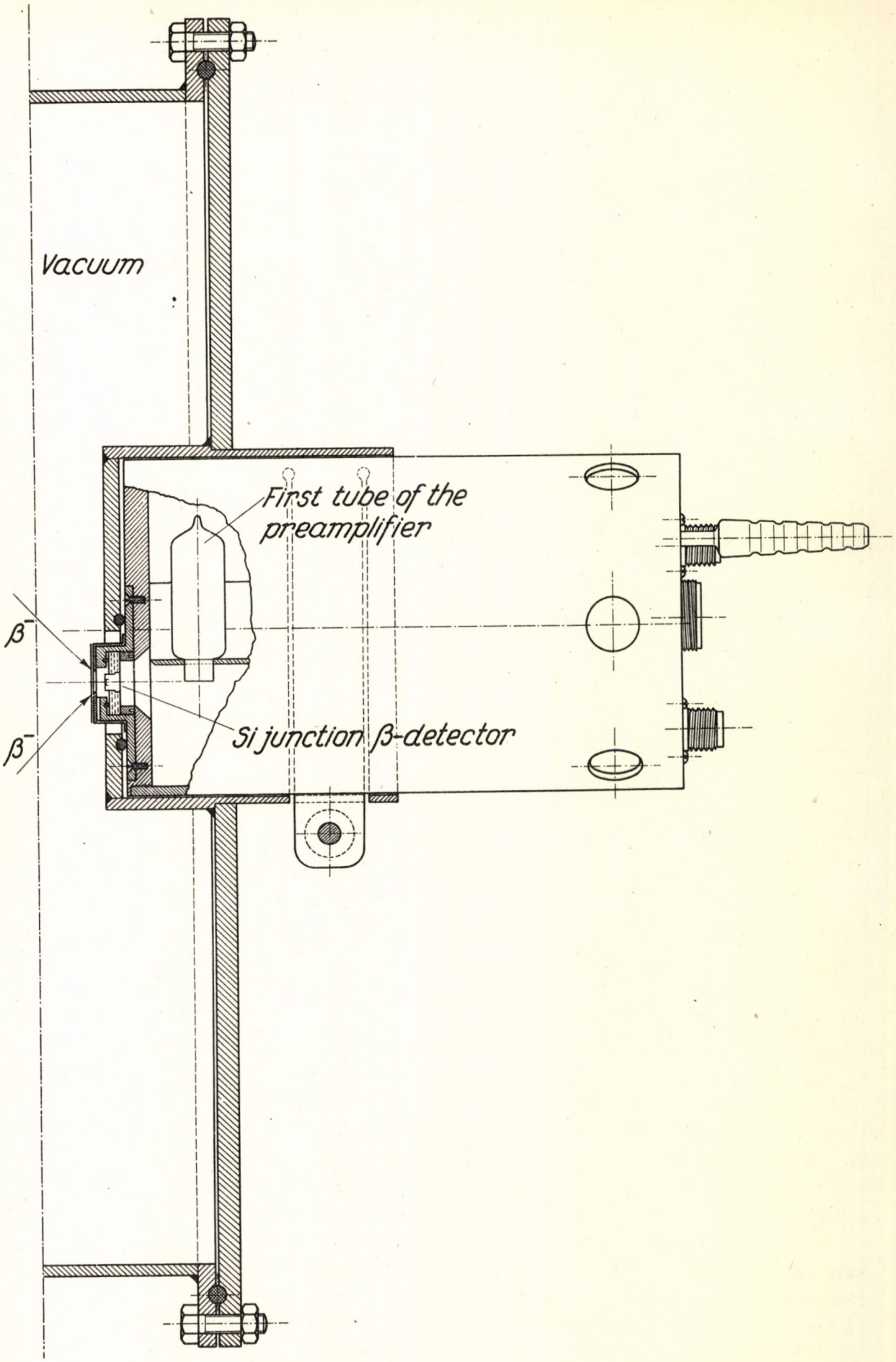

Fig. 1. Arrangement of the semiconductor detector in the β-ray spectrometer

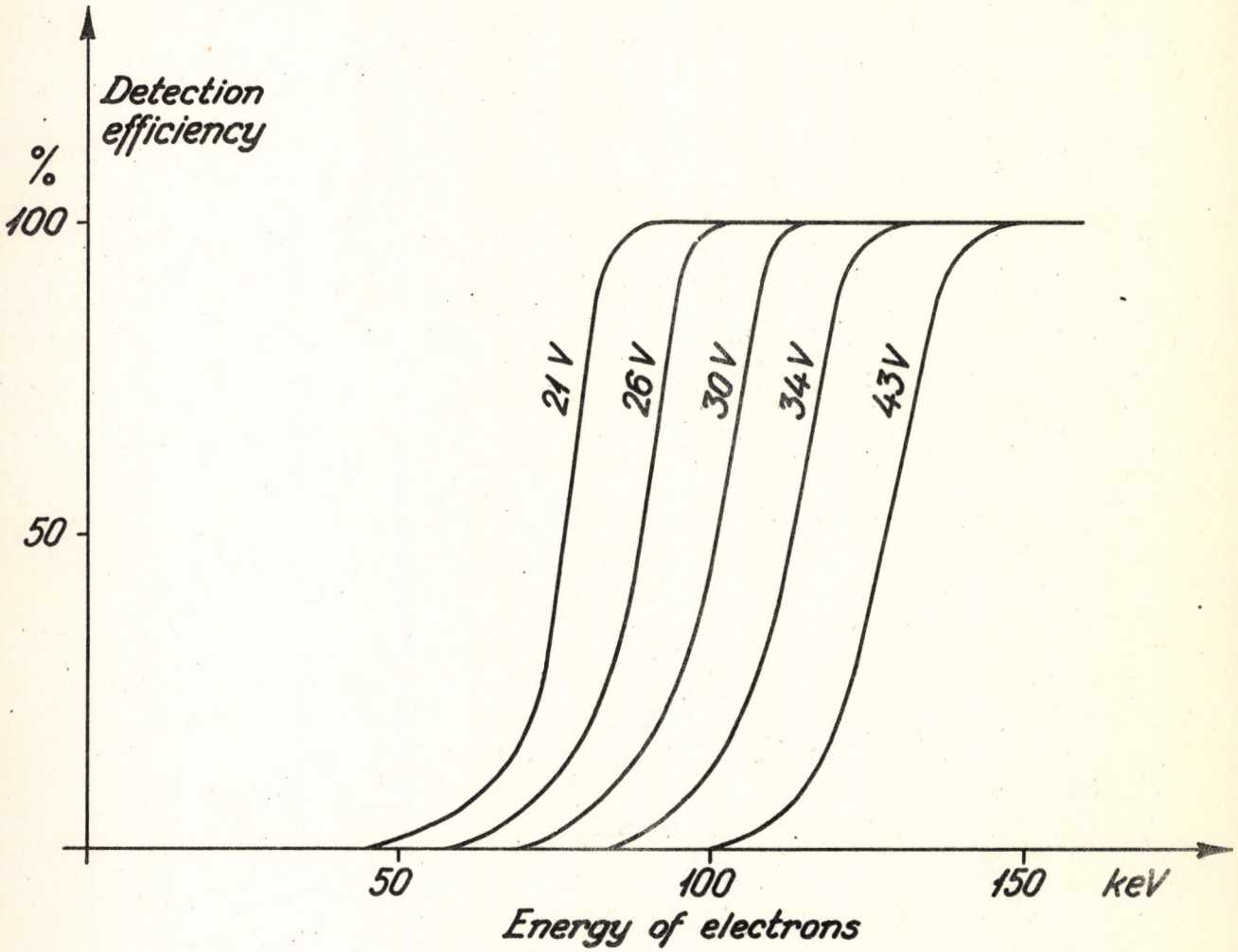

Fig. 2. Detection efficiency curves for low energy electrons in the function of the electron energies at different setting of the discrimination level (integral setting).

The magnetic beta-ray spectrometer may be applied also as a source of monoenergetic electrons and with its aid we investigated the pulse height - energy linearity of the detector in the region formerly mentioned, and the alteration of the resolving power as the function of energy.

The relative detection efficiency was determined by the detection of the Co^{60} β-ray spectrum in the well known manner [4, 5] by the deviation of the Fermi--Curie diagramm from the linearity at lower energies (Fig. 2.). With the aid of the curves it is possible to answer such a practical question as to which discriminator position is the most advantageous to be choosen in the case of a given measurement. It is obvious that the detector examined has a cut-off practically about 50 keV, even at the most suitable discriminator position. On the other hand if it is not necessary to detect such low energies, it is not advantageous to choose such relatively low discriminator position, because the signal to noise ratio will be very small in this case and the measurement becomes unreliable. See fig. 3.

Here the signal to noise ratio means the ratio of counting rates measured at the intensity maximum of the Co^{60} beta-ray spectrum i.e. at electrons of ≈150 keV and in case current does not flow through the beta-ray spectrometer coil.

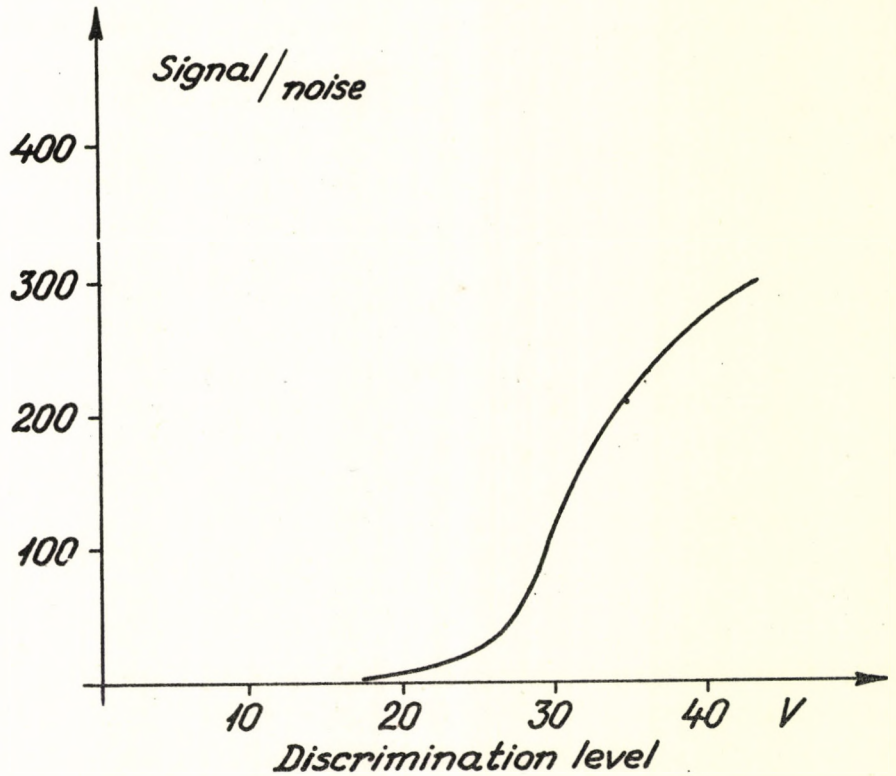

Fig. 3. The signal-to-noise ratio in the function of the discrimination level. The signal/noise is given here as the ratio of the counting rate at the intensity maximum of the Co^{60} β-ray spectrum and at the magnetic field of the spectrometer switched off.

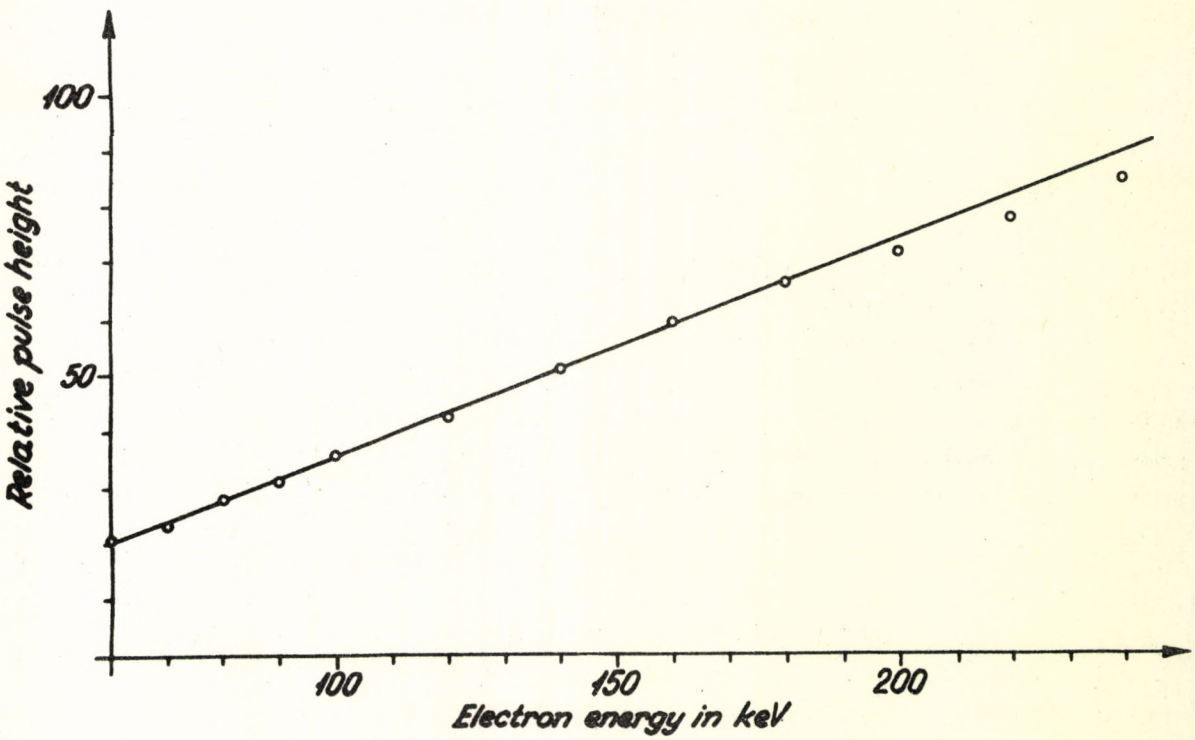

Fig. 4. The pulse height in the function of electron energy for the total absorption peaks in the spectrum taken by the detector as a β-ray spectrometer for monoenergetic electrons.

Putting Cs^{137} source in the magnetic beta-ray spectrometer and calibrating the spectrometer with the K conversion line, we set different current-intensities in the coil of the beta-ray spectrometer and thus different near monoenergetic electrons reached the semiconductor detector. Than we analised the beam at the different electron energies using the semiconductor detector as a spectrometer.

The pulse-height (i.e. the magnitude of the total absorption peak expressed in terms of the discriminator voltages) as a function of electron energies is plotted in Fig. 4.

We may see that the function shows deviation in the examined interval from the linear dependence only if the energy of electrons exceeds the energy of those electrons the range of which equal to the barrier depth. Towards small energy values up to the smallest examined energy (60 keV) we did not find any deviation from the linearity. The similar investigations referred to in the literature led to the same result. *McKenzie* and *Ewan* [6], *Bosch* et al. [7] investigated the pulse - height - energy correlation down to 100 keV and to 195 keV, respectively. We checked the linearity of the electronic system with two different precision mercury relay pulse generators. The pulse-height measured at the output of the amplifier depends linearly (within $\pm 1,5$ %) on the magnitude of signal measured at the input of the amplifier.

In the former measurements we determined also the full width of the total absorption peak at half maximum (FWHM) as a function of energy. The values are plotted in Fig. 5 (circles).

The detector leakage current noise and the noise of the electronic system (together: system noise) in the investigated interval had a constant value of 20 keV. We got this value by giving monoenergetic signals to the input of the amplifier from a mercury relay pulse generator and measuring the FWHM at the output of the amplifier.

One may see in Fig. 5. that the FWHM increases with the increasing electron energy. This increasing may have been expected because not wholly monoenergetic beam reaches the detector from the spectrometer and with increasing electron energy the energy dipersion of the beam will also increase. To characterize increasing of FWHM to be expected, we plotted in Fig. 5. the

$$\alpha = \alpha_S^2 + \alpha_\beta^2$$

quantity (crosses), where

α_S is the FWHM generated by the system noise,

α_β is the FWHM generated by the electron energy dispersion in the beta-ray spectrometer,

α is the FWHM generated by both system noise and electron energy dispersion.

The α_β quantity was determined by taking up a conversion e^- peak spectrum as a function of magnetic field strength (at constant radius of curvature). At this measurement we used the semiconductor only as a detector.

Fig. 5. shows, that the FWHM is nearly equal to the α quantity, i.e. about 60 keV electron energy the system noise, and at increasing energies - the system noise and the energy dispersion of the electron beam are mainly responsible for the full width at half-maximum.

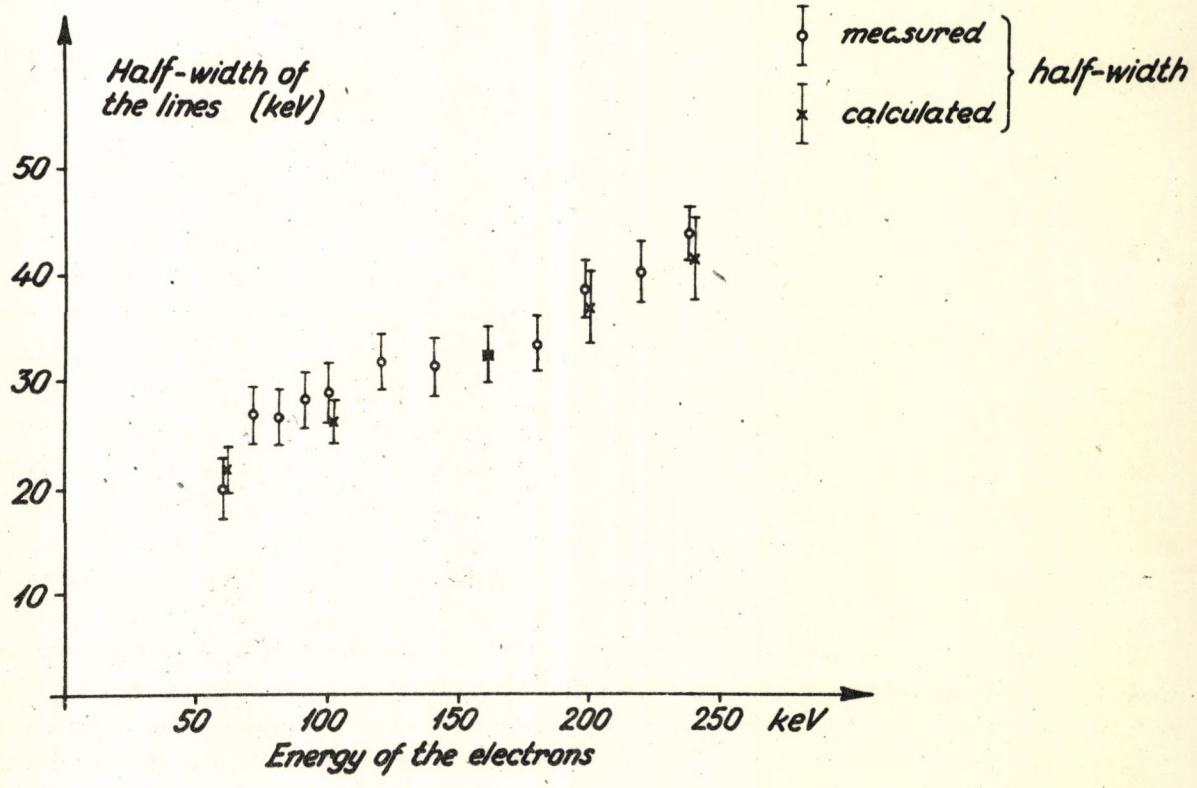

Fig. 5. The variation of the half-width of the total absorption peaks for monoenergetic electrons with electron energy (circles). Crosses: calculated half-width on the basis of system noise and electron energy distribution due to the final resolution in the β-spectrometer.

The authors express their thanks to *Prof. A. Szalay*, Director of the Institute, for excellent working conditions in the Institute and to our physicist colleaque *I. Mahunka* for help in different problems. A knowledgement is due to *Mrs. T. Halász* for technical aid at the measurements.

References

[1] *A. Szalay - D. Berényi:* Izv. AN SSSR, Ser. Fiz., *22*/1958/877 (in Russian).
[2] *A. Szalay - D. Berényi:* Acta Phys. Hung., *10*/1959/57.
[3] *C. Cottini - E. Gatti - G. Giannelli - G. Rozzi:* Nuovo Cimento, *3*/1956/473.
[4] *F.T. Porter - M.S. Freedman - T.B. Novey - F. Wagner Jr.:* Phys. Rev., *103*/1956/921.
[5] *D. Berényi - Gy. Máthé:* Nuclear Instr. and Methods, *13*/1961/161.
[6] *J.M. McKenzie - G.T. Ewan:* IRE Transactions on Nuclear Science, Vol. NS-8, /1961/ No. 1. p. 50.
[7] *H. Bosch - F. Krompotic - A. Plastino:* Nuclear Instruments, *23*/1963/79.

Kiadja a
Magyar Tudományos Akadémia
Atommag Kutató Intézete
D e b r e c e n
A kiadásért és szerkesztésért felelős
Szalay Sándor az Intézet igazgatója
Készült az Intézet "*Zetaprinton*" tipusu
sokszorositó gépén "*Rotaprint*" eljárással.
Foto és nyomdatechnikai kivitelező
Vencsellei István

Példányszám: 300
12/1963